5-2019

Targeting Sec61α by Ipomoeassin F Leads to Highly Cytotoxic Effect

Zhijian Hu
University of Arkansas, Fayetteville

Targeting Sec61α by Ipomoeassin F Leads to Highly Cytotoxic Effect

A dissertation submitted in partial fulfillment
of the requirements for the degree of
Doctor of Philosophy in Cell and Molecular Biology

by

Zhijian Hu
Huazhong University of Science and Technology
Bachelor of Science in Clinic Medicine, 2009
Huazhong University of Science and Technology
Master of Science in Surgery, 2012

May 2019
University of Arkansas

This thesis is approved for recommendation to the Graduate Council.

_____
Wei Shi, Ph.D.
Dissertation Chair

_____
Sun-OK Lee, Ph.D.
Committee Member

_____
Yuchun Du, Ph.D.
Committee Member.

_____
Gisela F. Erf, Ph.D.
Committee Member

_____
Suresh Thallapuranam, Ph.D.
Committee Member

Abstract

Ipomoeassin F is a flagship congener of a resin glycoside family that inhibits growth of many tumor cell lines with only single-digital nanomolar IC_{50} values. However, biological and pharmacological mechanisms of ipomoeassin F have been undefined. To facilitate exploration of the biological and pharmacological properties, we performed sophisticate SAR (Structure–activity relationship) studies of ipomoeassin F to understand its pharmacophore and structure properties so that we can design favorable probes for further biological investigation. By applying appropriate deviates that possess fluorescent groups and similar bio-activity, the target protein was found to be localized in endoplasmic reticulum (ER). Through biotin affinity pull down and proteomics studies, the target protein Sec61α (protein transport protein Sec61 subunit alpha isoform 1) was successfully isolated and confirmed. The isolated protein validation by Western blot provides convincing evidence to support the conclusion that Sec61α is the primary molecular target. Subsequently, the binding mode between ipomoeassin F and Sec61α was proved to be non-covalent or reversible covalent binding with the help of reverse/delayed competition. Based on competition result between ipomoeassin F and the derivatives with different activities, future applications of those derivatives to search for detect Sec61α-specific bio-active compounds by high throughput screening (HTS) are proposed. As a novel plant-derived carbohydrate-based macrocyclic molecule, ipomoeassin F was proved to have an exclusive mode of action. The successfully identification of its target protein Sec61α provides a new molecular tool to further understand the Sec61α biological properties and its potential to be a new therapeutic target for drug discovery. Most importantly, the information about this distinct mode of action would lead to a new way to design and develop more effective anti-cancer drugs.

Acknowledgements

I thank Dr. Sun-OK Lee, Dr. T.M.S. Kumar and Dr. Gisela F. Erf for being my committee member, treating each committee meeting as their special class to teach me more scientific thinking and academic management.

I gratitude for the generous guidance and teaching from Dr. Yuchun Du and Mrs. Jianhong Zhou all through my research. with their kindly help, I not only learned lots of fancy techniques but also enjoyed the charm of biologic research, which would benefit my whole life.

I thank my advisor, Dr. Wei Shi, for accepting me into the research group, helping me adjust to the academic life, mentoring me to be a creative biologist step by step, and patiently guiding me to overcome all kinds of obstacles. His is more than a thoughtful advisor but also a reliable friend who would always stand by me whenever I needed help.

I thank all the members of the Shi group for long time support, thank Dr. Gunaghui Zong for helping me adjust to the life in the first couple of weeks when I came here and support me in the chemistry lab.

I thank Dr. Hazim Al-jewari and Dr. Xianwei Sun for teaching me basic biological and chemical techniques. Thank Dr. Lucas Whisenhunt, Dr. Eric Barber and Dr. Mugunthan Govindarajan for their work and assistance in the chemistry lab.

Most importantly, I thank God for putting so many awesome people in my life. And we know that in all things God works for the good of those who love him, who have been called according to his purpose. (Romans 8:28)

Dedication

This work is dedicated to my family for the unconditional love, tolerance, and guidance since the beginning of my life. Thanks for their support and encourage whenever I was down. I appreciate my wife Ping Zhang for her unconditional support and irreplaceable help during this journey. Thanks for being the most important person in my life and teaching me to always be serious with everything I am doing.

Table of Contents

CHAPTER 1. BACKGROUND AND INTRODUCTION 1

1.1. Cancer Epidemiology 1

1.1.1. Cancer 1

1.1.2 Breast Cancer 2

1.2. Nature Product Ipomoeassins F 4

1.2.1. Nature product 4

1.2.2. Resin Glycosides and Ipomoeassin family 5

1.2.3. Target identification 7

1.3. Statement of the Problem 9

1.4. References 11

CHAPTER 2. SAR STUDY AND PROBE EXPLORATION 15

2.1. SAR study 15

2.1.1. Structure-activity information from ipomoeassin family members 15

2.1.2 Structure-activity information from characteristic structure modification 16

2.1.3. Structure-activity information from cinnamate and tiglate modification 18

2.1.4. Structure-activity information from hydrophilic moieties modification 21

2.1.5. Structure-activity information from aglycone modification 22

2.1.5.1. Impact of stereogenic center C-11 on ipomoeassin F bioactivity. 22

2.1.5.2. Impact of open-chain aglycone on ipomoeassin F bioactivity. 23

2.1.5.3. Impact of cyclic structure size on ipomoeassin F bioactivity. 25

2.1.6. Structure-activity information from fucose modification 26

2.1.7. Summarize of structure-activity relationship study 27

2.2. Probe Design and Selection 29

2.2.1. Probes for stepwise target protein identification 30

2.2.2. Probes for ABPP by fluorophore reporter 32

2.2.3. Probes for ABPP by affinity tag reporter 34

2.2.4. Summary of Probes design and selection. 36

2.3. References 37

CHAPTER 3. IPMOEASSIN F TARGET PROTEIN IDENTIFICATION AND VALIDATION 39

3.1. Abstract 39

3.2. Introduction 39

3.3. Results and Discussion 42

3.3.1. Proteomics Evaluations of Chemical Probes derived from Ipomoeassin F. 42

3.3.2. Cell Imaging Studies. 49

3.3.3. Pulldown from ER Microsomes. 50

3.3.4. Pulldown from ER Microsomes. 51

3.3.5. ipomoeassin F and Sec61α interaction mode exploration 51

3.4. Conclusions 54

3.5. Supporting Information 55
3.5.1. Cytotoxicity Assay 55
3.5.1.1. Cell Culture 55
3.5.1.2. MTT Cytotoxicity Assay 55
3.5.1.3. AlamarBlue Cytotoxicity Assay 56
3.5.2. Stepwise Activity Based Protein Profiling 56
3.5.3. Biotin Affinity Pulldown 57
3.5.3.1. Live Cell-based Pulldown 57
3.5.3.2. Cell Lysate-based Pulldown 58
3.5.3.3. ER Microsome-based Pulldown 59
3.5.4. Mass Spectrometry (MS) Analysis and MS Data Processing 59
3.5.5. Cell Imaging 60
3.5.6. Figures and Tables 62
3.5.6.1. Cell Cytotoxicity Assay 62
3.5.6.2. Stepwise Activity Based Protein Profiling 63
3.5.6.3. Biotin Affinity Pulldown 64
3.5.6.4. Cell Imaging 66
3.5.6.5. Pulldown in ER Microsomes. 67
References 84

CHAPTER 4. FUTURE PROJECT: APPLICATION FOR HIGH-THROUGHPUT SCREENING 87

4.1. Fluorescent probe based HTS study 88

4.1.1. Mechanism for fluorescent probe based HTS research 88

4.1.2. Optimal work concentration exploration for cell imaging 90

4.1.3. Optimal treatment time exploration for cell imaging 92

4.1.4. Optimal fold competition of ipomoeassin F for cell imaging 95

4.1.5. Optimal competition time of ipomoeassin F for cell imaging 97

4.1.6. Procedure design for fluorescent probe based HTS research 99

4.1.7. Result interpretation 100

4.2. Biotin probe based HTS study 101

4.2.1. Mechanism for biotin probe based HTS research 101

4.2.2. HTS work condition optimization. 102

4.2.3. Procedure design for biotin probe based HTS research 102

4.2.4. Result interpretation 104

4.3. Conclusion 104

4.4. References 106

SUMMARY AND CONCLUSIONS 107

Appendix: Biosafety Approval Letter 108

List of Figures

CHAPTER 1. BACKGROUND AND INTRODUCTION 1

Figure 1.1 Estimated New Cancer Cases and Deaths by Sex, United States, 2019. 1

Figure 1.2 Trends in Incidence Rates for Selected Cancers by Sex, United States, 1975 to 2015.. 3

Figure 1.3. Target protein identification by affinity purification. 8

CHAPTER 2. SAR STUDY AND PROBE EXPLORATION 15

Figure2. 1. Structures of ipomoeassin F and its analogues **2.1**-**2.4**. 17

Figure2. 2. Structure of ipomoeassin F analogues **2.5**-**2.8**. 19

Figure2. 3. Structure of ipomoeassin F analogues **2.8**-**2.10**. 20

Figure2. 4. Viability curves of ipomoeassin F and analogues **2.8**, **2.9**, **2.10** in breast cancer cell lines 21

Figure2. 5. Structures of ipomoeassin F analogues **2.11**-**2.12.** 22

Figure2. 6. Structures of ipomoeassin F and its C-*11R* epimer **2.13.** 23

Figure2. 7. Structures of ipomoeassin F analogues **2.14** and **2.15**. 24

Figure2. 8. Structures of ipomoeassin F and its analogues **2.16** and **2.17.** 25

Figure2. 9. Structures of ipomoeassin F analogues **2.18** and **2.19**. 26

Figure2. 10. Viability curves of ipomoeassin F and analogues **2.18** and **2.19** in breast cancer cell lines 27

Figure2. 11. Cytotoxicity loss by pharmacophore editing. 28

Figure2. 12. The four pillars of cell-based target validation using chemical probes. 30

Figure2. 13. Structure and cytotoxicity of ipomoeassin F analogues **2.20** and **2.21**.. 31

Figure2. 14. Diagram of stepwise target protein identification. 32

Figure2. 15. Structure of ipomoeassin F analogues **2.22-2.28**..... 33

Figure2. 16. Structures of ipomoeassin F analogues **2.29 - 2.33**. 35

CHAPTER 3. IPMOEASSIN F TARGET PROTEIN IDENTIFICATION AND VALIDATION..... 39

Figure 3. 1. Structures of ipomoeassins A, D, and F. 41

Figure 3. 2. Structure of ipomoeassin F analogues **3.1**-**3.3**..... 42

Figure 3. 3. Affinity pulldown using probe **3.3**. 45

Figure 3. 4. Structure and cytotoxicity of ipomoeassin F analogues **3.4**-**3.5**.. 46

Figure 3. 5. Affinity pulldown using probe **3.3**, **3.4** and **3.5.**..... 47

Figure 3. 6. Structures of ipomoeassins F analogues **3.1** and **3.6**. 48

Figure 3. 7. Structures of fluorescent derivative **3.7** 49

Figure 3. 8. Cell imaging studies with fluorescent probe **3.7** in MDA-MB-231 cells..... 50

Figure 3. 9. Traditional completion and reverse competition between ipomoeassin F and analogue **3.3**:. 53

Figure S 1. Cytotoxicity in MDA-MB-231: Cell viability curves of analogues **3.1**, **3.2**, **3.3**, **3.7** and ipomoeassin F..... 62

Figure S 2. Click reaction performed after incubating cells with competitor and its corresponding alkyne probe.. 63

Figure S 3. Biotin affinity pulldown with probes **3.2** and **3.3**..... 64

Figure S 4. Biotin affinity pulldown with probe **3.3** or **3.5** in the presence of the competitor ipomoeassin F or **3.6.**. 65

Figure S 5. Live cell imaging-based competition experiments..... 66

Figure S 6. Biotin affinity pulldown with probe **3.3** in ER microsomes.. 67

CHAPTER 4. FUTURE PROJECT: APPLICATION FOR HIGH-THROUGHPUT SCREENING..... 87

Figure 4. 1. Ipomoeassin F analogues **4.1, 4.2**..... 88

Figure 4. 2. Live cell imaging-based competition experiments.. 89

Figure 4. 3. Live cell imaging from **4.1** incubation at different concentration.. 92

Figure 4. 4. Live cell imaging from **4.1** 100nM treatment at different time incubation. 95

Figure 4. 5. Live cell confocal fluorescent microscopy imaging from 1h **4.1** 100nM treatment and 30min ipomoeassin F competition at different competition fold difference:..... 97

Figure 4. 6. Live cell imaging from 1h **4.1** 100nM treatment and 100-fold ipomoeassin F competition at different competition time..... 99

Figure 4. 7. Structure of ipomoeassin F analogues **4.3.**..... 101

Figure 4. 8. Work flow of biotin-based HTS. 103

List of Tables

CHAPTER 1. BACKGROUND AND INTRODUCTION 1

Table 1.1. Structures and IC_{50} Values of Ipomoeassin A–F. 6

CHAPTER 2. SAR STUDY AND PROBE EXPLORATION 15

Table 2. 1. Structures and IC_{50} Values of Ipomoeassin A–F. 16

Table 2. 2. Cytotoxicity (IC_{50}, nM) of Ipomoeassin F and Its analogues **2.1**-**2.4** 18

Table 2. 3. Cytotoxicity (IC_{50}, nM) of Ipomoeassin F and Its analogues **2.5**-**2.8** 19

Table 2. 4. Cytotoxicity (IC_{50}, nM) of Ipomoeassin F and Its analogues **2.11**-**2.12** 22

Table 2. 5. Cytotoxicity (IC_{50}, nM) of Ipomoeassin F and Its epimer **2.13** 23

Table 2. 6. Cytotoxicity (IC_{50}, nM) of Ipomoeassin F and Its analogues **2.14**-**2.15** 24

Table 2. 7. Cytotoxicity (IC_{50}, nM) of Ipomoeassin F and Its analogues **2.16**-**2.17** 26

Table 2. 8. Cytotoxicity (IC_{50}, nM) of Ipomoeassin F and its Probes **2.22**-**2.28** 34

Table 2. 9. Cytotoxicity (IC_{50}, nM) of Ipomoeassin F and its Probes **2.29**-**2.33** 36

CHAPTER 3. IPMOEASSIN F TARGET PROTEIN IDENTIFICATION AND VALIDATION……39

Table 3. 1. Cytotoxicity (IC_{50}, nM) of Ipomoeassin F and Its Probes 3.1-3.7 43

Table S 1. Data of proteomics form LC/MS……68

Abbreviations

IC_{50}: Half Maximal Inhibitory Concentration

SAR: Structure–Activity Relationship

ER: Endoplasmic Reticulum

HTS: High Throughput Screening

TNBC: Triple-negative breast cancer

PR: Progesterone Receptor

HER-2: Human Epidermal Growth Factor Receptor 2

FDA: U.S. Food and Drug Administration

NCEs: New Chemical Entities

NCI: National Cancer Institution

MOA: Mechanism of Action

MS: Mass Spectrometry

ABPP: Active-Based Protein Profiling

Glc*p:* Glucose

Fuc*p:* Fructose

CuAAC: Copper-catalyzed Alkyne-Azide Coupling

FBS: Fetal Bovine Serum

DMSO: Dimethyl Sulfoxide

DDM: n-Dodecyl-ß-D-Maltoside

FDR: False Discovery Rate

ELISA: Enzyme-Linked Immunosorbent Assay

List of Published Papers

Portion of **Chapter 3** is from the paper listed below

- Zong G.; * **Hu Z**.; * O'Keefe S.; Tranter D.; Iannotti M.; Baron L.; Hall B.; Corfield K.; Paatero A.; Henderson M.; Roboti P.; Zhou J.; Sun X.; Govindarajan M.; Rohde J.; Blanchard N.; Simmonds R.; Inglese J.; Du Y.; Demangel C.; High S.; Paavilainen V.; Shi W.Q. Ipomoeassin F Binds Sec61α to Inhibit Protein Translocation. J Am Chem Soc. *(under revision)* *Author contributions: Zong G. and Hu Z. contributed equally to the work.

CHAPTER 1. BACKGROUND AND INTRODUCTION

1.1. Cancer Epidemiology

1.1.1. Cancer

Cancer is one of the leading public health problems worldwide, and yet the most difficult research area due to its intricate physiopathology. It is threatening public health as second cause of death in the United States,[1] leading to heavy burden on the medical care system and the society.

Estimated New Cases

Males			Females		
Prostate	174,650	20%	Breast	268,600	30%
Lung & bronchus	116,440	13%	Lung & bronchus	111,710	13%
Colon & rectum	78,500	9%	Colon & rectum	67,100	8%
Urinary bladder	61,700	7%	Uterine corpus	61,880	7%
Melanoma of the skin	57,220	7%	Melanoma of the skin	39,260	4%
Kidney & renal pelvis	44,120	5%	Thyroid	37,810	4%
Non-Hodgkin lymphoma	41,090	5%	Non-Hodgkin lymphoma	33,110	4%
Oral cavity & pharynx	38,140	4%	Kidney & renal pelvis	29,700	3%
Leukemia	35,920	4%	Pancreas	26,830	3%
Pancreas	29,940	3%	Leukemia	25,860	3%
All Sites	**870,970**	**100%**	**All Sites**	**891,480**	**100%**

Estimated Deaths

Males			Females		
Lung & bronchus	76,650	24%	Lung & bronchus	66,020	23%
Prostate	31,620	10%	Breast	41,760	15%
Colon & rectum	27,640	9%	Colon & rectum	23,380	8%
Pancreas	23,800	7%	Pancreas	21,950	8%
Liver & intrahepatic bile duct	21,600	7%	Ovary	13,980	5%
Leukemia	13,150	4%	Uterine corpus	12,160	4%
Esophagus	13,020	4%	Liver & intrahepatic bile duct	10,180	4%
Urinary bladder	12,870	4%	Leukemia	9,690	3%
Non-Hodgkin lymphoma	11,510	4%	Non-Hodgkin lymphoma	8,460	3%
Brain & other nervous system	9,910	3%	Brain & other nervous system	7,850	3%
All Sites	**321,670**	**100%**	**All Sites**	**285,210**	**100%**

Figure 1.1 Estimated New Cancer Cases and Deaths by Sex, United States, 2019.[1]

From the data predicted, probability of being diagnosed with invasive cancer all through the lifetime is as high as 37.7%-39.3%.[1] According to the most recent data analysis,[1] there will be approximately 1,762,450 cancer cases diagnosed in the United States. That corresponding to more than 4,800 new cases will be diagnosed every day. Despite great breakthroughs in modern surgery, chemotherapy, radiotherapy, radiotherapy, newly established targeted therapies and immunotherapy significantly lessened morbidity and ameliorated survival over the past decades,[2] cancer remains one of the most dangerous killers in the United States.[3] It is estimated that 606,880 Americans will die from cancer in 2019, which is equivalent to nearly 1,700 deaths each day. From the literature report (Figure 1.1), there will be 268,600 new cases of breast cancer to be diagnosed, occupying 30% of all new woman cancers cases in 2019; and breast cancer is the second leading cause of death after lung cancer in woman cancer cases.

1.1.2 Breast Cancer

Breast cancer is the leading cause of death among women aged 20 to 59.[1] It was first described as a breast bulging in ancient Egyptian medical papyri.[4] Over the past few decades, the overall cancer incidence rate in woman was relatively stable, however, breast cancer incidence rates increased approximately 0.3% to 1.8% from 2006 - 2015.[5] This trend is clearly illustrated by data collected from 1975 - 2015 (Figure 2). Breast cancer survival rates vary significantly all over the world with an 80% 5-year survival rate in developed countries which is below 40% in developing countries.[6]

Breast cancer has been a worldwide critical public health problem for decades. The modern breast cancer treatment began in 1880s, when Halsted applied surgical approach.[7] With almost 140 years of continuous endeavor by innumerable physicians and scientists, prognosis of breast cancer improved significantly. However, due to the complexity of breast cancer and drug development, it

is still one of the most life threating diseases to women. It is a never-ending fight against breast cancer, extensive research is required to identify specific treatment and ameliorate its prognosis. Cancer cell lines are commonly used as the primary *in vitro* experimental models to understand cancer biology and molecular pharmacology of anticancer drugs.

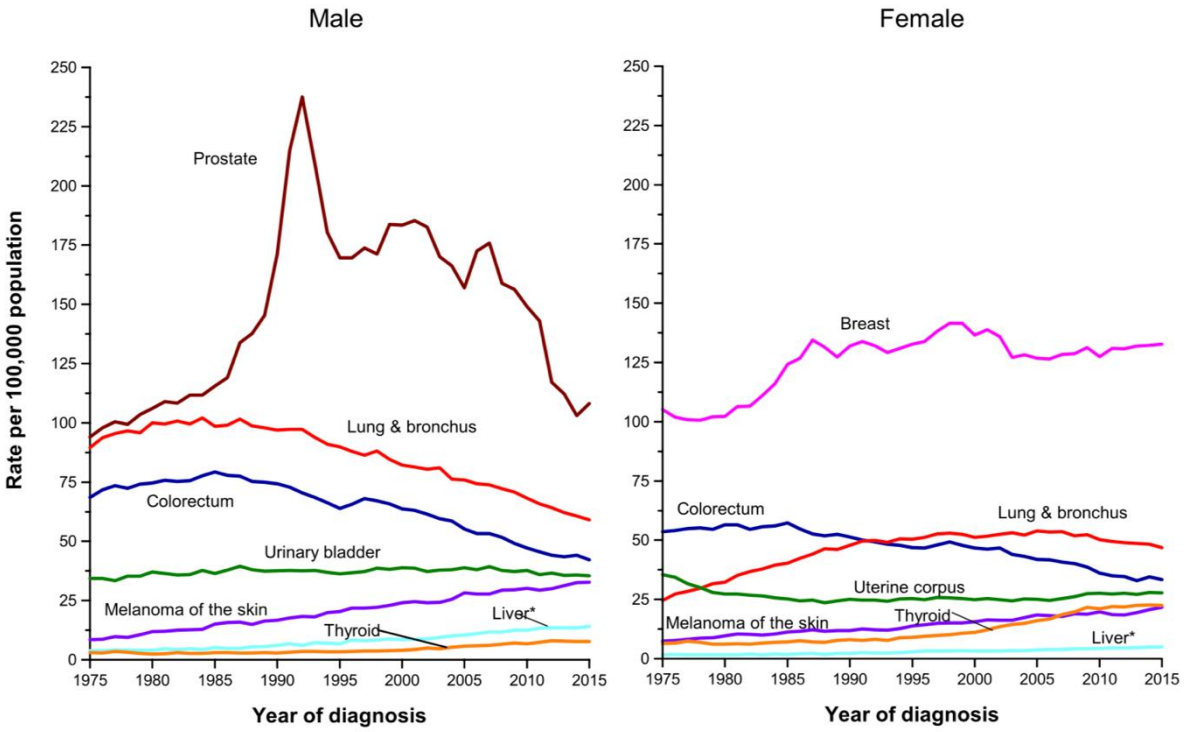

Figure 1.2 Trends in Incidence Rates for Selected Cancers by Sex, United States, 1975 to 2015.[1]

As a heterogeneous disease, breast cancer consists of a series of clinical and molecular distinct subtypes.[8] Triple-negative breast cancer (TNBC) is a destructive type of breast cancer which lacks expression of progesterone receptor (PR), human epidermal growth factor receptor 2 (HER-2) and estrogen receptor (ER), and the gene expression profile is often a basal-like cancer cell line.[9] TNBC is an invasive subtype and occupies around 15% of all invasive breast cancers.[10] MDA-MB-231 cell line is a well-established human breast cancer epithelial cell line originated from a pleura effusion of a Caucasian female breast cancer patient.[11] It is commonly used as a

TNBC cell model characterized with highly aggressive, invasive and poorly-differentiated cancer, endowing its great value in anti-cancer drug research.

MCF-7 is a commonly used breast cancer cell line established by Dr. Soule and his colleagues in 1973.[12] It was first isolated from pleural effusion of a breast cancer metastatic case. MCF-7 is a luminal A molecular subtype cell line which is estrogen receptor (ER) - positive and progesterone receptor (PR) - positive.[13,14] It is a non-invasive cell line and proved to be a suitable model cell line for anticancer drugs investigation.[14,15]

MCF-10 is a human breast epithelial cell line derived from s.c. mastectomy tissue from a patient with fibrocystic disease.[16] MCF-10A is an attaching immortal cell line which originated from a mortal cell line MCF-10M. Electron microscopy revealed that MCF-10A has the same characteristics of luminal ductal cells, moreover it maintains their epithelial cell characteristics.[16] MCF-10A is considered as an important tool for investigating cell growth and carcinogenesis,[16] therefore we include this cell line as a non-cancer control to evaluate compound selectivity among breast cell derived cell lines.

In our bio-activity study, cytotoxicity of synthesized compounds was tested against the highly invasive breast cancer cell line MDA-MB-231, non-invasive breast cancer cell line MCF-7 and the breast epithelial cell line MCF-10A separately. Half maximal inhibitory concentration (IC_{50}) was calculated to evaluate compound potency, and the ratio between the IC_{50} from cancer cell lines versus IC_{50} from epithelial cell was used to estimate selectivity of each compound.

1.2. Nature Product Ipomoeassins F

1.2.1. Nature product

Nature product consists of a significant amount of families with various chemical entities that plays import roles in biological activities. Throughout human history, people have been

exploring nature for treatment of a wide spectrum of diseases regardless of their different location and culture. Natural products have been the most widely used source for drug development, especially in anti-infectives and anti-cancer studies.[17-20] Over the past 75 years since the discovery of penicillin, more than 23,000 natural products have been identified and characterized. [21] It is reported that 60% of the 1500 FDA approved new chemical entities (NCEs) from 1981 to 2014 were natural products, derivatives or mimicked natural products.[17] Among the 136 approved anti-cancer drugs, nearly 83% of the reagents were developed from natural products or were direct derivates.[22] Within the intense competition of drug development, more and more people are realizing that there would be more chance of getting successful drugs from natural products rather than collections of synthetic compounds. [23,24]

Nowadays numerous incurable diseases have been conquered, however cancers, a series of comprehensive systematic diseases, are still out of control due to the dilemma of killing cancer cells together with normal cells damaged while applying anti-cancer drugs. This double-edged sword effect originated from the lack of pinpointing effective target-oriented medicine. Therefore, looking for an active natural product, identifying its druggable target and designing the corresponding acting analogues without triggering off target effects, would be an ideal approach for anti-cancer development.

1.2.2. Resin Glycosides and Ipomoeassin family

Resin glycosides, which are part of glycolipids or lipo-oligosaccharides family, consist of complex resins (glycoresins).[25] They are a group of compounds isolated from *Convolvulaceae*, and widely used as traditional medicine to perform various biological activities including purgative, haemolytic, laxative, antifungal, anti-bacterial and even cytotoxicity.[26-30] All parts of *Convolvulaceae*, including roots, leaves, stems, bulbs and flowers have been explored and used as

medication for different diseases.[26,31] A large number of glycoconjugate natural products have been identified to harbor anti-cancer bioactivity.[32]

The ipomoeassins, a representative of resin glycosides family, was first isolated from Suriname rainforest by Kingston and his colleagues in 2005 from the leaves of *Ipomoea squamosa*.[33] This small class of six resin glycosides family is reported to have a range of biological properties including antifungal, antibacterial and cytotoxicity.[27,31] Kingston et al. isolated ipomoeassin family A-E, and revealed their potency against an ovarian cancer cell line.[33] While resin glycosides are reported to be potent anti-cancer reagents based on their micromolar IC_{50} values against certain cancer cell lines, certain members in ipomoeassin family exhibit their anti-cancer toxicity at nanomolar IC_{50} values.[34]

NCI-60 was developed by US National Center Institute in the 1980s to maintain their own collection of stable, differentiated cancer cell lines.[21] The panel of 60 cell lines have been employed to investigate the efficacy and specificity of all kinds of natural products. As the most abundant in ipomoeassin family, ipomoeassin A was tested against NCI-60 cell lines and found to have antiproliferation activity.[34] What's more, the activity pattern was found to be unmatchable among known anticancer agents in National Cancer Institution (NCI) database.

Table 1.1. Structures and IC_{50} Values of Ipomoeassin A–F.[34,35]

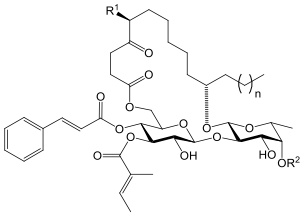

Ipomoeassin	Structure			IC_{50} (nM)						
	R^1	R^2	n	HeLa	L-929	A2780	U937	HT-29	MDA-MB-435	H522-T1
A	H	Ac	1	64	77.8	500	20.2	46.1	42.6	108.9
B	H	H	1	2500		400	134	396	2700	1070
C	OH	Ac	1	1500	> 1000	2900	-	-	-	-
D	OAc	Ac	1	32	135	35	7.9	11.8	19.9	23.2
E	OAc	H	1	4300	> 1000	3300	163	393	1633	967
F	H	Ac	3	-	7.4	36	2.6	4.2	9.4	12.9

Two years after the extensive study on ipomoeassin family, Kingston group isolated another family member ipomoeassin F, which possesses distinguished potency against multiple cancer cell lines.[35] According to previous *in vitro* cytotoxicity test, it inhibits cancer cells proliferation mostly with IC_{50} value nanomolar range (Table 1.1). The impressive cytotoxicity is even more potent than many clinical chemotherapeutic drugs. Interestingly, when we submitted our home made ipomoeassin F for test against NCI-60 cell lines, the report not only confirmed its nanomolar potency against couple of cell lines but also reflected its unique functional mechanism that was different from all existing agents in NCI databases.[36] The conclusion perfectly matches previous research on ipomoeassin A.

Such high degree bioavailability of this newly discovered natural product endows its potential promising candidacy for efficient anti-cancer drug development. Therefore, uncovering the possible mode of action may pave a new road for anti-cancer development.

1.2.3. Target identification

An increasing number of natural products are well studied for potential therapeutical candidates, however, their further development into application is always time consuming and costly due to the limited understanding of the mechanism of action (MOA) and unexpected side effects.[37] Active small molecules perform their bioactivity through various ways of interaction with their specific target in biological environment, As a result, identification of the pivot target could significantly facilitate the understanding of their MOA as well as the unwanted side effects.[37] It's almost impossible to ignore the drug target whiling developing a mechanism-based drug. Revealing the target can not only predict the future clinic efficacy and safety, but also provide clue to understand and deal with side effects. For natural products, structural modifications through synthesis are a widely used approach to uncover MOA, and may lead to potential clinical drug

development. Proteins are one of the most often targets, hence development of high-accuracy research method will greatly improve the chance of identifying target proteins.

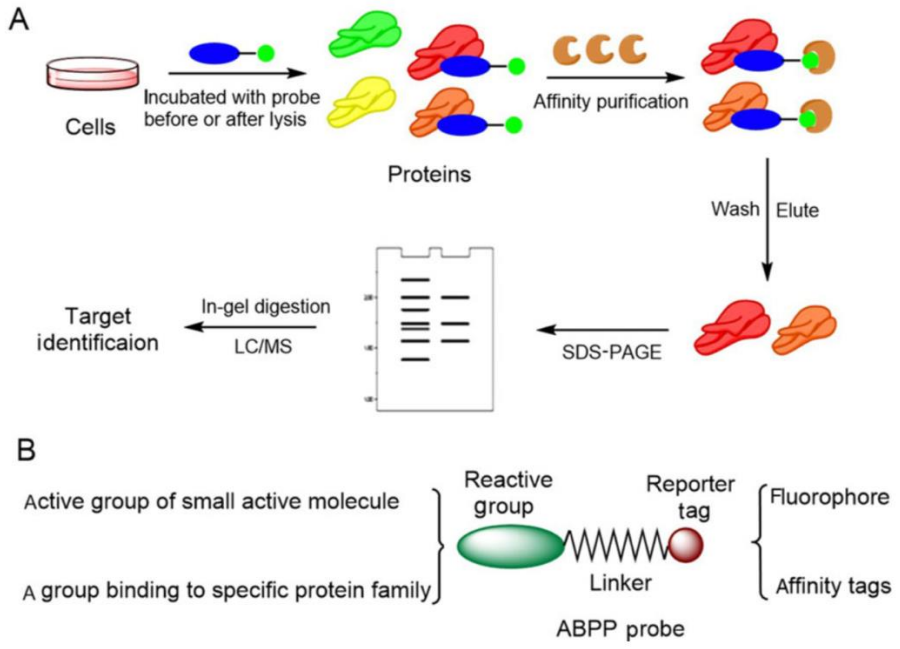

Figure 1.3. Target protein identification by affinity purification. (A) Workflow of target protein identification by affinity purification and LC/MS. (B) Typical ABPP probe constitution.[38]

The combination of affinity chromatography and Mass spectrometry (MS) have been proved to be successful way of unveiling target proteins. Based on specific bioactive interactions, application of chemical proteomics and active-based protein profiling (ABPP) further improved the rapid process and accurate target protein identification, minimizing the unspecific protein disturbance.[38-40] While working with chemical proteomics, molecular-protein interaction was studied through applying various synthesized probes with functional moieties. This approach often works together with MS to further push up greater precision and comprehensiveness than traditional western blot.[38,41] In ABPP chemical proteomics study, active functional probes are design and synthesize by modification from compounds of interest. They identify the target protein by probing covalent or strong non-covalent binding. Usage of ABPP coupling quantitative

chemical proteomics has played an important role in many insightful studies and proven to be a powerful tool in identifying target identification.[38,42]

Probes (Figure 1.3B) designed for ABPP normally consist of three core elements: (1) reactive group that specifically binds the target protein; (2) a traceable tag that enables affinity purification （Figure 1.3A）and further image study; (3) a linker between reactive group and reporter tags. The linker may act as an associated target protein purification or tracing facilitator by introducing crosslinking or cleavable functional groups. Typical target protein identification by ABPP is composed of cell or cell lysate incubation, probe-target protein complex isolation and target protein identification.

1.3. Statement of the Problem

Since Kingston group isolated and reported the ipomoeassin family in 2005, more and more scientists dedicate their research on exploring different properties of this potent anti-cancer agent. Even through certain chemical and biological characteristics have been unveiled, the understanding of the properties of this small family is still very limited.

Structure-activity relationship (SAR) study is one of the most frequently used as the first approach to explore the MOA of a compound. By understanding the contribution of each individual moiety to the bioactivity, appropriate modification could be introduced accordingly to introduce favorable function groups with minimum disturbance to the original bioactivity. Probes that maintain the biomedical properties of the compound of interest could be developed to further define the MOA as well as the mechanism of side effects, endowing the possibility to produce ideal drugs for serious diseases. From the data reported in the literature, some pieces of information could be obtained about certain aspects of the structure-activity character of ipomoeassin F. However, knowledge collected from available literature are far from sketching the contours of

ipomoeassin F structure - activity relationship due to the lack of appropriate analogue library to systematically study ipomoeassin F from all aspects.

As the most potent member of ipomoeassin family, ipomoeassin F has distinguished cytotoxic effects on different cancer cells with unknown exclusive functional mechanism, indicating the new compound has distinguished MOA by interacting with some novel molecular targets. Deciphering the action mode of ipomoeassin F could probably open a new window for manipulating the uncurbable cancer growth.

The goal of this project is to illustrate the contribution of each group of ipomoeassin F to its potency, and to identify the corresponding target by using applicable probes, ultimately illuminate the MOA of ipomoeassin F. Based on our research, we hope to apply the available discovery to explore potential practical applications.

1.4. References

1. Siegel RL.; Miller KD.; Jemal A., Cancer statistics, 2019. *CA: A Cancer Journal for Clinicians* **2019**, *69*(1), 7-34.

2. Mahvi DA.; Liu R.; Grinstaff MW.; Colson YL.; Raut CP., Local Cancer Recurrence: The Realities, Challenges, and Opportunities for New Therapies. *CA: A Cancer Journal for Clinicians* **2018**, *68*(6), 488-505.

3. National Center for Health Statistics (US). Health, United States, 2016: With Chartbook on Long-Term Trends in *Health. Report No. 2017–1232*. Hyattsville, MD: National Center for Health Statistics; **2017**.

4. Breasted JH., The Edwin Smith Surgical Papyrus. *In Translation for The New York Historical Society*. Chicago, IL: University of Chicago Press, **1930**.

5. Surveillance, Epidemiology, and End Results (SEER) Program. *SEER*Stat Database: Incidence-SEER 18 Regs Research Data with Delay-Adjustment, Malignant Only, Nov. 2017 sub (2000–2015) <Katrina/Rita Population Adjustment>-Linked To County Attributes-Total US, 1969–2016 Counties*. Bethesda, MD: National Cancer Institute, Division of Cancer Control and Population Sciences, Surveillance Research Program, Surveillance Systems Branch; **2018**.

6. Coleman MP.; Quaresma M.; Berrino F.; Lutz JM.; De Angelis R.; Capocaccia R.; Baili P.; Rachet B.; Gatta G.; Hakulinen T.; Micheli A.; Sant M.; Weir HK.; Elwood JM.; Tsukuma H.; Koifman S.; E Silva GA.; Francisci S.; Santaquilani M.; Verdecchia A.; Storm HH.; Young JL., Cancer survival in five continents: a worldwide population-based study (CONCORD). *The Lancet Oncology* **2008**; *9*(8), 730–56.

7. Zurrida S.; Veronesi U., Milestones in breast cancer treatment. *The Breast Journal* **2015**; *21*(1), 3-12.

8. Perou CM.; Sorlie T.; Eisen MB.; van de Rijn M.; Jeffrey SS.; Rees CA.; Pollack JR.; Ross DT.; Johnsen H.; Akslen LA.; Fluge O.; Pergamenschikov A.; Williams C.; Zhu SX.; Lonning PE.; Borresendale AL.; Brown PO.; Botstein D., Molecular portraits of human breast tumors. *Nature* **2000**; *406*(6797), 747-752.

9. Liedtke C.; Mazouni C.; Hess KR.; André F.; Tordai A.; Mejia JA.; Symmans WF.; Gonzalez-Angulo AM.; Hennessy B.; Green M.; Cristofanilli M.; Hortobagyi GN.; Pusztai L., Response to neoadjuvant therapy and long-term survival in patients with triple-negative breast cancer. *Journal of Clinical Oncology* **2008**; *26*(8), 1275–1281.

10. Foulkes W.; Smith I.; Reis-Filho J., Triple-negative breast cancer. *The New England Journal of Medicine* **2010**; *363*(20), 1938-1948.

11. Cailleau R.; Olive M.; Cruciger QV., Long-term human breast carcinoma cell lines of metastatic origin: preliminary characterization. *In Vitro* **1978**; *14*(11), 911-915.

12. Soule HD.; Vazguez J.; Long A.; Albert S.; Brennan M., A human cell line from a pleural effusion derived from a breast carcinoma. *Journal of the National Cancer Institute* **1973**; *51*(5), 1409-1416.

13. Done SJ., Preface. *In Breast Cancer - Recent Advances in Biology, Imaging and Therapeutics*. Rijeka, InTech, p IX, **2011**.

14. Shirazi FH., Remarks in Successful Cellular Investigations for Fighting Breast Cancer Using Novel Synthetic Compounds. In: *Breast Cancer – Focusing Tumor Microenvironment, Stem Cells and Metastasis (Gunduz M, Gunduz E (eds.)*. Rijeka, InTech, pp. 85-102, **2011**.

15. Gest C.; Joimel U.; Huang L.; Pritchard LL.; Petit A.; Dulong C.; Buquet C.; Hu CQ.; Mirshahi P.; Lauren M.; Fauvel-Lafève F.; Cazin L.; Vannier JP.; Lu H.; Soria J.; Li H.; Varin R.; Soria C., Rac3 induces a molecular pathway triggering breast cancer cell aggressiveness: differences in MDA-MB-231 and MCF-7 breast cancer cell lines. *BMC Cancer* **2013**; *13*, 63.

16. Tait L.; Soule HD.; Russo J., Ultrastructural and immunocytochemical characterization of an immortalized human breast epithelial cell line, MCF-10. *Cancer Research*. **1990**; *50*(18), 6087-6094.

17. Newman, D. J.; Cragg, G. M., Natural Products as Sources of New Drugs from 1981 to 2014. *Journal of Natural Products* **2016,** *79* (3), 629-661.

18. Cragg, G. M.; Grothaus, P. G.; Newman, D. J., Impact of Natural Products on Developing New Anti-Cancer Agents. *Chemical Reviews* **2009,** *109* (7), 3012-3043.

19. Cragg, G. M.; Grothaus, P. G.; Newman, D. J., New Horizons for Old Drugs and Drug Leads. *Journal of Natural Products* **2014,** *77* (3), 703-723.

20. Govindarajan, M., Amphiphilic glycoconjugates as potential anti-cancer chemotherapeutics. *European Journal of Medicinal Chemistry* **2018,** *143*, 1208-1253.

21. Katz L.; Baltz RH., Natural product discovery: past, present, and future. *Journal of Industrial Microbiology & Biotechnology* **2016**; *43*(2-3), 155-176.

22. Feher M.; Schmidt J.M., Property distributions: differences between drugs, natural products, and molecules from combinatorial chemistry. *Journal for Chemical Information and Computer scientists* **2003**; *43*(1), 218-227.

23. Grabowski K.; Schneider G., Properties and architecture of drugs and natural products revisited. *Current Chemical Biology* 2007; *1*, 115-127.

24. Lam, K. S., New aspects of natural products in drug discovery. *Trends in Microbiology* **2007,** *15* (6), 279-289.

25. Langenheim JH., Plant Resins. *Chemistry, Evolution, Ecology, and Ethnobotany*. Timber Press, Portland, Oregon, p 418, **2003**.

26. Pereda-Miranda, R.; Rosas-Ramírez, D.; Castañeda-Gómez, J., Resin Glycosides from the Morning Glory Family. In *Fortschritte der Chemie organischer Naturstoffe / Progress in the Chemistry of Organic Natural Products, Vol. 92*, Kinghorn, A. D.; Falk, H.; Kobayashi, J., Eds. Springer Vienna: Vienna, **2010**; pp 77-153.

27. Pereda-Miranda, R.; Bah, M., Biodynamic constituents in the Mexican morning glories: Purgative remedies transcending boundaries. *Current Topics in Medicinal Chemistry* **2003,** *3* (2), 111-131.

28. Dembitsky V. M., Chemistry and biodiversity of the biologically active natural glycosides, *Chemistry & Biodiversity* **2004**; *1*(5), 673-781.

29. Fürstner A., Total syntheses and biological assessment of macrocyclic glycolipids. *European Journal of Organic Chemistry*. **2004**; *2004*(5), 943-958.

30. Furukawa J.; Sahairi N., Synthetic studies on resin glycosides. *Trends in Glycoscience and Glycotechnology* **2001**; *13*(69), 1-10.

31. Pereda-Miranda, R.; Fragoso-Serrano, M.; Escalante-Sanchez, E.; Hernandez-Carlos, B.; Linares, E.; Bye, R., Profiling of the resin glycoside content of Mexican jalap roots with purgative activity. *Journal of Natural Products* **2006,** *69* (10), 1460-1466.

32. La Ferla B.; Airoldi C.; Zona C.; Orsato A.; Cardona F.; Merlo S.; Sironi E.; D'Orazio G.; Nicotra F., Natural glycoconjugates with antitumor activity. *Natural Product Reports* 2011; *28* (3), 630-648.

33. Cao, S. G.; Guza, R. C.; Wisse, J. H.; Miller, J. S.; Evans, R.; Kingston, D. G. I., Ipomoeassins A-E, cytotoxic macrocyclic glycoresins from the leaves of Ipomoea squamosa from the Suriname rainforest. *Journal of Natural Products* **2005,** *68* (4), 487-492.

34. Kingston DG., A natural love of natural products. *The Journal of Organic Chemistry* **2008**; *73*(11):3975-3984.

35. Cao S.; Norris A.; Wisse JH.; Miller JS.; Evans R.; Kingston DG., Ipomoeassin F, a new cytotoxic macrocyclic glycoresin from the leaves of Ipomoea squamosa from the Suriname rainforest. *Natural Product Research* **2007**; *21*(10), 872-876.

36. Zong G.; Whisenhunt L.; Hu Z.; Shi WQ., Synergistic contribution of tiglate and cinnamate to cytotoxicity of Ipomoeassin F. *The Journal of Organic Chemistry* **2017**; *82*(9), 4977-4985.

37. Brown, D., Unfinished business: target-based drug discovery. *Drug Discovery today* **2007**; *12*(23-24), 1007–1012.

38. Pichler, C. M.; Krysiak, J.; Breinbauer, R., Target identification of covalently binding drugs by activity-based protein profiling (ABPP). *Bioorganic & Medicinal Chemistry* **2016**; *24*(15), 3291–3303.

39. Chen X.; Wong YK.; Wang J.; Zhang J.; Lee YM.; Shen HM.; Lin Q.; Hua ZC., Target identification with quantitative activity-based protein profiling (ABPP). *Proteomics* **2017**; *17*, 3-4.

40. Heydenreuter W.; Kunold E.; Sieber S. A., Alkynol natural products target ALDH2 in cancer cells by irreversible binding to the active site. *Chemical Communications* **2015**; *51*(87), 15784–15787.

41. Kreuzer, J.; Bach, N. C.; Forler, D.; Sieber, S. A., Target discovery of acivicin in cancer cells elucidates its mechanism of growth inhibition. *Chemical Science* **2015**; *6*(1), 237-245.

42. Rix U.; Superti-Furga G., Target profiling of small molecules by chemical proteomics. *Nature Chemical Biology* **2009**; 5(9), 616-624.

CHAPTER 2. SAR STUDY AND PROBE EXPLORATION

The structures for ipomoeassin family were uncovered by spectroscopic data and chemical degradation.[1] The ipomoeassins are composed of a (1→2)-β-disaccharide as a core structure, and hydroxylated fatty acid derivatives connecting disaccharide with different acylation patterns. The core structure consists of a D-Glc*p* and D-Fuc*p*-derivatives, while the peripherally connects with cinnamate (cinn, C-4-Glc*p*), tiglate (tig, C-3Glc*p*) and aglycone. Within aglycone of ipomoeassins, unlike for most resin glycosides, there is an oxygenation at C-*4* position,[2-3] a sterogeinc center at C-*11* position; and in some family members (ipomoeassin C-E), it contains a stereogenic center at C-*5* position.[2,4]

2.1. Structure-Activity Relationship study

For newly discovered compound, structure-relationship study (SAR) study is a classical yet most rewarding medicinal chemistry method to understand the information of the compound structure. With the help SAR study, potential pharmacophores would be well illuminated and assigned in drug development. As a flagship congener of a resin glycoside family, ipomoeassin F is an ideal candidate of systematic SAR study for developing novel anti-cancer drugs. This is not only due to the distinguished potency of ipomoeassin F against cancer cell lines, but also because of the limited understanding of exclusive MOA of this underexplored natural product. In the systematical SAR study, all ipomoeassin F and its analogues are synthesized in our total synthesize lab.

2.1.1. Structure-activity information from ipomoeassin family members

According to previous cytotoxicity data (Table 2.1), R^1 in 4'-O site of D-fucose and R^2 in C-5 site of the fatty acid tether play a pivot role from the pharmacophoric point of view. This

conclusion is well elucidated by comparing the potency of ipomoeassin D and F with the rest of the family members. Substitution on the two moieties could even lead to two orders of magnitude potency change against different cancer cell lines. The available information from previous cytotoxicity assay (Table 2.1) suggests that additional two methylene units in fatty acid of ipomoeassin F result in lipophilicity increase, contributing to the potency of this amphiphilic glycoconjugate.[5] The conclusion that overall lipophilicity is vital to potency of the ipomoeassins is further confirmed by comparing the IC_{50} value variation by the difference of OAc and OH in R^1(ipomoeassin D vs C), as well as in R^2 (ipomoeassin A vs B, ipomoeassin D vs E).

Table 2. 1. Structures and IC_{50} Values of Ipomoeassin A–F.[2,4]

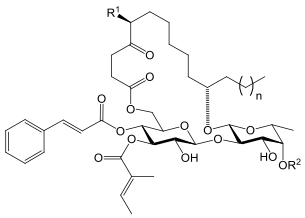

Ipomoeassin	Structure			IC_{50} (nM)						
	R^1	R^2	n	HeLa	L-929	A2780	U937	HT-29	MDA-MB-435	H522-T1
A	H	Ac	1	64	77.8	500	20.2	46.1	42.6	108.9
B	H	H	1	2500		400	134	396	2700	1070
C	OH	Ac	1	1500	> 1000	2900				
D	OAc	Ac	1	32	135	35	7.9	11.8	19.9	23.2
E	OAc	H	1	4300	> 1000	3300	163	393	1633	967
F	H	Ac	3		7.4	36	2.6	4.2	9.4	12.9

2.1.2 Structure-activity information from characteristic structure modification

Some ipomoeassin family members are found to have impressive toxicity against multiple cancer cell lines. Variation of peripheral oxygenation and acylation pattern in ipomoeassin structure may trigger significant cytotoxicity fluctuation toward cancer cell lines.[2] Ipomoeassins possesses two exclusive structure features differ from other glycosides: (1) the carbohydrate core structure is intensively connected to ester functionalities. (2) In the C-4 position of the fatty acid chain, there is a ketone group. To clarify the functionality of those unique properties, we designed and synthesized analogues **2.1**-**2.4** by removing those structure units one by one and then judging the functionality by evaluating their potency gain or loss.

A.

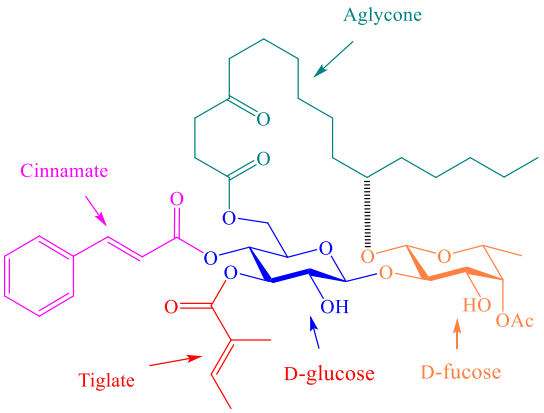

B.

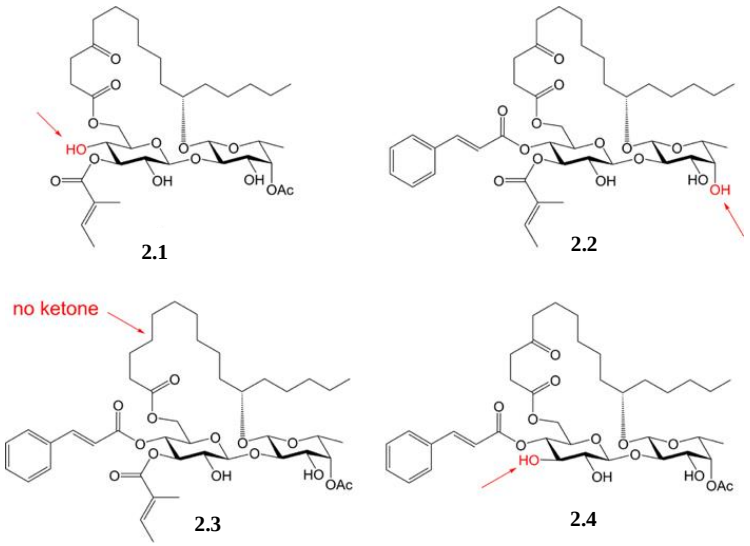

Figure 2. 1. Structures of ipomoeassin F and its analogues **2.1**-**2.4**. (A) Structure of ipomoeassin F; (B) Structure of **2.1**-**2.4**.

In the study of ipomoeassin family, the Fürstner group found that simultaneous migration of tiglate and cinnamate damage the bioactivity.[5] The importance of these two moieties was further confirmed by our research data (Table 2.2).[6] As we remove cinnamate (**2.1**) or tiglate (**2.4**), the analogue potency dropped significantly (more than 1,000-fold change in MDA-MB-231).

Fürstner and his colleagues also reported that removal of the C-4 ketone in the fatty acid chain impaired the potency.[5] However, when we removed the carbonyl group in the hydrophilic tether, analogue **2.3** almost retained its potency with a maximum 3-fold potency loss. Compared to analogue **2.3**, analogue **2.2** suffered relative more bioactivity loss when losing acetate group, further verifying the hypothesis that increasing lipophilicity could enhance the bioactivity of ipomoeassins. But the impact was limited at around 20-fold change, and the cytotoxicity of analogue **2.2** against MCF-7 was almost retained (dropped 2-fold). All the information above suggests the significance of influence on ipomoeassins potency in the order of cinnamoyl> tigloyl>>acetyl>ketone.

Table 2. 2. Cytotoxicity (IC_{50}, nM) of Ipomoeassin F and Its analogues **2.1**-**2.4**[a]

	MDA-MB-231	MCF7	MCF-10A
Ipomoeassin F	6.3	36.4	5.3
2.1	7129.2	9090.0	ND[b]
2.2	131.0	86.7	297
2.3	16.1	33.0	30.7
2.4	6848.0	5929.0	ND

[a] The data were obtained from at least two independent experiments, and the standard errors are within 20%; [b] ND = not determined.

2.1.3. Structure-activity information from cinnamate and tiglate modification

Since both cinnamate and tiglate are confirmed to be the most important moieties that contribute to ipomoeassins, we executed deep exploration within those two structure elements. Both of the two moieties contain an α,β-unsaturated double bond, so we concluded that the common structure double bond might contribute to the high cytotoxicity. Phenyl group, as a structural constitution element in cinnamate, may also have something to do with its functionality.

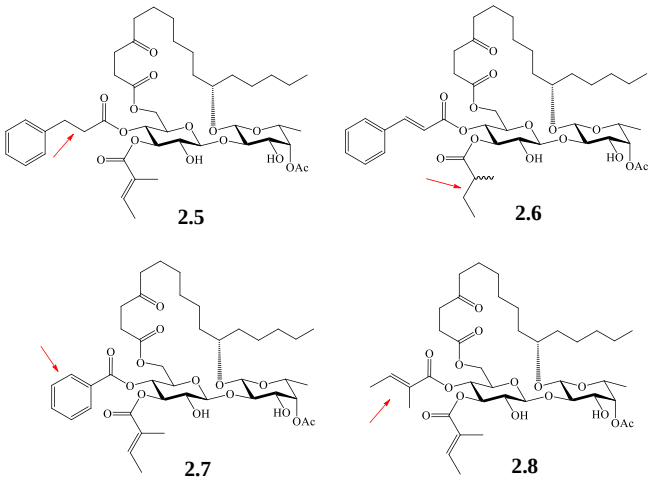

Figure 2. 2. Structure of ipomoeassin F analogues **2.5**-**2.8**.

To verify these hypotheses, we designed and synthesized analogue **2.5** with cinnamate double bond reduced, **2.6** with tiglate double bond reduced, **2.7** with the cinnamate double bond missing and **2.8** with the phenyl group missing (Figure 2.2). The bioactivity change was evaluated by comparing IC_{50} value against breast cancer cell line MDA-MB-231 and MCF-7 respectively.

Table 2. 3. Cytotoxicity (IC_{50}, nM) of Ipomoeassin F and Its analogues **2.5**-**2.8**[a]

	MDA-MB-231	MCF7	MCF-10A
Ipomoeassin F	6.3	36.4	5.3
2.5	980	2560	ND[b]
2.6	429	477	ND
2.7	930	2890	ND
2.8	4500	3930	ND

[a] The data were obtained from at least two independent experiments, and the standard errors are within 20%; [b] ND = not determined.

Through cytotoxicity screening, the importance of double bond in cinnamate and tiglate is uncovered (Table 2.3). As expected, removing any of the double bonds in cinnamate or tiglate result in significant potency loss. But the cytotoxicity loss of reducing or removing cinnamate (dropped 150-fold in **2.5** and **2.7**) is more obvious than that of tiglate (dropped 66-fold in **2.6**),

indicating the cinnamate double bond may play more important role than tiglate double bond in cytotoxicity. When we removed the phenyl group by substituting cinnamate with tiglate, the analogue **2.8** suffered dramatically potency loss (dropped almost 700-fold), suggesting the pivot role of aromatic group in biological activities.

Since cinnamate was shown to be more important than tiglate and both of these two α,β-unsaturated esters were critical to retain ipomoeassin F potency, we were interested to know whether substituting tiglate with cinnamate could increase or maintain the cytotoxicity and whether those two moieties were interchangeable. To answer these follow-up questions, we designed another two analogues **2.9** and **2.10** (Figure 2.3).

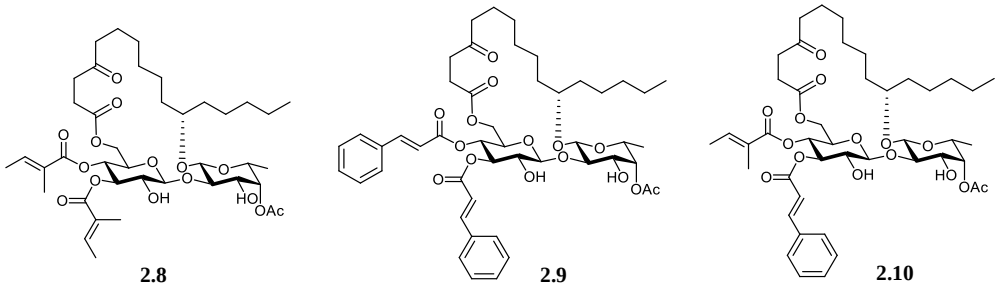

Figure 2. 3. Structure of ipomoeassin F analogues **2.8**-**2.10**.

A.

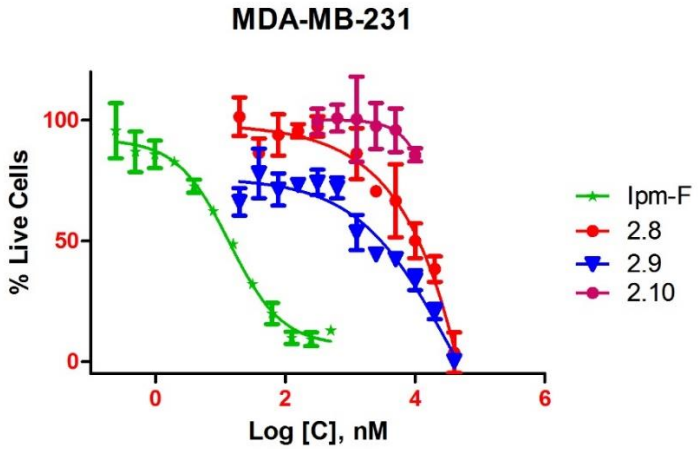

B.

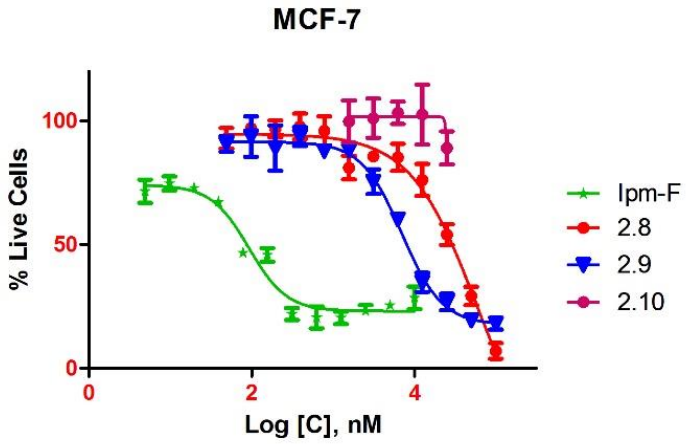

Figure 2. 4. Viability curves of ipomoeassin F and analogues **2.8**, **2.9**, **2.10** in breast cancer cell lines: (A) Cytotoxicity in MDA-MB-231 cell line; (B) Cytotoxicity in MCF-7 cell line. (72h incubation)

Cytotoxicity evaluation[7] indicates any of the changes on these two groups leads to significant potency loss (Figure 2.4). The cytotoxicity data further confirmed the irreplaceable role of cinnamate and tiglate, and also suggested the optimal combination for ipomoeassin F to perform its biological activity to be the aromatic α,β-unsaturated ester at C-4-Glc*p* and an aliphatic α,β-unsaturated ester at C-3-Glc*p*.

2.1.4. Structure-activity information from hydrophilic moieties modification

Ipomoeassin F is an amphiphilic glycoconjugate with only two hydrophilic hydroxyl groups at 3-OH-Fuc*p* and 2-OH-Glc*p*. To better understand the function of the two groups in the molecular, we designed analogue **2.11** and **2.12** by introducing acetylation to the corresponding site and then evaluate the cytotoxicity on breast cell lines (Figure 2.5).

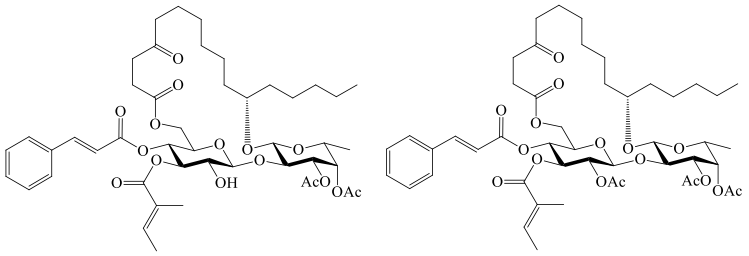

2.11 **2.12**

Figure 2. 5. Structures of ipomoeassin F analogues **2.11**-**2.12.**

The cytotoxicity data indicates that amphiphilic character is a one of the important factors that retain the molecular biologic activity (Table 2.4). The two hydrophilic sites may serve as an exit tunnel to the aqueous environment and maintain the conformational stability. With a hydrophilic hydroxyl group left at 2-OH-Glc*p*, analogue **2.11** still exhibit strong potency even its potency decreases compared with ipomoeassin F. But analogue **2.12** on the other hand, totally lost its biological activity, which may be caused by poor aqueous solubility due to lack of hydrophilic group.

Table 2. 4. Cytotoxicity (IC_{50}, nM) of Ipomoeassin F and Its analogues **2.11**-**2.12**[a]

	MDA-MB-231	MCF7	MCF-10A
Ipomoeassin F	6.3	36.4	5.3
2.11	16.5	216	24.0
2.12	>10,000	>10,000	ND[b]

[a] The data were obtained from at least two independent experiments with the same condition, and the standard errors are within 20%; [b] ND = not determined.

2.1.5. Structure-activity information from aglycone modification

2.1.5.1. Impact of stereogenic center C-11 on ipomoeassin F bioactivity.

Within aglycone of ipomoeassin F, there is a unique stereogenic center at C-*11* position. We hypothesized the exclusive structure may have a close relationship with molecular cytotoxicity,

switching C-*11S* of ipomoeassin F into C-*11R* could inevitably impair its biological activity. To verify the hypothesis, we synthesized epimer analogue **2.13** and test its cytotoxicity against breast cancer cell lines (Figure 2.6).

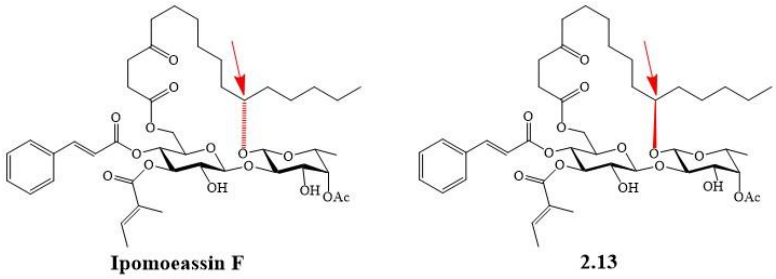

Figure 2. 6. Structures of ipomoeassin F and its C-*11R* epimer **2.13.**

As expected, the cytotoxicity result perfectly supported the hypothesis.[8] Cytotoxicity of constructed C-*11R* epimer leads to a 38-fold potency loss in MDA-MB-231 cytotoxicity assay compared with C-*11S* configuration of ipomoeassin F, giving the conclusion that C-*11S* is a favorable configuration for the impressive cytotoxicity.

Table 2. 5. Cytotoxicity (IC_{50}, nM) of Ipomoeassin F and Its epimer **2.13**[a]

	MDA-MB-231	MCF7	MCF-10A
Ipomoeassin F	6.3	36.4	5.3
2.13	240.2	830.7	159.2

[a] The data were obtained from at least two independent experiments, and the standard errors are within 20%.

2.1.5.2. Impact of open-chain aglycone on ipomoeassin F bioactivity.

Other than chiral center, cyclic structure framework is another key character of ipomoeassin F. In literature, people believe cyclic structure framework is critical in retaining macrocycle biological activities.[9-10] In order to clarify whether this hypothesis is applicable to the macrocyclic

skeleton of ipomoeassin F, we designed an open-chain analogue **2.14** and its terminal reduced analogue **2.15** to expel the disturbance introduced by terminal double bond (Figure 2.7).

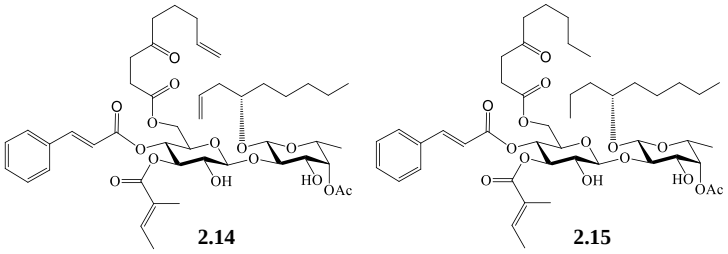

Figure 2. 7. Structures of ipomoeassin F analogues **2.14** and **2.15**.

However, the cytotoxicity result doesn't quite follow the hypothesis. Open chain analogue **2.14** retained good potency even though experience some limited cytotoxicity loss (Table 2.6). While reducing the double bond, the analogue **2.15** recovered the cytotoxicity obviously, leaving the impression that integrity of macrocyclic structure is not the key requirement for maintaining high biological activity in ipomoeassin F.

Table 2. 6. Cytotoxicity (IC_{50}, nM) of Ipomoeassin F and Its analogues **2.14**-**2.15**[a]

	MDA-MB-231	MCF7	MCF-10A
Ipomoeassin F	6.3	36.4	5.3
2.14	59.1	124	151
2.15	18.8	78.2	11.8

[a] The data were obtained from at least two independent experiments, and the standard errors are within 20%.

Cytotoxicity data conveyed another interesting piece of information that interruption of the ring structure of ipomoeassin F evidently improve its selectivity. Before opening the cyclic structure, the selectivity index（IC_{50} values in MCF-10A / IC_{50} in MDA-MB-231) is 0.84. But when the ring structure is opened, this index increases dramatically to 2.55. However, as double

bond in open chain reduced, the index drops back to 0.63. The variation of selectivity index suggests double bond in open chain terminal increase the selectivity of this macrocyclic glycoside, providing valuable information for future anti-cancer drug development.

2.1.5.3. Impact of cyclic structure size on ipomoeassin F bioactivity.

Although the cytotoxicity data of open chain analogues is not aligned with literature, the import role of cyclic structure in ipmoeassin F biological activity is not ignorable. Even so, the influence of cyclic structure size to ipomoeassin F potency is not fully understood. So, we try to change the ring size by adding (**2.16**) or chopping (**2.17**) one or two members to the skeleton and explore the impact on its cytotoxicity.

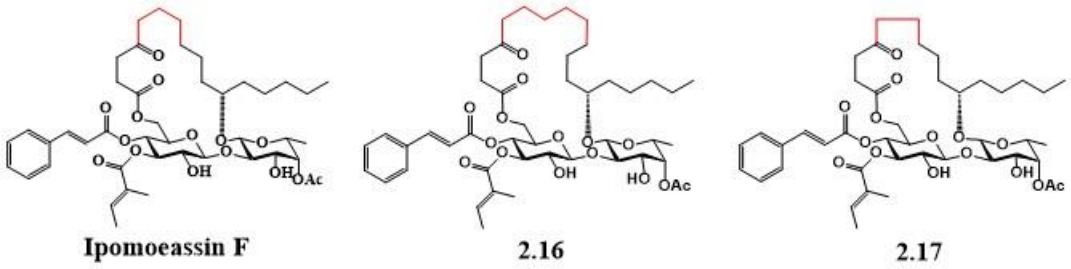

Figure 2. 8. Structures of ipomoeassin F and its analogues **2.16** and **2.17.**

Since cyclic structure is one of the exclusive characters, the modification on the size lead to evident cytotoxicity difference (Table 2.7). Interestingly, as aglycon ring size becomes larger, molecular potency increases 4-fold. On the other hand, decreasing the ring size gives rise to even 10-fold potency loss. A possible explanation for the bioactivity change is that as the size of aglycon increase, the molecular becomes easier to be incarcerated after binding to the target protein functional pocket, facilitating compound-target protein interaction. The result not only firmly supports the critical role of cyclic structure framework in maintaining biological activities, but also

provides solid evidence for the conclusion that overall lipophilicity is vital to maintain potency of ipomoeassin F.

Table 2. 7. Cytotoxicity (IC_{50}, nM) of Ipomoeassin F and Its analogues **2.16**-**2.17**[a]

	MDA-MB-231	MCF7	MCF-10A
Ipomoeassin F	6.3	36.4	5.3
2.16	1.3	9.1	0.6
2.17	67.8	291.6	98.6

[a] The data were obtained from at least two independent experiments, and the standard errors are within 20%.

2.1.6. Structure-activity information from fucose modification

D-Glc*p* and D-Fuc*p* connecting with functional groups constitute the core structure of ipomoeassin F. According to the structure-activity relationship discussed above, certain modifications around D-Fuc*p* didn't significantly diminish the molecular cytotoxicity. To further explore the biological contribution of D-Fuc*p*, we plan to truncate the whole fucose and design monosaccharide analogues **2.18** and **2.19** (Figure 2.9).

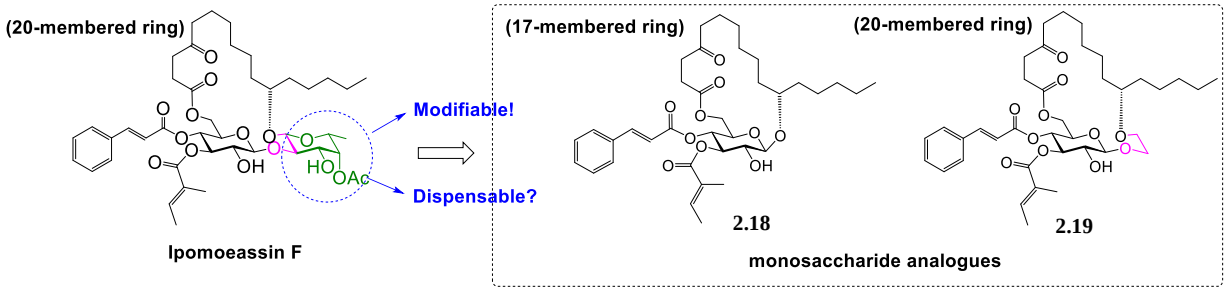

Figure 2. 9. Structures of ipomoeassin F analogues **2.18** and **2.19**.

The biological activity of analogues was evaluated against two breast cancer cell lines MDA-MB-231 and MCF-7.[11] Compared with ipmoeassin F, the two monosaccharides almost lost any inhibition of cell proliferation (Figure 2.10). Without doubt, D-Fuc*p* is indispensable in the

bioactivities of impomoeassin F. Accompanied with the information that modification of peripheral groups could cause very limited potency loss, it is not hard to come to the conclusion that the existence of D-Fuc*p* provides stability to maintain the appropriate confirmation of ipomoeassin F structure, so it can work properly with the target protein.

A. B.

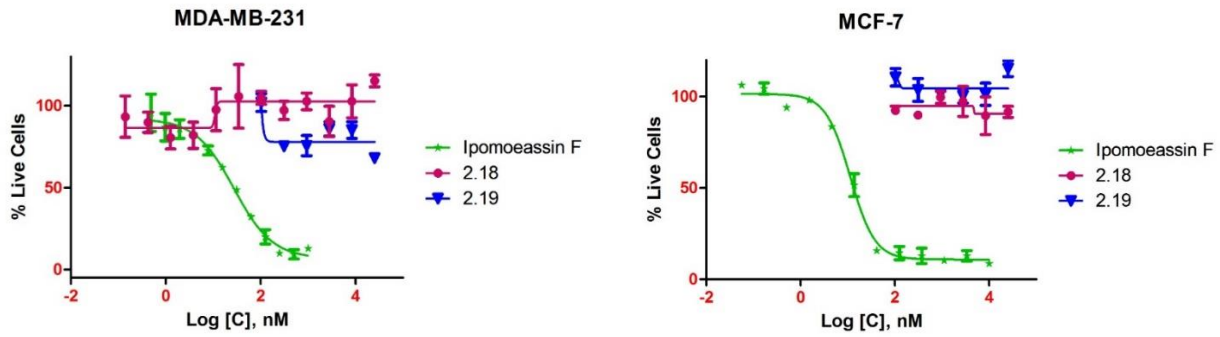

Figure 2. 10. Viability curves of ipomoeassin F and analogues **2.18** and **2.19** in breast cancer cell lines: (A) Cytotoxicity in MDA-MB-231 cell line; (B) Cytotoxicity in MCF-7 cell line. (72h incubation)

2.1.7. Summary of structure-activity relationship study

In conclusion, by deliberate design, synthesis and cytotoxicity screening, we built up a systematic analogue library of ipomoeassin F. With the help of complicated structure modification *vs* cytotoxicity variation, the importance of each moiety was illuminated. The influence significance of different groups can be summarized at the rank of D-Fuc*p* >cinnamate >tiglate >alkene in cinnamate > alkene in tiglate > acetate > 3-OH-Fuc*p* >cyclic skeleton ≈ ketone (Figure 2.11).

As an amphiphilic glycoconjugate, both hydrophobic groups and hydrophilic groups are indispensable for ipomoeassin F to perform its cytotoxicity. Hydrophilic groups, work as a vessel, help the overall molecule stay soluble in an aqueous environment so that it could be transported

into the cell. Hydrophobic groups, work as anchors and functionality portions, facilitate ipomoeassin F anchoring inside hydrophobic binding pocket and interact with target protein in the hydrophobic environment. Therefore, increasing hydrophobicity appropriately would favor its interaction with target protein. However, introduction of hydrophobicity by blocking hydrophilic moieties will inevitably damage the potency due to the significant aqueous solubility loss.

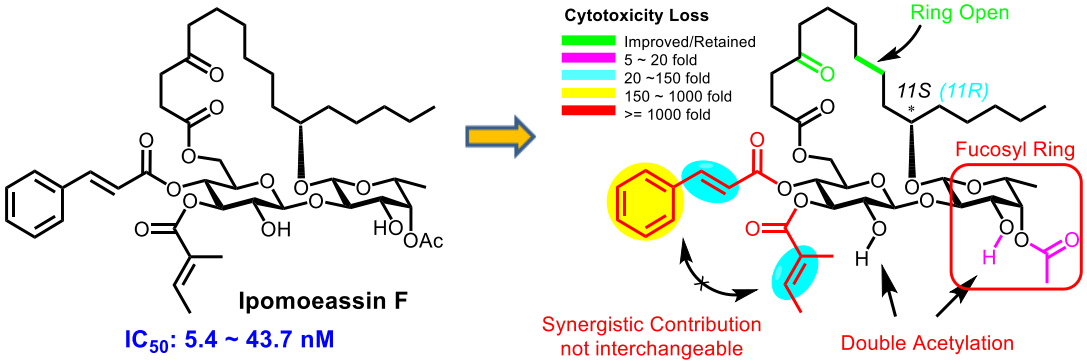

Figure2. 11. Cytotoxicity loss by pharmacophore editing.

All characteristic structures work together to maintain the distinguish potency of ipomoeassin F. Chiral center C-*11R* keeps ipomoeassin F function at an optimal configuration; ring structure aglycon helps the molecular stay firmly inside binding pocket facilitating further interaction with protein domains. Opening the cyclic structure retains cytotoxicity probably by limited conformational disturbance, and the modification evidently uncovered selectivity increase, providing a new approach for clinical drug development. The dramatical cytotoxicity disturbance along with modification of two α,β-unsaturated esters cinnamate and tiglate suggests that they may play important role in interacting with the target protein by covalent binding or strong non-valent interaction, directing a promising way for further MOA study and target protein identification.

2.2. Probe Design and Selection

Chemical probe is a series of modified molecular maintain original drug structural and bio-active similarity but has certain key chemical and structural differences.[12] The introduced key functional groups are essential to illustrate the unknown compound-cell/bio-molecular interaction and support unbiased interpretation of biological experiments. Developing appropriate chemical probe tool kit more than once has been documented to be beneficial towards action mode exploration and drug development.

Scientists at Pfizer Inc recently published the four pillars philosophy (Figure 2.12) in directing successful drug development program by retrospective analyzing 44 drug programs and 2 clinical trials.[13] Pillar 1 involves the efficacy exposure of probes at the expected site of action. The first pillar confirms cellular permeability of the probes by evaluating the pharmacologically relevant concentrations at the target site, therefore rule out the possibility that the response is due to unspecific binding. The pillar 2 proves target engagement and is the most challenging validation. But appropriate strategy approach such as activity-based proteomics profiling, fluorophore introduction would facilitate target identification and validation. Pillar 3 and pillar 4 further confirm the pharmacokinetic and pharmacodynamic properties of a drug to be developed and phenotype disturbance after probe application. Probes with poor access to the site of action would lead to the lack of pharmacological (pillar 3) or phenotypic (pillar 4) response, resulting in false negative result. According to their analysis, failed projects often are not able to fulfill some or all the four pillars.

With the employment of cytotoxicity screening, the different moiety properties of ipomoeassin F is well established. According to information collected from SAR study, most vital factors for maintaining ipomoeassin F cytotoxicity are position of cinnamate and tiglate, existence

of the two α,β-unsaturated double bond, existence of aromatic ring structure in cinnamate and the complete D-Fuc*p* structure. In order to avoid disturbing molecular potency at minimum extent, we design our probe by introducing functional groups at para position of the aromatic ring structure to push introduced moieties away from core structure as far as possible.

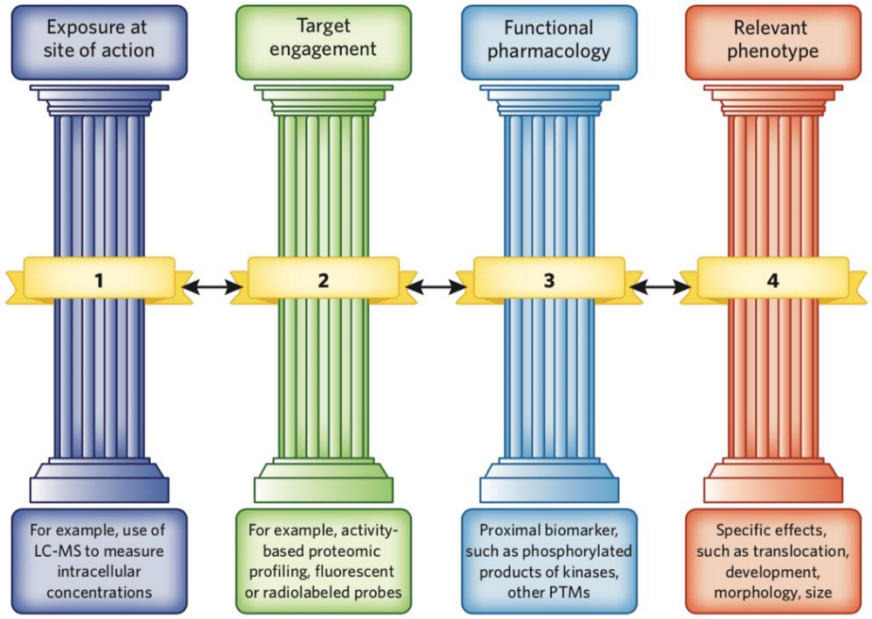

Figure 2. 12. The four pillars of cell-based target validation using chemical probes.[13]

2.2.1. Probes for stepwise target protein identification

Active-based protein profiling (ABPP) is a typical approach to identify target protein. Probes for ABPP typically consist of an active site, a linker and a traceable tag. These three constituents greatly facilitate the target identification efficacy, however, too many structures in the probe on the other hand causes steric hinderance between probe and the target protein, influencing the chance of successfully binding to expected targeting site.

To overcome this disadvantage, stepwise click chemistry is employed for target identification. In our project, we designed probe **2.20** by introducing alkyne into para position of benzene ring. According to our SAR study, α,β-unsaturated double bond is one of the most critical structure that

help maintain molecular cytotoxicity. As a result, a new analogue **2.21** with all double bonds reduced would be expected to be inactive, so that it can be used as an ideal negative control.

As expected, slight modifications on aromatic ring did not disturb the biological activity too much (Figure 2.13B), indicating the change have little impact on MOA of ipomoeassin F.

A.

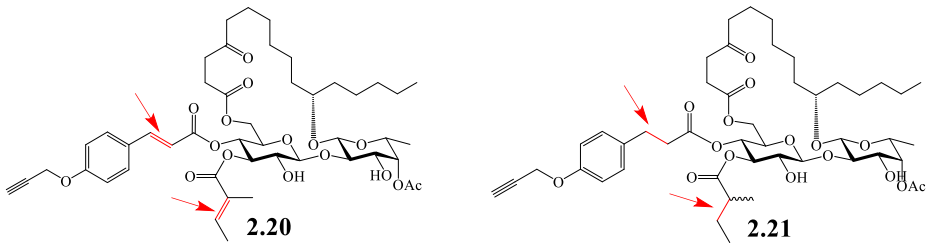

B.

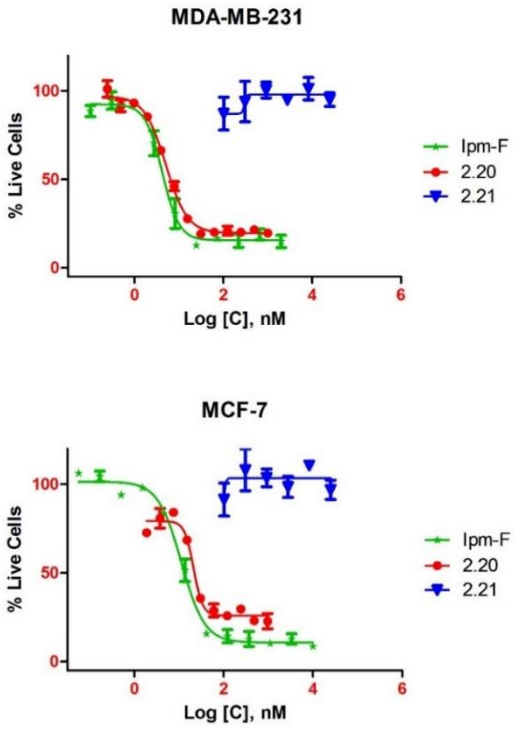

Figure 2. 13. Structure and cytotoxicity of ipomoeassin F analogues 2.20 and 2.21. (A) Structure of 2.20 and 2.21. (B). Viability curve of **2.20**, **2.21** and ipomoeassin F in MDA-MB-231 and MCF-7 (72h incubation).

It is a high probability that **2.20** could bind the same target, hence introduction of traceable tags like fluorophore or biotin by click chemistry reaction following **2.20** specifically binding the target protein may provide great chance to capture and trace the target protein (Figure 2.14). Being an inactive analogue, **2.21** is a perfect corresponding side by side negative control of any probe that labels target protein for identification by introducing function groups into **2.21**.

A.

B.

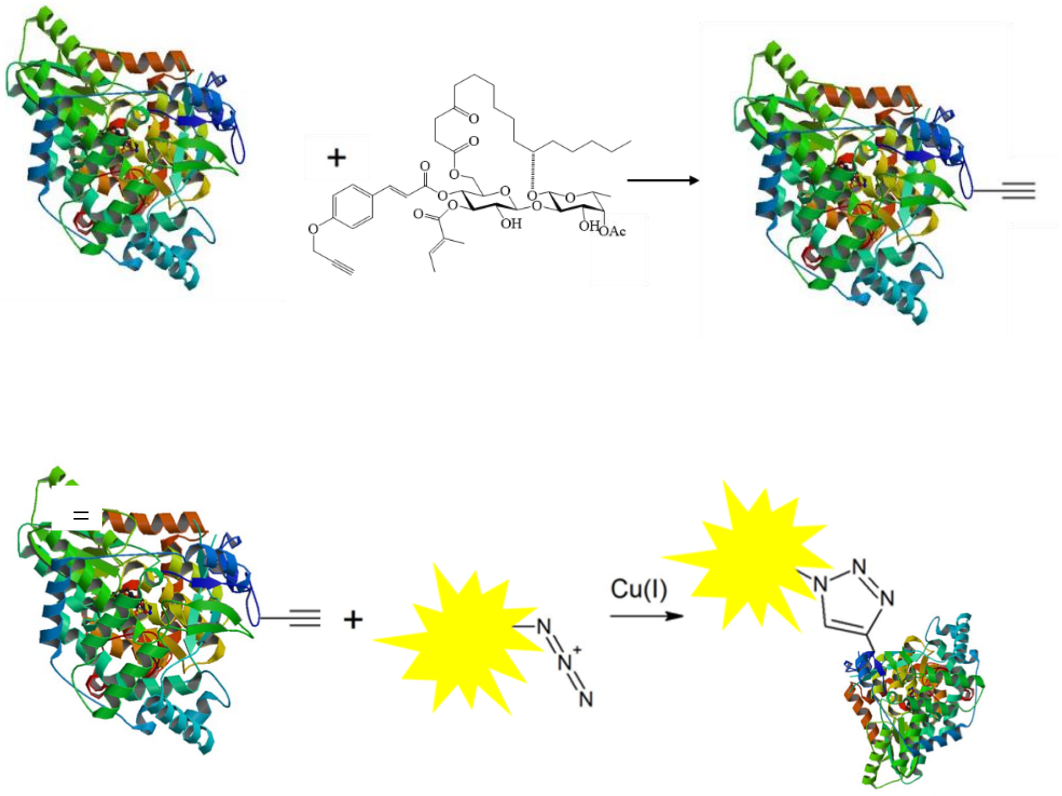

Figure 2. 14. Diagram of stepwise target protein identification. (A) Target protein labelling; (B) Introduction of traceable moieties for protein isolation and identification.

2.2.2. Probes for ABPP by fluorophore reporter

Fluorophore is commonly used strategies for tracking biological action mode not only in subcellular level but also in molecular level studies due to its high sensitivity. To make good use of the great advantage, we designed fluorescent probes **2.22 - 2.28** (Figure 2.15).

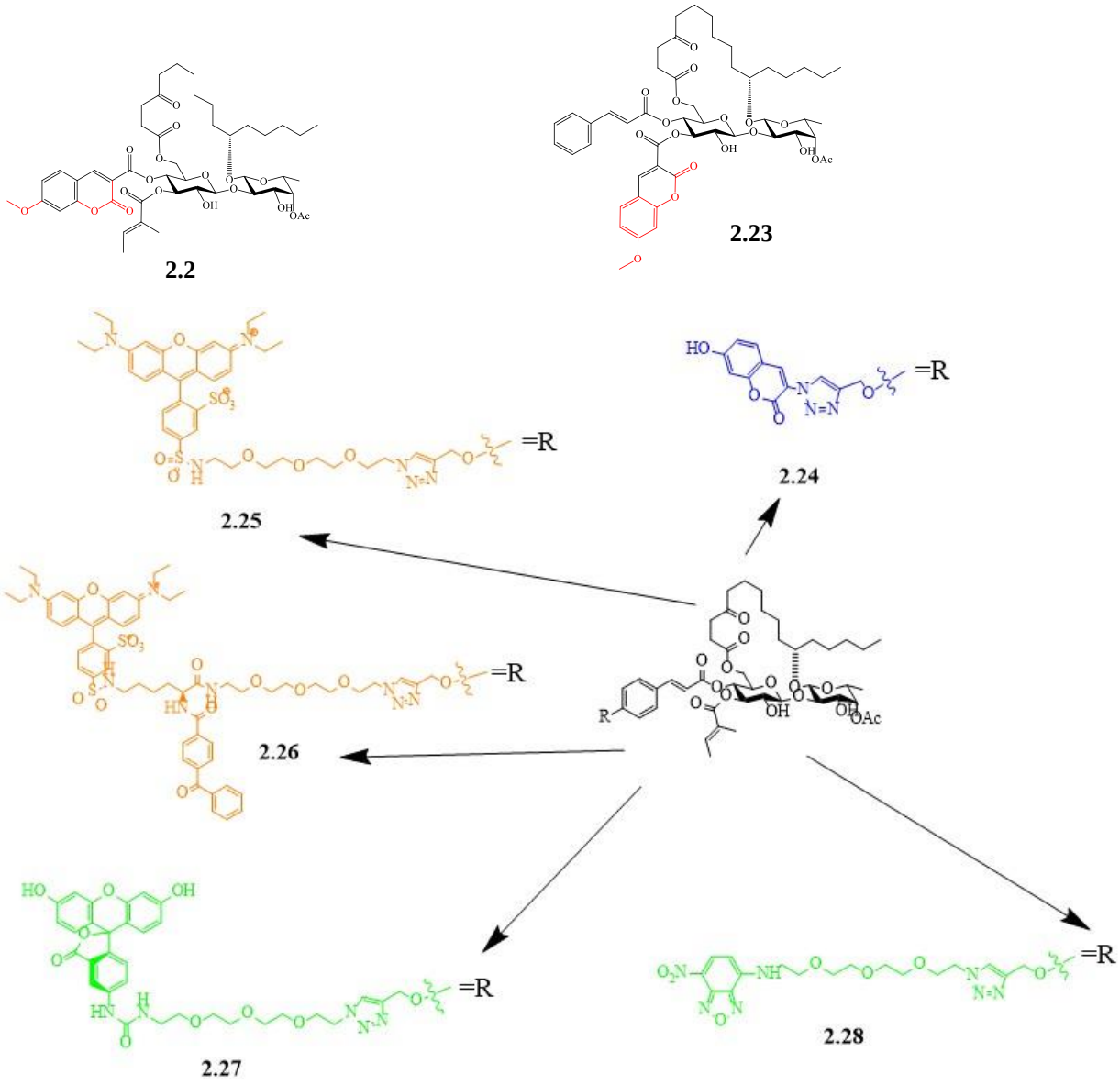

Figure 2. 15. Structure of ipomoeassin F analogues **2.22-2.28**.

Based on cytotoxicity screening in breast cancer line MDA-MB-231 and MCF-7, analogue **2.22**, **2.23**, **2.26, 2.27** were expelled due to significant potency loss (Table 2.8). Both coumarin-coupled probe **2.24** and NBD-coupled probe **2.28** retained substantial cytotoxicity with **2.28** being even more potent than ipomoeassin F. Unfortunately, **2.28** underwent photobleaching very easily and could not be used for imaging studies. In contrast, **2.24** gave a rather weak fluorescent signal,

presumably due to an internal photo-induced electron transfer effect combined with its shorter excitation maximum (365 nm). Fluorescent signal from probe **2.25** was strong and stable in different situation, and therefore was selected for further cell imagine studies.

Table 2. 8. Cytotoxicity (IC_{50}, nM) of Ipomoeassin F and its Probes **2.22**-**2.28**[a]

	MDA-MB-231	MCF7	MCF-10A
Ipomoeassin F	6.3	36.4	5.3
2.22	5,500.3	5,825.1	ND[b]
2.23	8,547.6	10,565	ND
2.24	8.9	172.2	11.3
2.25	253.4	172.2	133.8
2.26	7,225.5	>25,000	ND
2.27	1,270.6	>25,000	ND
2.28	2.8	21.1	2.0

[a] The data were obtained from at least two independent experiments, and the standard errors are within 20%; [b] ND = not determined.

2.2.3. Probes for ABPP by affinity tag reporter

Biotin affinity pull down experiment is a widely used approach for target protein purification and identification. The strategy is based on strong non-covalent binding between biotin and streptavidin, specifically reserving target protein that forms complex with biotin containing probes. Since high specificity is a great advantage of biotin affinity target protein identification, we designed probes **2.29** - **2.33** (Figure 2.16). **2.29** is expected to be an active probe with short linker, its reduced form **2.30** is expected to be corresponding negative control.

Accordingly, probe **2.31** and probe **2.33** are designed to be active probes with long linkers. In order to better exclude noise signal from non-specific binding protein, we introduced a photocleavage moiety into the linker. Probe **2.32**, a reduced form of **2.33,** was designed to be the corresponding negative control.

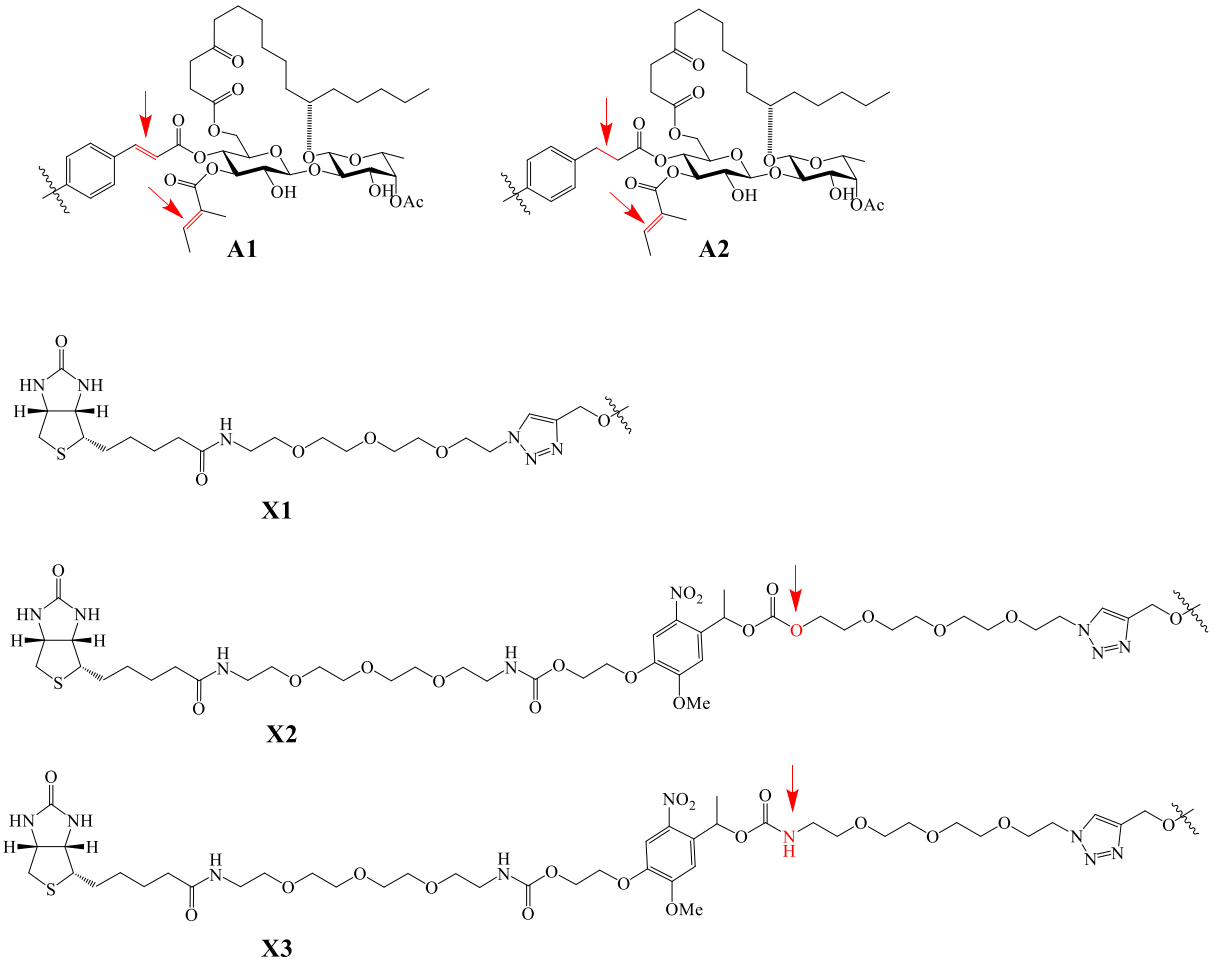

Figure2. 16. Structures of ipomoeassin F analogues **2.29 - 2.33**.

As expected, active analogues **2.29**, **2.31** and **2.33** keep the cytotoxicity loss within 5-fold (Table 2.9). Among these potential applicable probes, **2.31** almost withholds disturbance of structure modification, suggesting the high probability that it shares identical target protein as ipomoeassin F. Probes **2.30** and **2.32** were proved to be perfect negative controls that have no biological activity against test cells.

Table 2. 9. Cytotoxicity (IC_{50}, nM) of Ipomoeassin F and its Probes **2.29**-**2.33**[a]

	MDA-MB-231	MCF7	MCF-10A
Ipomoeassin F	6.3	36.4	5.3
2.29	29.5	187.4	21.7
2.30	>25,000	>25,000	ND[b]
2.31	7.0	19.8	5.1
2.32	>25,000	25,000	ND
2.33	24.1	225.3	21.9

[a] The data were obtained from at least two independent experiments, and the standard errors are within 20%; [b] ND = not determined.

2.2.4. Summary of Probes design and selection.

Active based protein profiling (ABPP) is a widely accepted as an efficiency strategy for target protein identification. According to our systematic SAR study of ipomoeassin F, we designed and tested probe **2.20** and its corresponding negative control **2.21** for stepwise ABPP. We designed a couple of fluorescent probes and picked up **2.25** for future study because of its acceptable potency, strong fluorescent intensity and fluorophore stability. We also designed biotin probes and verified their applicability from their cytotoxicity. **2.29** and **2.30** are selected to be short linker pairs for affinity purification; **2.31** is selected to be an ideal candidate for MOA study; **2.32** and **2.33** are selected to be long linker pairs for affinity purification.

2.3. References

1. Pereda-Miranda, R.; Rosas-Ramirez, D.; Castaneda-Gomez, J., Resin glycosides from the morning glory family. *Progress in the Chemistry of Organic Natural Products* **2010,** *92*, 77-153.

2. Cao, S. G.; Guza, R. C.; Wisse, J. H.; Miller, J. S.; Evans, R.; Kingston, D. G. I., Ipomoeassins A-E, cytotoxic macrocyclic glycoresins from the leaves of Ipomoea squamosa from the Suriname rainforest. *Journal of Natural Products* **2005,** *68* (4), 487-492.

3. Ono, M., Resin glycosides from Convolvulaceae plants. *Journal of Natural Medicines* **2017,** *71* (4), 591-604.

4. Cao S.; Norris A.; Wisse JH.; Miller JS.; Evans R.; Kingston DGI., Ipomoeassin F, a New Cytotoxic Macrocyclic Glycoresin from the Leaves of Ipomoea squamosa from the Suriname Rainforest. *Natural Product Research* **2007**, *21*(10), 872-876.

5. Nagano T.; Pospísil J.; Chollet G.; Schulthoff S.; Hickmann V.; Moulin E.; Herrmann J.; Müller R.; Fürstner A., Total synthesis and biological evaluation of the cytotoxic resin glycosides ipomoeassin A-F and analogues. *Chemistry* **2009**, *15*(38), 9697-9706.

6. Zong G.; Aljewari H.; Hu Z.; Shi WQ., Revealing the pharmacophore of ipomoeassin F through molecular editing. *Organic Letters* **2016**, *18*(7), 1674-1677.

7. Zong G,.; Whisenhunt L.; Hu Z,.; Shi WQ., Synergistic contribution of tiglate and cinnamate to cytotoxicity of Ipomoeassin F. *The Journal of Organic Chemistry* **2017**, *82*(9), 4977-4985.

8. Zong G.; Barber E.; Aljewari H.; Zhou J.; Hu Z.; Du Y.; Shi WQ., Total Synthesis and Biological Evaluation of Ipomoeassin F and Its Unnatural 11R-Epimer. *The Journal of Organic Chemistry* **2015**, *80*(18), 9279-9291.

9. Driggers, E. M.; Hale, S. P.; Lee, J.; Terrett, N. K. The exploration of macrocycles for drug discovery-an underexploited structural class. *Nature Reviews Drug Discovery* **2008**, *7*(7), 608-624.

10. Marsault, E.; Peterson, M. L., Macrocycles are great cycles: applications, opportunities, and challenges of synthetic macrocycles in drug discovery. *Journal of Medicinal Chemistry* **2011**, 54(7), 1961-2004.

11. Zong G.; Hirsch M.; Mondrik C.; Hu Z.; Shi WQ., Design, synthesis and biological evaluation of fucose-truncated monosaccharide analogues of ipomoeassin F. *Bioorganic & Medicinal Chemistry Letters* **2017**, *27*(12), 2752-2756.

12. Schenone, M.; Dancik, V.; Wagner, B. K.; Clemons, P. A., Target identification and mechanism of action in chemical biology and drug discovery. *Nature Chemical Biology* **2013,** *9* (4), 232-240.

13. Bunnage, M. E.; Chekler, E. L. P.; Jones, L. H., Target validation using chemical probes. *Nature Chemical Biology* **2013,** *9* (4), 195-199.

CHAPTER 3. IPMOEASSIN F TARGET PROTEIN IDENTIFICATION AND VALIDATION

3.1. Abstract

Ipomoeassin F is a potent natural cytotoxin that inhibits growth of many tumor cell lines with single-digit nanomolar potency by an undefined mechanism. However, its biological and pharmacological properties have remained largely unexplored. Building upon our earlier achievements in total synthesis and medicinal chemistry, we used chemical proteomics to identify Sec61α (protein transport protein Sec61 subunit alpha isoform 1), the pore-forming subunit of the Sec61 protein translocon, as a direct binding partner of ipomoeassin F in living cells. The interaction is specific and strong enough to survive lysis conditions, enabling ipomoeassin F to pull down Sec61α from live cells, yet it is also reversible as judged by fluorescent streptavidin staining and reverse competition. Sec61α provides the central subunit of the ER protein translocation complex, and the binding of ipomoeassin F results in cell proliferation inhibition. Therefore, ipomoeassin F represents the first plant-derived, carbohydrate-based member of a novel structural class that offers new opportunities to explore Sec61α function and to further explore its potential as a therapeutic target for drug discovery.

3.2. Introduction

Historically, natural products have significantly contributed to the development of drugs for human disorders,[1] most notably as anticancer chemotherapeutics.[2] Structurally and functionally unique natural products also provide a spectrum of valuable chemical tools for examining biological systems in translational biomedical research.[3,4] To continue our battle against various unsolved problems of human health, including those arising from drug resistance, it is crucial to

systematically investigate underexplored areas of existing chemical space such as those offered by bioactive natural products with unique structures and/or mechanisms.[5]

Resin glycosides, also called glycoresins, are a large collection of amphiphilic glycolipids isolated from the morning glory family of plants,[6] and these compounds are considered active ingredients of many morning glory-based traditional medicines that are used worldwide. Resin glycosides consist of a differently-acylated oligosaccharide glycosylated with a mono- or dihydroxy C14 or C16 fatty acid, with more than 300 family members discovered to date. Through an ester bond, the fatty acid chain is usually folded back to form a macrolactone ring of various sizes spanning one or more carbohydrate units. Because of their unique macrocyclic architecture with embedded carbohydrates, and their broad spectrum of biological activities exhibited in phenotypic screens, resin glycosides have attracted considerable attention from the synthetic chemistry community, but not much beyond.[7-9]

In 2005, a new family of glycoresins, ipomoeassins A–E, was isolated from the leaves of Ipomoea squamosa found in the Suriname rainforest and shown to inhibit the proliferation of A2780 human ovarian cancer cells.[10] Among these compounds, ipomoeassin D (Figure 1) displayed the greatest potency with an IC_{50} value of 35 nM. Two years later, a new member of the family, ipomoeassin F (Figure 1), was isolated and showed a cytotoxicity comparable to ipomoeassin D.[11] Because of their promising antiproliferative activity and unique molecular skeleton with carbohydrates being part of the macrocycle, these newly discovered natural glycoconjugates quickly inspired synthetic chemists, including ourselves, to tackle their total syntheses.[12-16] Subsequently, ipomoeassin F was confirmed to be the most cytotoxic resin glycoside discovered to date with single-digit nanomolar IC_{50} values against several cancer-derived cell lines.[13] Intriguingly, ipomoeassins A and F (see Figure 1) have distinct cytotoxicity

profiles, as revealed in the NCI 60-cell lines screen, suggesting that the ipomoeassins may possess an unusual mode of action.[16,17] On this basis, ipomoeassin F is a very promising candidate for molecular probe and chemotherapeutic development; however, the absence of knowledge about the cellular targets of ipomoeassin F has significantly impeded such efforts. To overcome this challenge, after improving our understanding of the structure–activity relationship (SAR) of ipomoeassin F through medicinal chemistry studies,[18-20] we employed a chemical proteomics approach to identify its binding partner(s) in human cells. Here we describe the evolution of our chemoproteomic studies that enabled the discovery of Sec61α (protein transport protein Sec61 subunitalpha isoform 1) as a primary molecular target of ipomoeassin F, and our subsequent mechanistic investigations which validate this component as a key target. We define the inhibitory effects of ipomoeassin F on Sec61-mediated bioactivity within endoplasmic reticulum (ER), corroborating our contemporaneous observations of the potent inhibition of cellular secretion by ipomoeassin F.

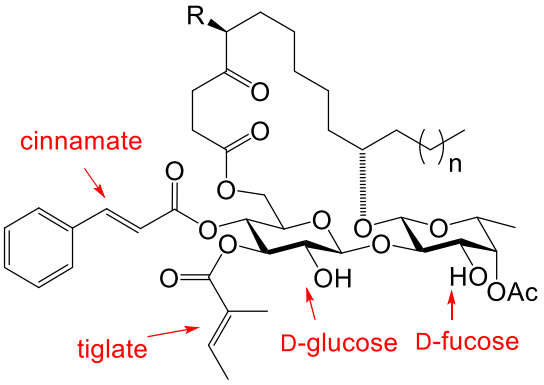

Ipomoeassin A: R = H, n = 1
Ipomoeassin D: R = OAc, n = 1
Ipomoeassin F: R = H, n = 3

Figure 3. 1. Structures of ipomoeassins A, D, and F.

3.3. Results and Discussion

3.3.1. Proteomics Evaluations of Chemical Probes derived from Ipomoeassin F.

Michael acceptor systems are present in many electrophilic natural products, allowing the formation of covalent adducts with bio-macromolecules, which are often responsible for their biological activities.[21] Because of significant activity loss (up to 160-fold) after reducing one of the two double bonds in the α,β-unsaturated esters to a single bond,[22] we hypothesized that the cinnamate and/or the tiglate (Figure 3.1) may enable irreversible binding between ipomoeassin F and its biological target(s). Therefore, we initially designed and synthesized a potential activity-based probe[23-25] **3.1** (Figure 3.2) by introducing a small propargyloxy group to the para position of the benzene ring.

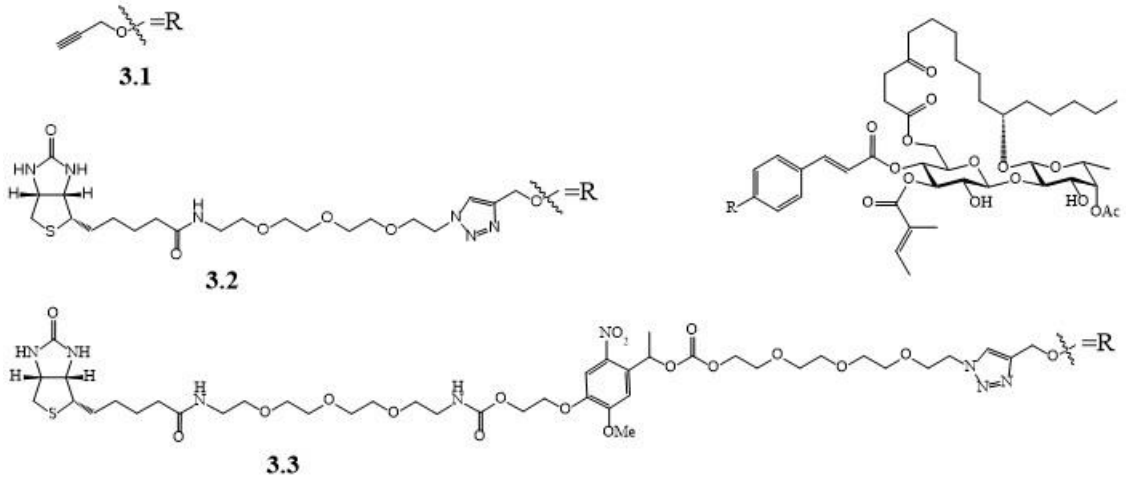

Figure 3. 2. Structure of ipomoeassin F analogues **3.1**-**3.3**.

With probe **3.1** in hand, we conducted activity-based protein profiling experiments for target identification both in the soluble fraction of cell lysates made from MDA-MB-231 breast cancer cells and live MDA-MB-231 cells. Unfortunately, after in situ click chemistry with a fluorescent rhodamine azide [26], we detected no differences in labeled proteins between negative control (lane

1), probe **3.1** (lane 2), and probe **3.1** plus ipomoeassin F (competition; lane 3) (Figure S2A), while an unrelated probe used as a positive control for pulldown gave clear signals (Figure S2A, lanes 4 and 5). We considered two possible explanations for this negative result: firstly, ipomoeassin F is not a covalent protein modifier; secondly, target proteins of ipomoeassin F are in low abundance. Due to the dramatic loss in activity with alkene-reduced compounds,[22] we favored the second possibility.

Table 3. 1. Cytotoxicity (IC_{50}, nM) of Ipomoeassin F and Its Probes 3.1-3.7[a]

	MDA-MB-231[b]	MCF7	MCF-10A
Ipomoeassin F	6.3	36.4	5.3
3.1	6.3	22.2	9.6
3.2	29.5	187.4	21.7
3.3	7.0	19.8	5.1
3.4	24.1	225.3	21.9
3.5	> 25,000	> 25,000	ND[c]
3.6	> 25,000	> 25,000	ND
3.7	253.4	172.2	133.8

[a] The data were obtained from at least two independent experiments, and the standard errors are within 20%; [b] See Figure S1 for IC_{50} curves; [c]ND = not determined.

With probe **3.1** in hand, we conducted activity-based protein profiling experiments for target identification both in the soluble fraction of cell lysates made from MDA-MB-231 breast cancer cells and live MDA-MB-231 cells. Unfortunately, after in situ click chemistry with a fluorescent rhodamine azide [26], we detected no differences in labeled proteins between negative control (lane 1), probe **3.1** (lane 2), and probe **3.1** plus ipomoeassin F (competition; lane 3) (Figure S2A), while an unrelated probe used as a positive control for pulldown gave clear signals (Figure S2A, lanes 4 and 5). We considered two possible explanations for this negative result: firstly, ipomoeassin F is not a covalent protein modifier; secondly, target proteins of ipomoeassin F are in low abundance.

Due to the dramatic loss in activity with alkene-reduced compounds,[22] we favored the second possibility.

In order to enrich for relatively low abundance cellular proteins, we next synthesized a biotin-labeled analogue **3.2** of ipomoeassin F by reacting the alkyne probe **3.1** with biotin azide [27] under chemo-selective copper-catalyzed alkyne-azide coupling (CuAAC) conditions.[28] The synthesis was successful in producing biotin probe **3.2** that remained cytotoxic (Table 3.1), showing only ~5-fold decrease. After incubating **3.2** with either detergent solubilized cell lysate or intact cells, we ued streptavidin beads to recover the biotin probe **3.2**-bound proteins followed by electrophoresis and silver staining of the captured material. However, no proteins were selectively enriched by probe **3.2** (Figures S3A and S3C, lanes 1 to 3), nor was any enrichment apparent when these samples were probed using a fluorophore-labeled streptavidin (Figure S3B, lanes 1 to 3).

We hypothesized that if the target protein(s) of ipomoeassin F is of relatively low abundance, then endogenously biotinylated proteins could outcompete, and thereby mask, any positive signal. To minimize interference from endogenously biotinylated proteins, we synthesized a new biotin probe **3.3** (Figure 3.2) containing a photo-cleavable nitrobenzene moiety[29] by coupling the alkyne analogue **3.1** with the biotin azide fragment containing an o-nitrobenzyl photolabile linker, the latter synthesized by modifying previously reported procedures[26-28] . Notably, the capacity of **3.3** to inhibit cancer cell proliferation was close to that of parental ipomoeassin F (Table 3.1), despite the large size of the appendage at the para-position of the cinnamate benzene ring. We then used probe **3.3** to label target proteins in live MDA-MB-231 cells, performed a streptavidin pulldown on the resulting cell lysate and selectively released bound proteins by UV photocleavage. When the resulting products were analyzed by SDS-PAGE, probe **3.3** strongly enriched a ~40 kDa protein and, to a lesser extent, a second protein of ~100 kDa (Figure 3.2A, lane 2, red arrows),

both of which were absent from the negative control (Figure 3.3A, lane 1). In support of their bona fide interaction with **3.3**, these two proteins were lost when a 100-fold excess of unmodified ipomoeassin F was included during the incubation (Figure 3.3A, lane 3). Because no proteins were selectively recovered with probe **3.3** when it was incubated with detergent-solubilized (1% NP40 and 0.25% sodium deoxycholate) extracts of MDA-MB-231 cells (Figure S3C, lanes 1, 4 and 5), we believe that the interaction between ipomoeassin F and its target protein(s) may require a particular subcellular environment that is detergent sensitive.

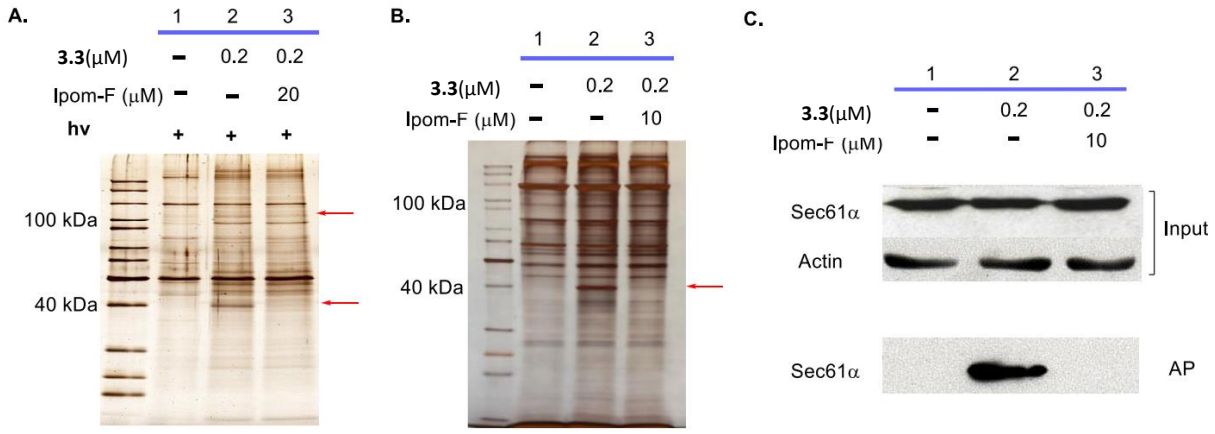

Figure 3. 3. Affinity pulldown using probe **3.3** with (A) or without (B) photo cleavage. Red arrows indicate positive results; (C) Target validation by western blot with a Sec61α antibody. Ipom-F, ipomoeassin F; AP, affinity pulldown.

We next investigated whether photocleavage is essential for the selective recovery of the two putative target protein bands using probe **3.3**. Strikingly, the ~40 kDa protein was also recovered without photocleavage. It was substantially enriched by **3.3** when total streptavidin-bound products were analyzed, and was lost in the presence of excess ipomoeassin F (Figure 3.3B, lanes 1–3). In contrast, an enrichment of the ~100 kDa component under these conditions was not apparent (Figures 3.3A and 3.3B).

A.

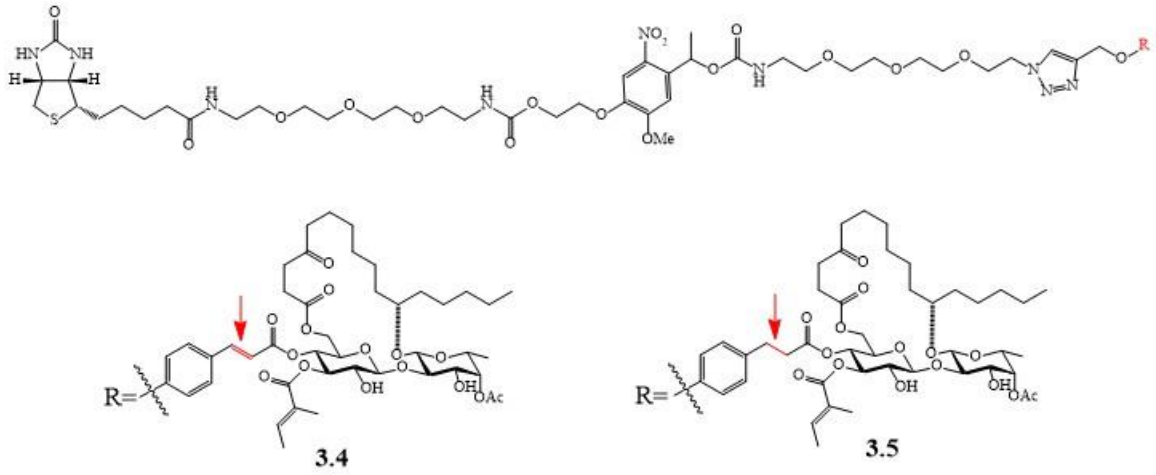

B.

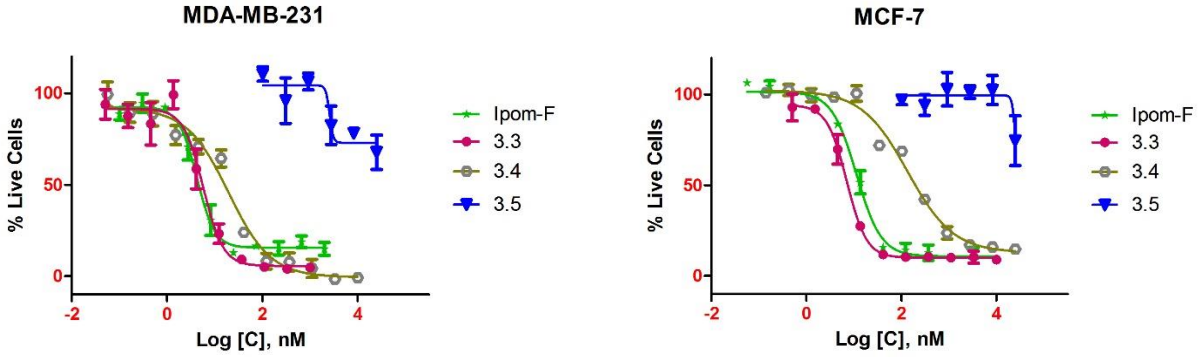

Figure 3. 4. Structure and cytotoxicity of ipomoeassin F analogues **3.4**-**3.5**. (A) Structure of probe **3.4** and **3.5**; (B) Viability curve of **3.3**, **3.4**, **3.5** and ipomoeassin F in MDA-MB-231 and MCF-7 (72h incubation).

To further investigate the factors that facilitate ~40 kDa protein recovery, we designed biotin probe **3.4** (Figure 3.4) which contains -N- rather than -O- in the linker compared with probe **3.3** and its reduced analogue **3.5** (Figure 3.4) as reference compound. While substituting -N- with -O- in the linker triggers limited cytotoxicity disturbance, further reduction of the two α,β-unsaturated double bonds leads to significant loss of the biological activity (Figure 3.4B). Then we performed

biotin affinity pull down parallel with different probes and analyzed collected sample with SDS-PAGE gel. Probe **3.4** (Figure 3.5, lane 4) specifically enriched ~40 kDa protein the same amount of probe **3.3** (Figure 3.5, lane 2), inactive probe **3.5** (Figure 3.5, lane 3) exhibit no specific enrichment as reference group.

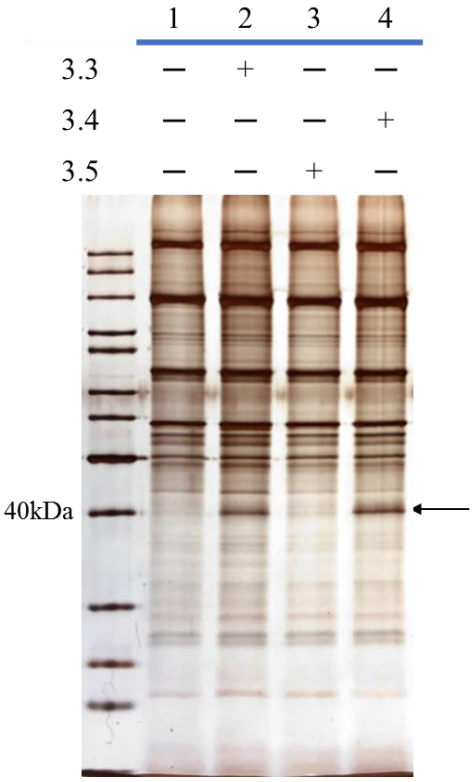

Figure 3. 5. Affinity pulldown using probe **3.3**, **3.4** and **3.5.** Cells are treated with 20nM 1h accordingly in each group.

Since photocleavage and subtle linker change were not essential for probe **3.3** to selectively recover the 40 kDa protein, it is very likely that the increased linker length between the biotin moiety and the ipomoeassin F region, but not its capacity for selective cleavage, significantly improved the performance of probe **3.3** over probe **3.2**. Another factor that plays critical role in selectively isolating the 40 kDa protein is the exitance of double bound in cinnamate and tiglate groups. The conclusion is supported by absence of the ~40 kDa protein recovery in 20nM incubation after reducing the two double bonds (Figure 3.5, lane 2 and 3), even with 500 nM of

3.5 affinity pull down (Figure S4B, lanes 1 and 4). Our data also suggest that, once formed, the complex between probe **3.3** and the ~40 kDa protein is tight and can survive detergent mediated cell lysis. This is further supported by pulldown of the ~40 kDa target protein with low concentrations of probe **3.3** (10 nM) and ipomoeassin F (50 nM) (Figure S4A, lanes 1–3).

We next submitted both the ~40 kDa protein(s) (Figure 3.3B, lane 2) and the corresponding regions of the gel for the negative control (Figure 3.3B, lane 1) and the ipomoeassin F competition sample (Figure 3.3B, lane 3) for mass spectrometry analysis. When spectral counts were compared, Sec61α (protein transport protein Sec61 subunit alpha isoform 1) stood out as the only protein that was both substantially enriched in the pulldown with probe **3.3** and showed a corresponding reduction when excess ipomoeassin F was present (Table S1). The selective recovery of Sec61α by probe **3.3** was further confirmed by Western blotting (Figure 3C, cf. signals between input and AP).

To further support Sec61α as a target protein responsible for the biological activity of ipomoeassin F, we synthesized another reference compound **3.6** (Figure 3.6 and Table 3.1) by removing both double bonds in cinnamate and tiglate. Inactive analogue **3.6** was ineffective at competing with probe **3.3** binding, even when **3.6** was present in 50-fold excess (Figure S4B, cf. lanes 1 to 3). Taken together, these findings further support the specificity of Sec61α as a primary cellular target of ipomoeassin F.

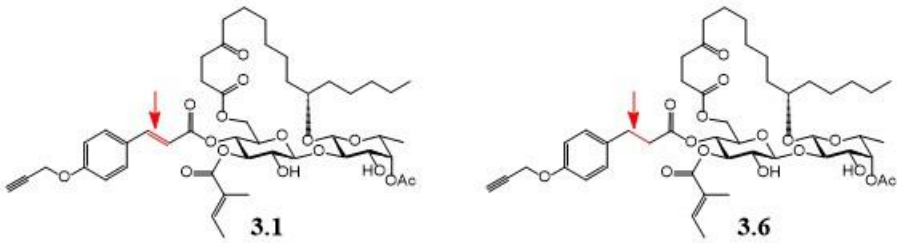

Figure 3. 6. Structures of ipomoeassins F analogues **3.1** and **3.6**.

3.3.2. Cell Imaging Studies.

The Sec61 protein translocon plays an essential role in translocating newly synthesized membrane and secretory polypeptides into and across the membrane of the endoplasmic reticulum (ER).[30,31] Sec61α forms the membrane conduit that nascent secretory polypeptides pass through. To examine the subcellular localization of ipomoeassin F, we performed live cell imaging studies using fluorescent analogue **3.7** (Figure 3.7) prepared from alkyne probe **3.1** using CuAAC. To overcome the low fluorescent signal caused by internal photo-induced electron transfer and photobleaching often encountered in fluorescent probe studies, rhodamine analogue **3.7** was synthesized from the rhodamine azide precursor. Although **3.7** is between 5- and 40-fold less potent than ipomoeassin F depending on the cell type analyzed, it retains substantial cytotoxicity when compared to inactive analogues **3.5** and **3.6** (see Table 3.1), and we therefore used it for our imaging studies.

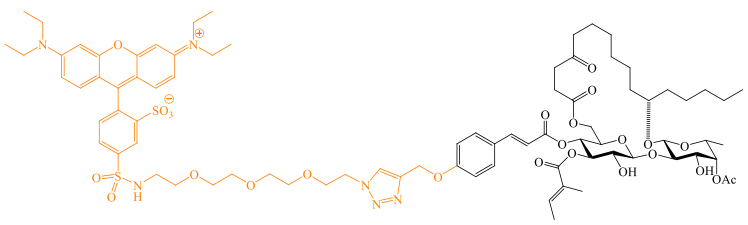

Figure 3. 7. Structures of fluorescent derivative **3.7** of ipomoeassin F.

Subsequently, we confirmed that **3.7** could penetrate the cell membrane in a concentration- and time dependent manner and gave a strong fluorescent signal. Hence, **3.7** stained cells within 30 mins when present at 2 μM, but took >3 h to give clear images when used at 20 nM. When cells labelled with **3.7** were co-stained with markers for either the ER or the nucleus, it was apparent that **3.7** strongly labeled the ER (Figure 3.8), but not the nucleus (Figure S5A). To confirm the specificity of ER labelling by **3.7**, competition experiments were performed using ipomoeassin F

or inactive compound **3.6**. The fluorescence signal of **3.7** was almost completely abolished when the cells were preincubated for 30 minutes with a 100-fold excess of free ipomoeassin F (Figure S5B), yet preincubation with compound **3.6** had little effect (Figure S5C). The apparent ER localization of the cellular interacting partner(s) of ipomoeassin F strongly supports the notion that its target is Sec61α.

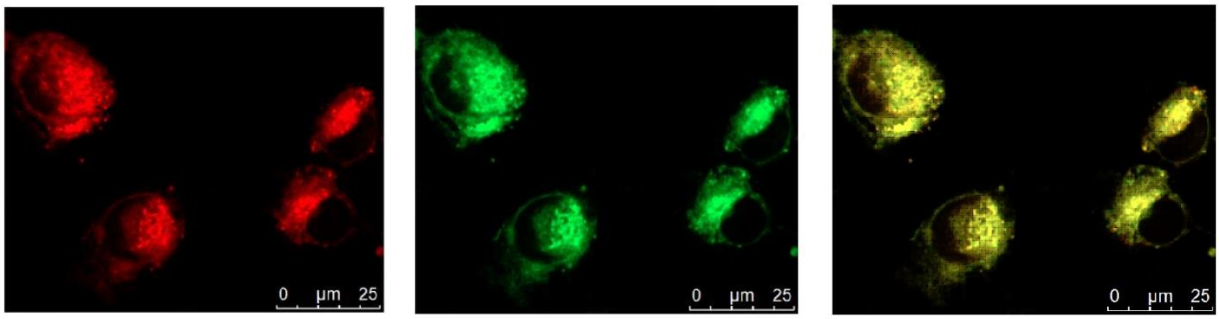

Figure 3. 8. Cell imaging studies with fluorescent probe **3.7** in MDA-MB-231 cells. Rhodamine-conjugated ipomoeassin F analogue **3.7** (0.2 µM) was added to cells and after 1 hours, cells were imaged to analyze localization of **3.7** relative to ER staining.

3.3.3. Pulldown from ER Microsomes.

As evidenced by the negative results from our pulldown experiments using cell lysates prepared with detergent, we propose that the membrane environment of the ER may be required to maintain Sec61α in a conformation that can bind to ipomoeassin F effectively. In this regard, it would be unlikely that purified Sec61α alone could recapitulate a direct interaction with the natural product. However, since the biological function of Sec61α is maintained in isolated ER microsomes (provide by cooperation lab),[32] and once pre-bound to probe **3.3** in intact cells the resulting complex appears stable to detergent treatment (Figures 3.2A and 3.2B), we attempted to pulldown Sec61α from purified ER-derived microsomes. After incubation with probe **3.3** and detergent solubilization (10% n-dodecyl-ß-D-maltoside) to release biotin-bound proteins from the

phospholipid bilayer, only a single protein was visible after pulldown (Figure S6A). The identity of this product was confirmed as Sec61α by western blotting (Figure S6B). This finding strongly supports our previous conclusion made with live cells, namely that Sec61α directly interacts with ipomoeassin F.

3.3.4. Pulldown from ER Microsomes.

As evidenced by the negative results from our pulldown experiments using cell lysates prepared with detergent, we propose that the membrane environment of the ER may be required to maintain Sec61α in a conformation that can bind to ipomoeassin F effectively. In this regard, it would be unlikely that purified Sec61α alone could recapitulate a direct interaction with the natural product. However, since the biological function of Sec61α is maintained in isolated ER microsomes,[32] and once pre-bound to probe **3.3** in intact cells the resulting complex appears stable to detergent treatment (Figures 3A and 3B), we attempted to pulldown Sec61α from purified ER-derived microsomes. After incubation with probe **3.3** and detergent solubilization (10% n-dodecyl-ß-D-maltoside) to release biotin-bound proteins from the phospholipid bilayer, only a single protein was visible after pulldown (Figure S6A). The identity of this product was confirmed as Sec61α by western blotting (Figure S6B). This finding strongly supports our previous conclusion made with live cells, namely that Sec61α directly interacts with ipomoeassin F.

3.3.5. ipomoeassin F and Sec61α interaction mode exploration.

According to the information we got from biotin affinity pull down experiment, Sec61α can form tight complex with probe **3.3** by direct interaction even at the concentration of 10nM in membrane complete environment. The question that whether this complex sustained by a covalent binding or strong non-covalent intermolecular interaction attracted our attention.

Since IC_{50} of probe **3.3** against MDA-MB-231 is 7.0nM, we further narrowed down its work concentration down to 5nM and found ~40 kDa protein enrichment still could be detectable (Figure S4C, lane 1), suggesting the binding between probe **3.3** and Sec61α is very sensitive and strong. Considering 5-fold of ipomoeassin F can easily keep the probe **3.3** out of binding site (Figure S4A) and the single digital nanomolar cytotoxicity IC_{50} value against multiple cell lines, the connection between ipomoeassin F and Sec61α seems to be a covalent binding.

Nevertheless, fluorescent streptavidin staining indicates that a stable covalent adduct between the ~40 kDa protein and probe **3.3** was not formed under SDS-PAGE electrophoresis (Figure S3B, lanes 4 and 5). The contradictory guided us to have a second thought on the understanding about the binding mode between ipomoeassin F and target protein Sec61α.

Traditional competition is performed by the order of treating cells with probes (analogue **3.3**) followed by half an hour original compound (ipomoeassin F) management. The result from the procedure would provide solid evidence that probe **3.3** and ipomoeassin F share the identical target, however the result could not provide evidence to convince people about the binding mode. To overcome this disadvantage, we switch the order of cell management. If the ipomoeassin F-protein complex binding is covalent, ipomoeassin F would have little chance to squeeze the probe **3.3** out binding pocket when treating cell after probe **3.3** management. Vice versa, If the secondary treatment of ipomoeassin F can peel its probe **3.3** off after the probe-protein complex fully generated, it is more likely that binding is non-covalent.

We gradually increase the reverse 100-fold competition intensity in the order of: ipomoeassin F 0.5h treatment followed by 1h probe 3.3 management (Figure 3.9A, lane 4), ipomoeassin F 1h treatment followed by 1h probe 3.3 management (Figure 3.9B, lane 4). Short time reverse competition competes away very limited protein binding compared with traditional pulldown

experiment (Figure 3.9A, lane 2). But with the elongation of competition time, more and more probe-protein complex become dissociated (Figure 3.9B, lane 4). The increase of competition effectiveness in the reverse treatment supports the idea that ipomoeassin F targets Sec61α most likely by strong non-covalent binding or through reversible weak covalent binding.

A.

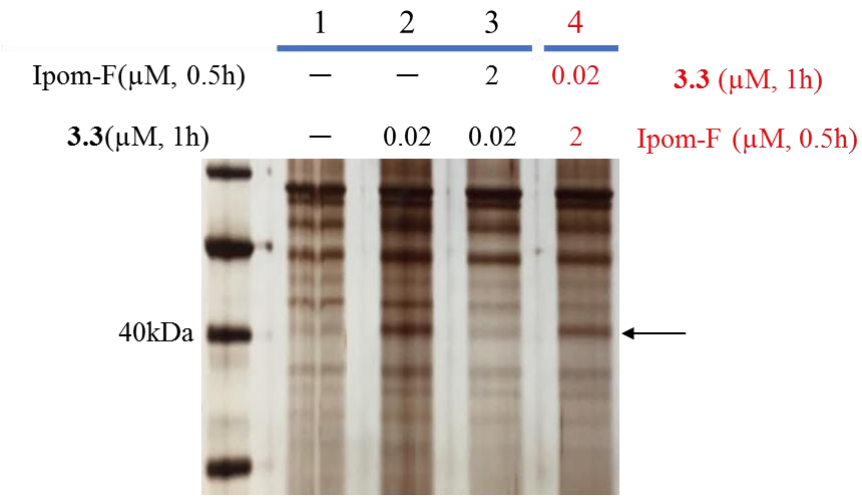

B.

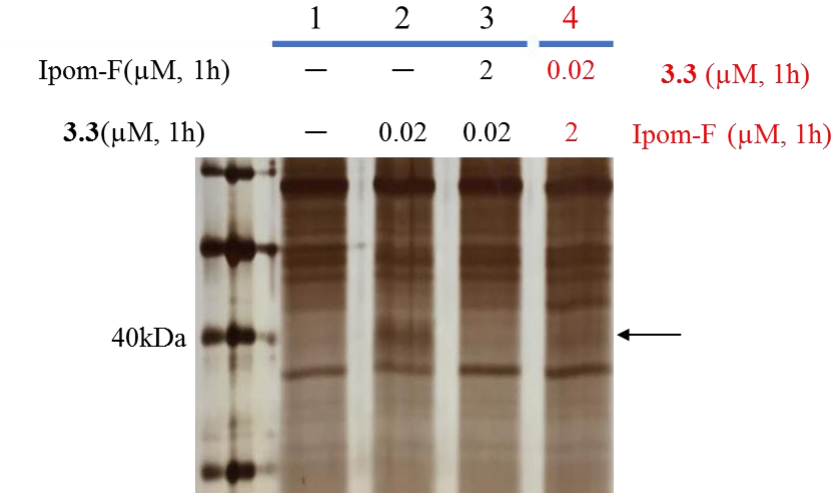

Figure 3. 9. traditional completion and reverse competition between ipomoeassin F and analogue **3.3**: (A) ipomoeassin F 0.5h competition after 1h **3.3** incubation; (B) ipomoeassin F 1h competition after 1h **3.3** incubation.

3.4.Conclusions

Here, we report comprehensive chemical biology studies of ipomoeassin F to understand the molecular basis for its potent cytotoxicity. By designing and evolving our chemical probes on an empirical basis, Sec61α was ultimately identified and validated as a direct and physiologically relevant target of ipomoeassin F. The absence of fluorescent streptavidin staining we observed indicates ipomoeassin F is unlikely to form a stable covalent complex with Sec61α, despite the presence of two Michael acceptor systems in its structure (cinnamate and tiglate, Figure 3.1). Moreover, reverse competition supports the non-covalent binding between ipomoeassin F and Sec61α. We therefore conclude that the pulldown of Sec61α with probe **3.3** represents a successful biotin affinity enrichment of a non-covalent ligand-membrane protein complex formed in live cells, most likely reflecting a slow disassociation rate of ipomoeassin F from Sec61α. The binding of ipomoeassin F to cellular Sec61α is supported by the ER staining seen with a fluorescent version of the compound, the highly selective pulldown of Sec61α from ER-derived microsomes and the ability of ipomoeassin F to compete with cotransin for Sec61α binding.

In short, we provide compelling evidence that the core α subunit of the Sec61 translocation complex is the major target for ipomoeassin F in a cellular context, thereby opening the way for the exploitation of ipomoeassin F for target-based drug discovery. More broadly, given its comparatively advantageous synthesis, we anticipate that ipomoeassin F and its analogues/probes will provide accessible new molecular tools that will help our efforts to fully define the molecular basis for Sec61-mediated protein translocation at the ER membrane.

3.5.Supporting Information

3.5.1. Cytotoxicity Assay

3.5.1.1. Cell Culture

Two human breast cancer cell lines (MDA-MB-231 and MCF7) and one human breast nontumorigenic epithelial cell line (MCF-10A) were maintained in a DMEM high glucose culture medium supplemented with 10% fetal bovine serum (FBS) and 2 mM L-glutamine. The cells were grown in a humidified atmosphere of 5% CO_2 and 95% air at 37 ºC. The culture medium was changed every 2–4 days depending on cell density. Cell cultures were passaged once a week using 0.125% trypsin-EDTA to detach the cells from culture flasks/dishes.

3.5.1.2. MTT Cytotoxicity Assay

Viable cells were counted with a hemocytometer immediately before each experiment. Experiments were done in triplicate. First, 100 µL of MCF7 cells at the density of 50,000 cells/mL were seeded in a 96-well plate (5,000 cells/well), which was incubated at 37 ºC and 5% CO_2 atmosphere for 24 h. The compounds were dissolved in DMSO (dimethyl sulfoxide) to make drug stocks (10 mM). The stock solutions were diluted with the complete DMEM high glucose culture medium to make a series of gradient fresh working solutions right before each test. Subsequently, the cells were treated with 100 µL of the freshly made gradient working solution in the total volume of 200 µL/well for 72 h. After that, the media were discarded and 200 µL of the fresh complete medium containing 10% of MTT stock solution (5 mg/mL) was added to each well. The plate was then incubated at 37 ºC and 5% CO_2 for 3 h. Next, 180 µL of the medium was discarded from each well, and 180 µL of DMSO was added to each well to dissolve formazan crystals. Absorbance of formazan was detected by a microplate reader (BioTek Synergy H1) at 570 nm with 650 nm as the reference wavelength. The percentage of viability compared to the negative control (DMSO-

treated cells) was determined. GraphPad Prism 6 software was used to make a plot of % viability versus sample concentration and to calculate the concentration at which a compound exhibited 50% cytotoxicity (IC_{50}).

3.5.1.3. AlamarBlue Cytotoxicity Assay

MDA-MB-231 and MCF-10A Viable cells were counted with a hemocytometer immediately before each experiment. Experiments were done in triplicate. First, 100 μL of MDA-MB-231 cells or MCF10A cells at the density of 50,000 cells/mL was seeded in a 96-well plate (5,000 cells/well) and then incubated at 37 ºC and 5% CO_2 for 24 h. The compounds were dissolved in DMSO (dimethyl sulfoxide) to make drug stocks (10 mM). The stock solutions were diluted with the complete DMEM high glucose culture medium to make a series of gradient fresh working solutions right before each test. Subsequently, the cells were treated with 100 μL of the freshly made gradient working solution in the total volume of 200 μL/well for 72 h. After that, the media were discarded and 200 μL of the fresh complete medium containing 10% of AlamarBlue (resazurin) stock solution (3 mg/27.15mL) (5 mg/mL) was added to each well. The plate was then incubated at 37 ºC and 5% CO_2 for another 3 h. Emission of each well at 620 nm was detected by a microplate reader (BioTek Synergy H1) at excitation 580 nm. The percentage of viability compared to the negative control (DMSO-treated cells) was determined. GraphPad Prism 6 software was used to make a plot of % viability versus sample concentration and to calculate the concentration at which a compound exhibited 50% cytotoxicity (IC_{50}).

3.5.2. Stepwise Activity Based Protein Profiling

MDA-MB-231 cells were seeded in five groups of 6 cm petri dishes with 3 ml DMEM high glucose culture and incubated at 37 ºC and 5% CO_2 until 90% confluency. Each group was treated

with fresh medium containing 20 µM competitor or an equal volume of DMSO vehicle for 30 min at 37 ºC and 5% CO_2, followed by addition of 0.2 µM probe or an equal volume of DMSO. After 1 h incubation at 37 ºC and 5% CO_2, the cells were harvested and washed with cold PBS for 3 times. The cells were then lysed in 100 µl of lysis buffer 1 (50 mM Hepes pH = 9.0, 100 mM NaCl, 10% glycerol, 5 mM $MgCl_2$, 1 mM $CaCl_2$, 0.2% NP40, 1x protease inhibitor) using ultrasound sonication. The supernatant of each group was collected after centrifugation at 21,100 g and 4 ºC for 10 min, and the protein concentration was quantified with a BCA kit. 10% SDS was then added into protein solution to make a final SDS concentration of 0.4%, and the solution was incubated at 95 ºC for 5 min. 1 µl TECP (100 mM stock solution in H_2O) was mixed with 1 µl TBTA (10 mM stock solution in a 4:1 ratio of *t*-butanol and DMSO), 1 µl $CuSO_4$ (100 mM stock solution in H_2O), and 1 µl rhodamine-azide (1 mM stock solution in DMSO). The mixed solution was added into the previously prepared protein solution containing 0.25 mg protein. The total volume was adjusted to 100 µl with the lysis buffer 1 to make a final protein concentration of 2.5 mg/ml, and the click reaction was performed at room temperature for 1.5 h. Proteins in 15 µl of the reactant were fractionated by an SDS-PAGE gel. The protein gel was scanned with a typhoon scanner (Typhoon™ FLA 9500) at 532 nm excitation with 700 mV gain setting and then stained with Coomassie blue.

3.5.3. Biotin Affinity Pulldown

3.5.3.1. Live Cell-based Pulldown

According to the experimental needs, MDA-MB-231 cells were seeded into 3-7 groups of 15-cm tissueculture dishes and incubated at 37 ºC and 5% CO_2 until 90% confluency. Each group was treated with fresh medium containing a competitor or an equal volume of DMSO vehicle for 30 min at 37 ºC and 5% CO_2, followed by addition of a probe or an equal volume of DMSO. After

1 h incubation at 37 ºC and 5% CO_2, the cells were harvested and washed with cold PBS for 3 times and lysed with the lysis buffer 2 (50 mM Tris pH=7.4, 150 mM NaCl, 1% NP40, 0.25% sodium deoxycholate, 10 mM NaF, 10 mM β-glycerophosphate, and 1 mM Na_3VO_4). The supernatant of each group was collected after centrifugation at 4 ºC and 21,100 g for 10 min, and the protein concentration was quantified with the BCA kit. After adjusting protein concentration with lysis buffer 2, each protein solution with equal amount of total protein in the same volume was incubated with 20 µl of washed streptavidin bead at 4 ºC for 2 h with rotation. After incubation, the beads were washed with washing buffer (50 mM Tris pH=7.4, 150mM NaCl, 1% NP40, 0.25% Sodium deoxycholate, 10 mM NaF, 10 mM β-glycerophosphate, and 1 mM Na_3VO_4) for 3 times and boiled at 95ºC for 5 min in 2x sample buffer (125 mM Tris-HCl PH=6.8, 20% Glycerol, 2% SDS, 2% β-mercaptoethanol and 0.02% Bromophenol blue). After centrifugation at 21,100 g and 4 ºC for 1 min, the cleared eluted proteins were divided into two parts. One part was fractionated by a 12% SDS PAGE and visualized by silver staining. The other part was analyzed by Western blotting, in which proteins on the nitrocellulose membrane were visualized by either fluorescently labeled streptavidin or an anti-Sec61α antibody.

3.5.3.2. Cell Lysate-based Pulldown

MDA-MB-231 cells from seven 15-cm tissue culture dishes were harvested and washed with PBS for 3 times and lysed in buffer 2 using ultrasound sonication. The supernatant of each group was collected after centrifugation at 21,100 g and 4 ºC for 10 min, and the protein concentration was quantified with the BCA kit and adjusted to be between 3.5–4 mg/mL with lysis buffer 2. Next, the cell lysate was equally divided into 7 fractions, 1 ml/each. Each fraction was treated with either a competitor or an equal volume of DMSO vehicle for 30 min at 4 ºC, followed by the addition of a probe or an equal volume of DMSO. All the samples were then incubated at 4 ºC for

1 h. After incubation, 20 µl of streptavidin washed bead was added to each sample followed by 2 h incubation at 4 ºC with rotation. The remaining procedures were the same as the live cell-based pulldown (see above).

3.5.3.3. ER Microsome-based Pulldown

1 ul of Ipomoeassin F (2 mM stock concentration) or DMSO vehicle was added to 198.6 ul ER microsome suspension in one of the three Eppendorf tubes to produce a final ipomoeassin F concentration of 10 µM and two blank tubes. The resulting mixtures were incubated at 4 ºC for 30 min, followed by addition of 0.2 µM probe (final concentration) to two tubes or an equal volume of DMSO to a blank tube. After 1 h incubation at 4 ºC, 10% DDM (*n*-dodecyl-ß-D-maltoside) was added to each tube to give the final concentration of 1%, and the mixtures were further incubated at 4 ºC for another 1 h. The supernatant of each group was collected after centrifugation at 4 ºC and 21,100 g for 10 min. 20 µl of washed streptavidin beads was added to each sample followed by 2 h incubation at 4 ºC with rotation. After washing with washing buffer (50 mM Tris pH=7.4, and 150 mM NaCl) for 3 times, the bound proteins were eluted by were boiling the beads in 20 µl of 2x sample buffer at 95 ºC for 5 min. The eluted proteins were analyzed by SDS-PAGE or Western blotting as described above.

3.5.4. Mass Spectrometry (MS) Analysis and MS Data Processing

In the pulldown, the bound proteins were eluted via boiling the high capacity streptavidin agarose beads in 1x sample buffer. The eluted proteins were fractionated with a 12% SDS-PAGE and the fractionated proteins were visualized by blue silver staining.[33] The 40 kDa protein band from the probe **3.3**-enriched sample and the corresponding regions of the gel for the negative control and the ipomoeassin F competition sample were cut, in-gel digested, the resulting peptides

were analyzed by an Orbitrap Fusion mass spectrometer (*Thermo Fisher Scientific*), and the MS/MS spectra were searched against a composite target-decoy UniProtkB human protein database (2018_02, 20317 entries) using Mascot (Matrix Science, London, UK; version 2.5.1) as described previously. [34-35] The parameters for database searching were as follows: MS tolerance of 3.0 ppm and MS/MS tolerance of 0.5 Da; tryptic enzyme specificity with a maximum of 2 missed cleavages; fixed modification, carbamidomethyl of cysteine; and variable modifications, oxidation of methionine and acetylation of the N-terminus. Search results were further processed by Scaffold software (version 4.8.6; Proteome Software, Portland, OR) for viewing protein and peptide identification information. In the Scaffold analysis, peptide identifications were accepted if they could achieve a false discovery rate (FDR) of <1.0% by the Scaffold Local FDR algorithm. Protein identifications were accepted if they could achieve an FDR of <1.0% and contained at least 2 identified peptides. Total spectral counts were exported from Scaffold and used to represent relative protein abundance from different samples based on the positive, linear correlation between spectral count and the abundance of a protein in complex samples.[36-38] Contaminant proteins such as keratins were discarded. For reliable representation of protein abundance, proteins identified with <4 spectra in the probe **3.3** - enriched sample were discarded.[37]

3.5.5. *Cell Imaging*

MDA-MB-231 cells were seeded on fibronectin-coated coverslips at 70% confluency in a 48-well plate and cultured at 37 ºC and 5% CO_2. After 24 h, culture medium was replaced with fresh medium containing a 20 µM competitor or an equal volume of DMSO vehicle for 30 min at 37 ºC and 5% CO_2, followed by addition of 0.2 µM (final concentration) fluorescent probe **3.7**. After 1 h incubation, the coverslips were mounted onto a glass slide with a mounting medium with or without 0.5 µg/ml DAPI. The fluorescent images were acquired with a confocal microscope

(Leica TCS SP5) using 405 nm excitation and 562 nm excitation. For the ER co-localization studies, 1uM ER-Tracker™ Blue-White DPX was added to the medium after 1 h incubation with probe **3.7**. After 5 min incubation, the coverslips were mounted onto a glass slide and the images were acquired as described above.

3.5.6. Figures and Tables

3.5.6.1. Cell Cytotoxicity Assay

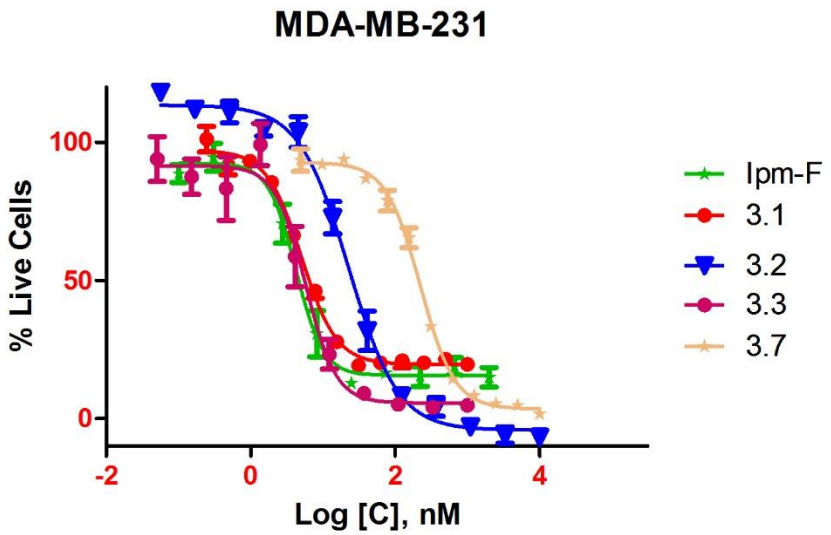

Figure S 1. Cytotoxicity in MDA-MB-231: Cell viability curves of analogues **3.1**, **3.2**, **3.3**, **3.7** and ipomoeassin F (72 h incubation).

3.5.6.2. Stepwise Activity Based Protein Profiling

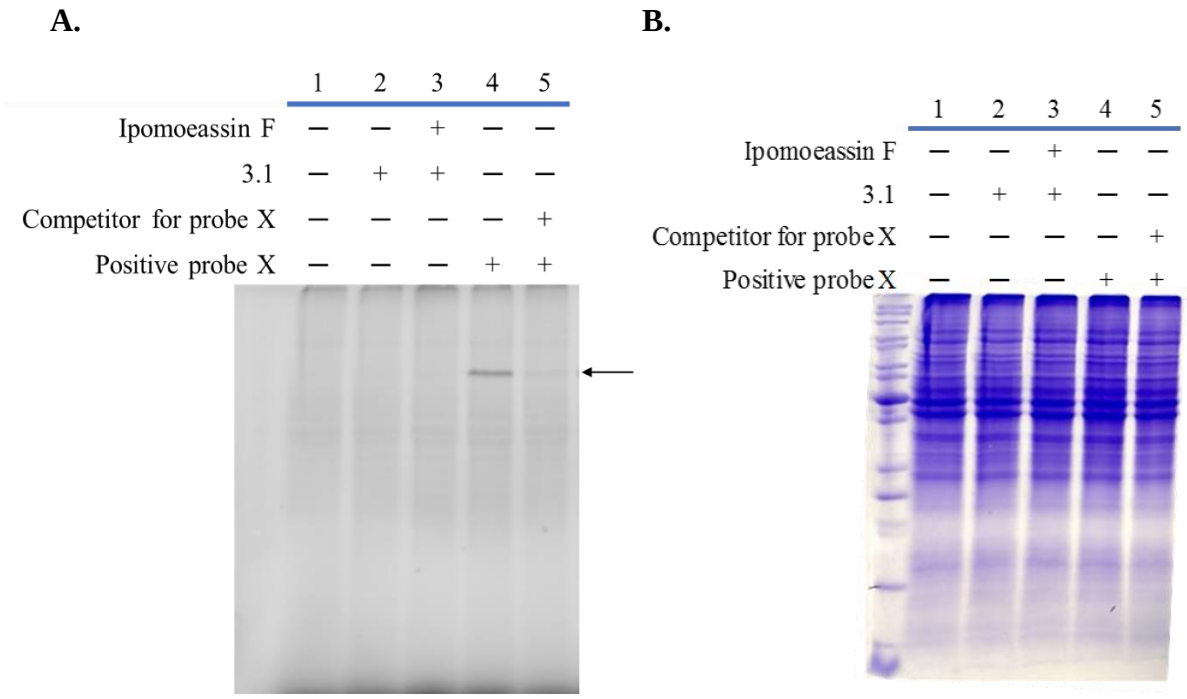

Figure S 2. Click reaction performed after incubating cells with competitor and its corresponding alkyne probe. (A) Fluorescent image by a Typhoon scanner. (B) Coomassie Blue stain of the gel. (The arrow indicates a positive result for probe X, where a protein band appeared in lane 4 but was absent in lanes 1 and 5.)

3.5.6.3. Biotin Affinity Pulldown

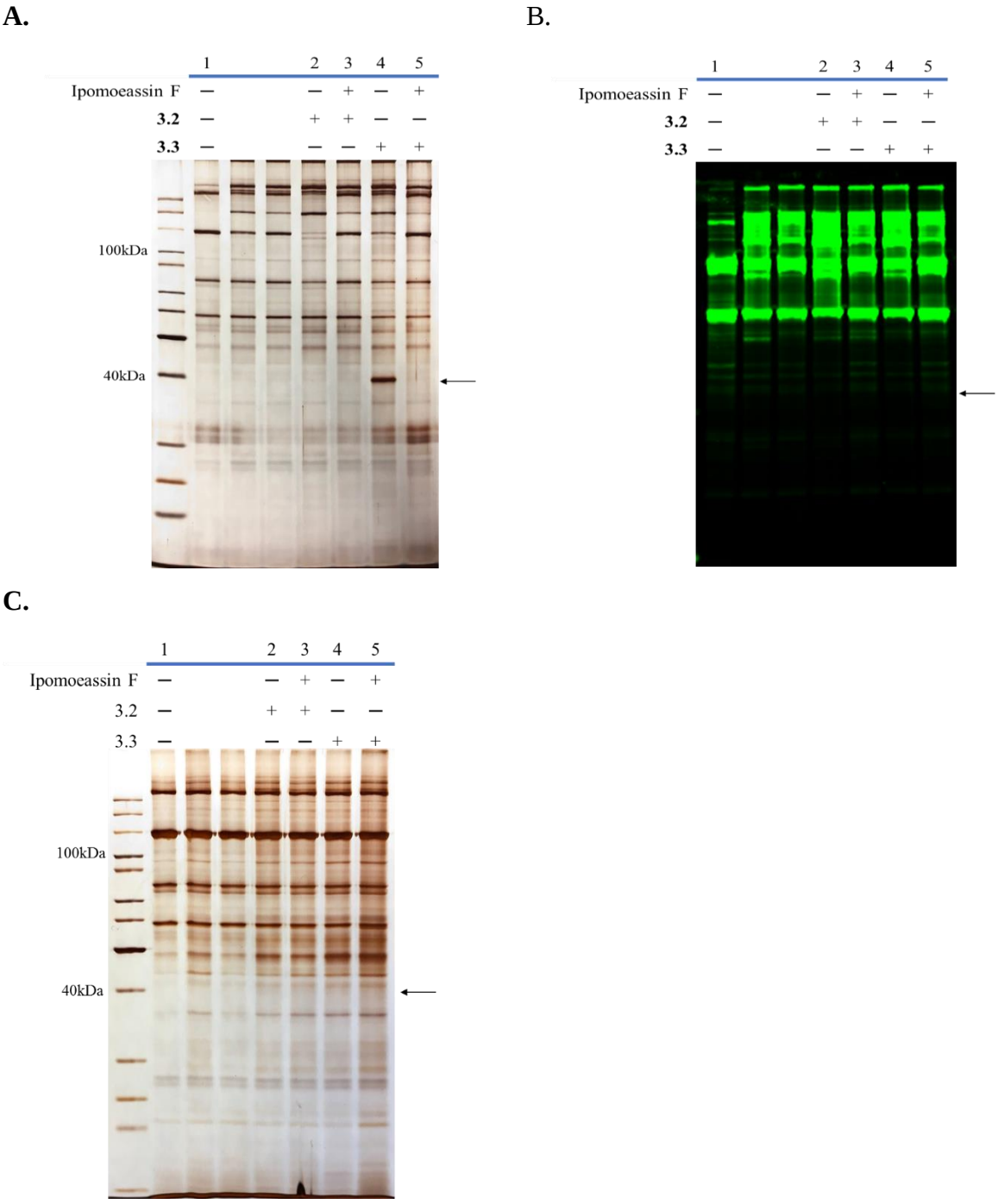

Figure S 3. Biotin affinity pulldown with probes 3.2 and 3.3. Cells were incubated with ipomoeassin F and probes, then lysed and subjected to biotin affinity pulldown with streptavidin beads. (A) SDS-PAGE and silver staining analysis of pulldown samples from live cells. (B) SDS-PAGE analysis of pulldown samples from live cells using fluorescently labeled streptavidin. (C) SDS-PAGE and silver staining analysis of pulldown samples from cell lysates. Arrows indicate the ~40 kDa position.

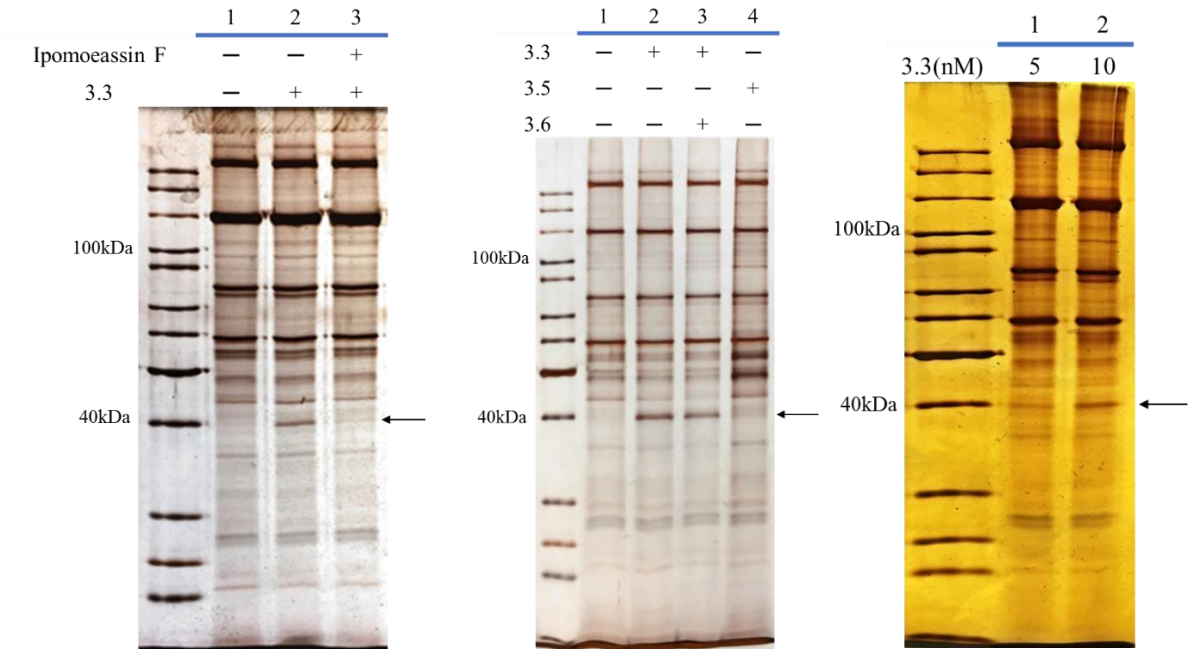

Figure S 4. Biotin affinity pulldown with probe **3.3** or **3.5** in the presence of the competitor ipomoeassin F or **3.6.** (A) Pulldown experiment with 10 nM **3.3** and 50 nM ipomoeassin F. (B) Pulldown experiments with either 20 nM **3.3** and 1 μM **3.6** or 500 nM **3.5** without competition. Arrows indicate the ~40 kDa position. (C) Pulldown experiment with 5nM and 10nM **3.3**.

3.5.6.4. *Cell Imaging*

A.

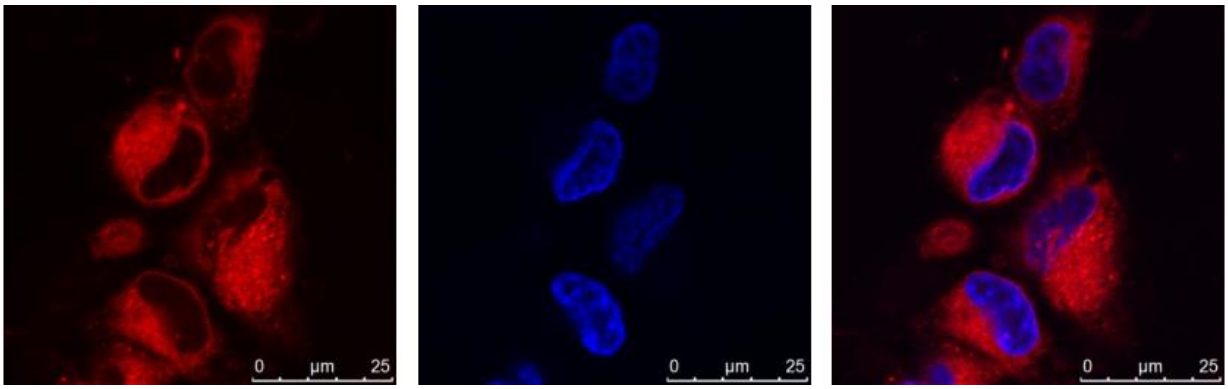

3.7, 0.2µM DAPI Merged

B.

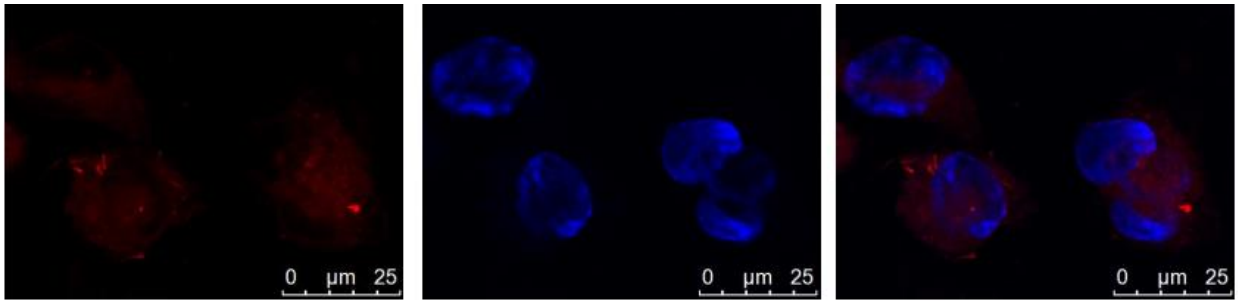

3.7 (0.2 µM) + Ipom-F (20 µM) DAPI Merged

C.

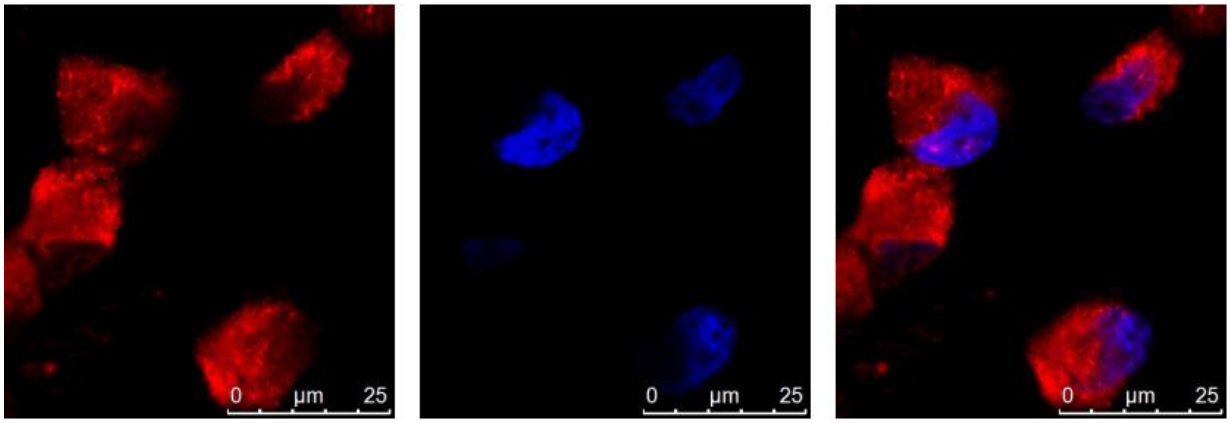

3.7 (0.2 µM) + **3.6** (20 µM) DAPI Merged

Figure S 5. Live cell imaging-based competition experiments. (A) Cells were treated with 1 µM **3.7**. (B) Cells were treated with ipomoeassin F (100-fold) and **3.7**; (C) Cells were treated with **3.6** (100-fold) and **3.7**.

3.5.6.5. Pulldown in ER Microsomes.

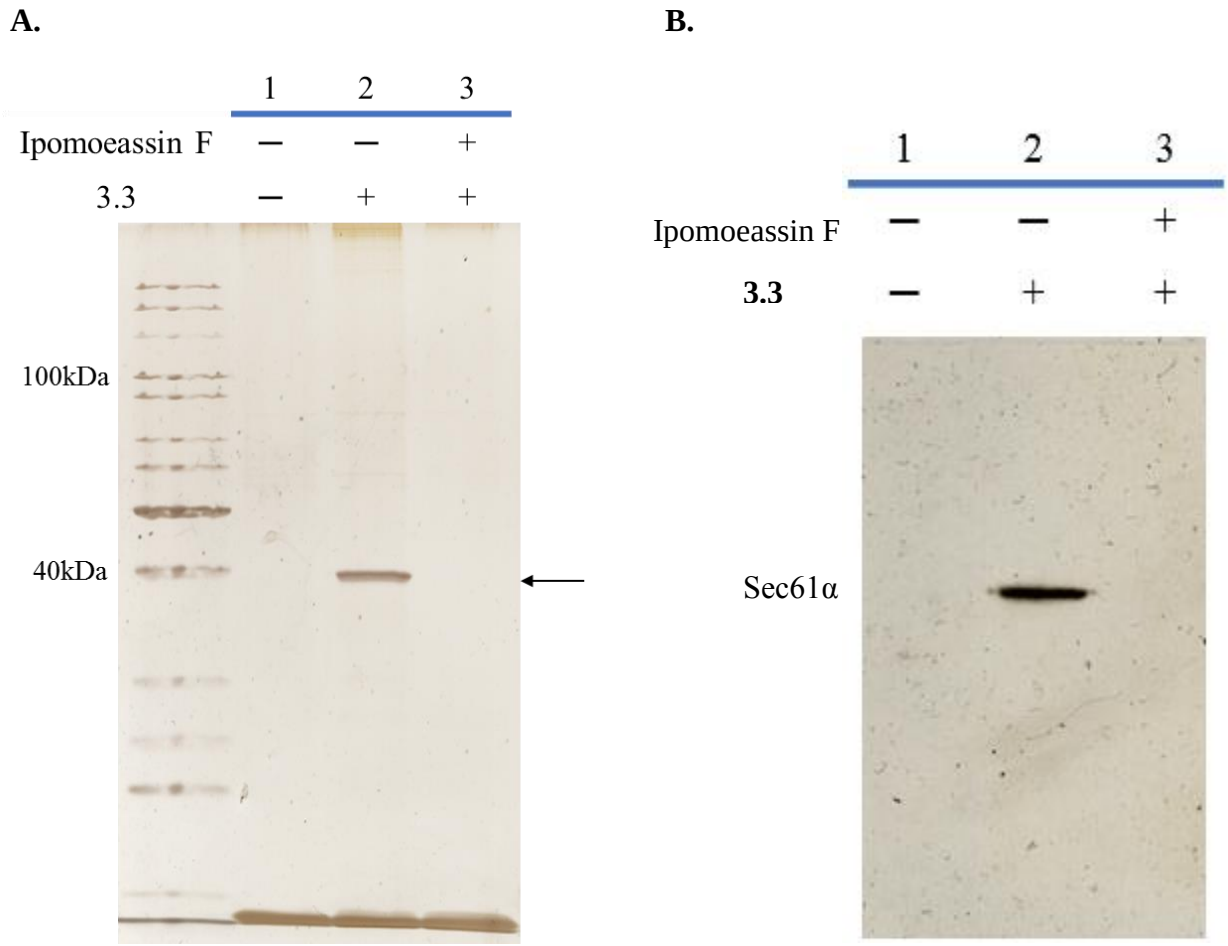

Figure S 6. Biotin affinity pulldown with probe 3.3 in ER microsomes. (A) The proteins were visualized by silver staining. The arrow indicates the positive result. (B) The proteins were transferred onto a nitrocellulose membrane and visualized by western blot using an anti-Sec61α antibody.

Table S 1.

Spectral Counts for Proteins Identified in ~40 kDa Bands from LC/MS						
Identified Proteins	**Accession Number**	**Molecular Weight**	**Spectral count**			
			DMSO	**Probe 7**	**7 + Ipom F**	**delta (Probe/probe + Ipom-F)**
Vimentin	VIME_HUMAN	54 kDa	108	88	126	**0.7**
Protein transport protein Sec61 subunit alpha isoform 1	S61A1_HUMAN	52 kDa	11	80	16	**5**
Pyruvate carboxylase, mitochondrial	PYC_HUMAN	130 kDa	97	68	109	**0.62**
Poly(rC)-binding protein 1	PCBP1_HUMAN	37 kDa	45	45	82	**0.55**
mRNA export factor	RAE1L_HUMAN	41 kDa	50	41	53	**0.77**
Actin, cytoplasmic 1	ACTB_HUMAN	42 kDa	45	40	54	**0.74**
Stomatin-like protein 2, mitochondrial	STML2_HUMAN	39 kDa	42	37	68	**0.54**
Enoyl-CoA delta isomerase 2, mitochondrial	ECI2_HUMAN	44 kDa	34	36	51	**0.71**

Spectral Counts for Proteins Identified in ~40 kDa Bands from LC/MS						
Identified Proteins	**Accession Number**	**Molecular Weight**	**Spectral count**			
			DMSO	**Probe 7**	**7 + Ipom F**	**delta (Probe/probe + Ipom-F)**
Plectin	PLEC_HUMAN	532 kDa	30	29	65	**0.45**
Methylcrotonoyl-CoA carboxylase subunit alpha, mitochondrial	MCCA_HUMAN	80 kDa	42	28	44	**0.64**
26S proteasome regulatory subunit 10B	PRS10_HUMAN	44 kDa	27	25	45	**0.56**
Acetyl-CoA acetyltransferase, mitochondrial	THIL_HUMAN	45 kDa	24	25	37	**0.68**
Core histone macro H2A.1	H2AY_HUMAN	40 kDa	30	24	50	**0.48**
Heterogeneous nuclear ribonucleoprotein A3	ROA3_HUMAN	40 kDa	35	24	47	**0.51**

Spectral Counts for Proteins Identified in ~40 kDa Bands from LC/MS						
Identified Proteins	**Accession Number**	**Molecular Weight**	**Spectral count**			
			DMSO	**Probe 7**	**7 + Ipom F**	**delta (Probe/probe + Ipom-F)**
Methylcrotonoyl-CoA carboxylase beta chain, mitochondrial	MCCB_HUMAN	61 kDa	36	23	37	**0.62**
DnaJ homolog subfamily B member 11	DJB11_HUMAN	41 kDa	25	21	28	**0.75**
Fructose-bisphosphate aldolase A	ALDOA_HUMAN	39 kDa	55	21	37	**0.57**
Succinate--CoA ligase [GDP-forming] subunit beta, mitochondrial	SUCB2_HUMAN	47 kDa	25	21	28	**0.75**
Poly(rC)-binding protein 2	PCBP2_HUMAN	39 kDa	23	20	34	**0.59**

Spectral Counts for Proteins Identified in ~40 kDa Bands from LC/MS						
Identified Proteins	**Accession Number**	**Molecular Weight**	**Spectral count**			
			DMSO	**Probe 7**	**7 + Ipom F**	**delta (Probe/probe + Ipom-F)**
Cytosolic acyl coenzyme A thioester hydrolase	BACH_HUMAN	42 kDa	23	19	23	**0.83**
Transmembrane protein 43	TMM43_HUMAN	45 kDa	19	18	21	**0.86**
HLA class I histocompatibility antigen, A-2 alpha chain	1A02_HUMAN	41 kDa	8	8	16	**0.5**
Mevalonate kinase	KIME_HUMAN	42 kDa	10	8	15	**0.53**
Mitotic checkpoint protein BUB3	BUB3_HUMAN	37 kDa	8	8	15	**0.53**
Nucleolar protein 7	NOL7_HUMAN	29 kDa	9	8	10	**0.8**
Nucleolysin TIAR	TIAR_HUMAN	42 kDa	9	8	13	**0.62**

Spectral Counts for Proteins Identified in ~40 kDa Bands from LC/MS						
Identified Proteins	**Accession Number**	**Molecular Weight**	**Spectral count**			
			DMSO	**Probe 7**	**7 + Ipom F**	**delta (Probe/probe + Ipom-F)**
Protein KTI12 homolog	KTI12_HUMAN	39 kDa	4	8	12	**0.67**
Protein SGT1 homolog	SGT1_HUMAN	41 kDa	8	8	22	**0.36**
Transcriptional activator protein Pur-alpha	PURA_HUMAN	35 kDa	15	8	19	**0.42**
Tropomodulin-3	TMOD3_HUMAN	40 kDa	15	8	19	**0.42**
40S ribosomal protein SA	RSSA_HUMAN	33 kDa	7	7	13	**0.54**
Cytoskeleton-associated protein 4	CKAP4_HUMAN	66 kDa	5	7	12	**0.58**
Erlin-1	ERLN1_HUMAN	39 kDa	8	7	9	**0.78**
Mitochondrial inner membrane protein OXA1L	OXA1L_HUMAN	49 kDa	8	7	9	**0.78**

Spectral Counts for Proteins Identified in ~40 kDa Bands from LC/MS						
Identified Proteins	**Accession Number**	**Molecular Weight**	**Spectral count**			
			DMSO	**Probe 7**	**7 + Ipom F**	**delta (Probe/probe + Ipom-F)**
Polymerase delta interacting protein 3	PDIP3_HUMAN	46 kDa	8	7	11	**0.64**
Rab11 family-interacting protein 5	RFIP5_HUMAN	70 kDa	7	7	10	**0.7**
T-complex protein 1 subunit delta	TCPD_HUMAN	58 kDa	14	7	13	**0.54**
tRNA methyltransferase 10 homolog C	TM10C_HUMAN	47 kDa	13	7	14	**0.5**
Ubiquitin-60S ribosomal protein L40	RL40_HUMAN	15 kDa	7	7	12	**0.58**
V-type proton ATPase subunit C 1	VATC1_HUMAN	44 kDa	10	7	15	**0.47**

Spectral Counts for Proteins Identified in ~40 kDa Bands from LC/MS						
Identified Proteins	**Accession Number**	**Molecular Weight**	**Spectral count**			
			DMSO	**Probe 7**	**7 + Ipom F**	**delta (Probe/probe + Ipom-F)**
28S ribosomal protein S5, mitochondrial	RT05_HUMAN	48 kDa	7	6	15	**0.4**
Activity-dependent neuroprotector homeobox protein	ADNP_HUMAN	124 kDa	6	6	9	**0.67**
Aspartate aminotransferase, cytoplasmic	AATC_HUMAN	46 kDa	21	6	16	**0.38**
COP9 signalosome complex subunit 4	CSN4_HUMAN	46 kDa	7	6	9	**0.67**
Eukaryotic translation initiation factor 3 subunit H	EIF3H_HUMAN	40 kDa	6	6	17	**0.35**

Spectral Counts for Proteins Identified in ~40 kDa Bands from LC/MS						
Identified Proteins	**Accession Number**	**Molecular Weight**	**Spectral count**			
			DMSO	**Probe 7**	**7 + Ipom F**	**delta (Probe/probe + Ipom-F)**
Ferrochelatase, mitochondrial	HEMH_HUMAN	48 kDa	9	6	13	**0.46**
Filamin-B	FLNB_HUMAN	278 kDa	8	6	10	**0.6**
Glutaminyl-peptide cyclotransferase-like protein	QPCTL_HUMAN	43 kDa	7	6	6	**1**
Heat shock protein HSP 90-beta	HS90B_HUMAN	83 kDa	14	6	15	**0.4**
Hemoglobin subunit alpha	HBA_HUMAN	15 kDa	10	6	2	**3**
Mannose-1-phosphate guanyltransferase beta	GMPPB_HUMAN	40 kDa	6	6	13	**0.46**
Nucleolin	NUCL_HUMAN	77 kDa	5	6	6	**1**

Spectral Counts for Proteins Identified in ~40 kDa Bands from LC/MS						
Identified Proteins	**Accession Number**	**Molecular Weight**	**Spectral count**			
			DMSO	**Probe 7**	**7 + Ipom F**	**delta (Probe/probe + Ipom-F)**
Proline-rich protein 11	PRR11_HUMAN	40 kDa	11	6	14	**0.43**
Protein arginine N methyltransferase 1	ANM1_HUMAN	42 kDa	11	6	14	**0.43**
Short/branched chain specific acyl-CoA dehydrogenase, mitochondrial	ACDSB_HUMAN	47 kDa	4	6	11	**0.55**
SUMO-activating enzyme subunit 1	SAE1_HUMAN	38 kDa	11	6	12	**0.5**
Ubiquitin-conjugating enzyme E2 Z	UBE2Z_HUMAN	38 kDa	8	6	10	**0.6**
Alpha-actinin-1	ACTN1_HUMAN	103 kDa	3	5	8	**0.63**

Spectral Counts for Proteins Identified in ~40 kDa Bands from LC/MS						
Identified Proteins	**Accession Number**	**Molecular Weight**	**Spectral count**			
			DMSO	**Probe 7**	**7 + Ipom F**	**delta (Probe/probe + Ipom-F)**
Alpha-actinin-4	ACTN4_HUMAN	105 kDa	11	5	11	**0.45**
Choline-phosphate cytidylyltransferase A	PCY1A_HUMAN	42 kDa	2	5	5	**1**
DnaJ homolog subfamily B member 2	DNJB2_HUMAN	36 kDa	5	5	3	**1.67**
Fructose-bisphosphate aldolase C	ALDOC_HUMAN	39 kDa	21	5	13	**0.38**
GDP-mannose 4,6 dehydratase	GMDS_HUMAN	42 kDa	9	5	11	**0.45**
Heat shock cognate 71 kDa protein	HSP7C_HUMAN	71 kDa	14	5	19	**0.26**
Hsp70-binding protein 1	HPBP1_HUMAN	39 kDa	6	5	8	**0.63**

Spectral Counts for Proteins Identified in ~40 kDa Bands from LC/MS						
Identified Proteins	**Accession Number**	**Molecular Weight**	**Spectral count**			
			DMSO	**Probe 7**	**7 + Ipom F**	**delta (Probe/probe + Ipom-F)**
Matrin-3	MATR3_HUMAN	95 kDa	2	5	7	**0.71**
Minor histocompatibility antigen H13	HM13_HUMAN	41 kDa	6	5	7	**0.71**
Nucleoside diphosphate kinase 7	NDK7_HUMAN	42 kDa	9	5	10	**0.5**
Probable ATP-dependent RNA helicase DDX5	DDX5_HUMAN	69 kDa	6	5	11	**0.45**
Probable methyltransferase-like protein 15	MET15_HUMAN	46 kDa	5	5	10	**0.5**

Spectral Counts for Proteins Identified in ~40 kDa Bands from LC/MS						
Identified Proteins	**Accession Number**	**Molecular Weight**	**Spectral count**			
			DMSO	**Probe 7**	**7 + Ipom F**	**delta (Probe/probe + Ipom-F)**
Propionyl-CoA carboxylase alpha chain, mitochondrial	PCCA_HUMAN	80 kDa	11	5	13	**0.38**
Propionyl-CoA carboxylase beta chain, mitochondrial	PCCB_HUMAN	58 kDa	7	5	6	**0.83**
Replication factor C subunit 2	RFC2_HUMAN	39 kDa	4	5	25	**0.2**
RNA 3'-terminal phosphate cyclase	RTCA_HUMAN	39 kDa	6	5	9	**0.56**
Serine/threonine-protein kinase MARK2	MARK2_HUMAN	88 kDa	3	5	4	**1.25**
Serpin B9	SPB9_HUMAN	42 kDa	11	5	9	**0.56**
Twinfilin-2	TWF2_HUMAN	40 kDa	10	5	10	**0.5**

Spectral Counts for Proteins Identified in ~40 kDa Bands from LC/MS						
Identified Proteins	**Accession Number**	**Molecular Weight**	**Spectral count**			
			DMSO	**Probe 7**	**7 + Ipom F**	**delta (Probe/probe + Ipom-F)**
7-dehydrocholesterol reductase	DHCR7_HUMAN	54 kDa	3	4	2	**2**
Alpha-2-macroglobulin receptor-associated protein	AMRP_HUMAN	41 kDa	2	4	4	**1**
Apoptosis-inducing factor 2	AIFM2_HUMAN	41 kDa	5	4	13	**0.31**
ATPase ASNA1	ASNA_HUMAN	39 kDa	3	4	5	**0.8**
BRISC and BRCA1-A complex member 1	BABA1_HUMAN	37 kDa	6	4	11	**0.36**
cAMP-dependent protein kinase catalytic subunit alpha	KAPCA_HUMAN	41 kDa	16	4	13	**0.31**

Spectral Counts for Proteins Identified in ~40 kDa Bands from LC/MS						
Identified Proteins	**Accession Number**	**Molecular Weight**	**Spectral count**			
			DMSO	**Probe 7**	**7 + Ipom F**	**delta (Probe/probe + Ipom-F)**
Cdc42 effector protein 1	BORG5_HUMAN	40 kDa	6	4	9	**0.44**
Desmocollin-1	DSC1_HUMAN	100 kDa	0	4	0	**#DIV/0!**
Filamin-A	FLNA_HUMAN	281 kDa	7	4	8	**0.5**
Flap endonuclease 1	FEN1_HUMAN	43 kDa	3	4	7	**0.57**
Glucose-fructose oxidoreductase domain containing protein 1	GFOD1_HUMAN	43 kDa	4	4	5	**0.8**
HAUS augmin-like complex subunit 4	HAUS4_HUMAN	42 kDa	1	4	11	**0.36**
Heat shock 70 kDa protein 1A	HS71A_HUMAN (+1)	70 kDa	6	4	7	**0.57**

Spectral Counts for Proteins Identified in ~40 kDa Bands from LC/MS						
Identified Proteins	**Accession Number**	**Molecular Weight**	**Spectral count**			
			DMSO	**Probe 7**	**7 + Ipom F**	**delta (Probe/probe + Ipom-F)**
HLA class I histocompatibility antigen, alpha chain E	HLAE_HUMAN	40 kDa	5	4	4	**1**
HLA class I histocompatibility antigen, B-41 alpha chain	1B41_HUMAN	41 kDa	2	4	4	**1**
Isovaleryl-CoA dehydrogenase, mitochondrial	IVD_HUMAN	46 kDa	8	4	8	**0.5**
MAP7 domain containing protein 3	MA7D3_HUMAN	98 kDa	4	4	8	**0.5**
Monocarboxylate transporter 4	MOT4_HUMAN	49 kDa	4	4	7	**0.57**
Muscleblind-like protein 1	MBNL1_HUMAN	42 kDa	3	4	5	**0.8**
Pinin	PININ_HUMAN	82 kDa	2	4	5	**0.8**
Polyhomeotic-like protein 2	PHC2_HUMAN	91 kDa	4	4	4	**1**
RelA-associated inhibitor	IASPP_HUMAN	89 kDa	1	4	7	**0.57**
Serum albumin	ALBU_HUMAN	69 kDa	4	4	4	**1**

Spectral Counts for Proteins Identified in ~40 kDa Bands from LC/MS						
Identified Proteins	**Accession Number**	**Molecular Weight**	**Spectral count**			
			DMSO	**Probe 7**	**7 + Ipom F**	**delta (Probe/probe + Ipom-F)**
Stress-70 protein, mitochondrial	GRP75_HUMAN	74 kDa	5	4	6	**0.67**
Synaptic vesicle membrane protein VAT-1 homolog	VAT1_HUMAN	42 kDa	3	4	10	**0.4**
Testis-expressed protein 264	TX264_HUMAN	34 kDa	7	4	10	**0.4**
Transcription factor jun B	JUNB_HUMAN	36 kDa	4	4	9	**0.44**
Transformer-2 protein homolog beta	TRA2B_HUMAN	34 kDa	5	4	6	**0.67**
UBX domain-containing protein 1	UBXN1_HUMAN	33 kDa	4	4	5	**0.8**

References

1. Newman DJ.; Natural Products as Sources of New Drugs from 1981 to 2014. *Journal of Natural Products* **2016,** *79*(3), 629-661.

2. Cragg GM.; Grothaus PG.; Newman DJ., Impact of natural products on developing new anti-cancer agents. *Chemical Reviews* **2009,** *109* (7), 3012-3043.

3. Carlson EE., Natural products as chemical probes. *ACS Chemical Biology* **2010**, *5(*7),639-653.

4. Rizzo S.; Waldmann H., Development of a natural-product-derived chemical toolbox for modulation of protein function. *Chemical Reviews* **2014**, *114*(9), 4621-4639.

5. Pye CR, Bertin MJ, Lokey RS, Gerwick WH, Linington RG. Retrospective analysis of natural products provides insights for future discovery trends. *Proceedings of the National Academy of Sciences of the United States of America* **2017**, *114*(22), 5601-5606.

6. Pereda-Miranda R.; Rosas-Ramírez D.; Castañeda-Gómez J., Resin glycosides from the morning glory family. *Fortschritte der Chemie organischer Naturstoffe* **2010**, *92*, 77-153.

7. Furukawa, J.-i.; Sakairi, N. Synthetic Studies on Resin Glycosides. *Trends in Glycoscience and Glycotechnology* **2001**, *13*(69), 1-10.

8. Fürstner, A. Eur. Cover Picture: Total Syntheses and Biological Assessment of Macrocyclic Glycolipids (Eur. J. Org. Chem. 5/2004). *European Journal of Organic Chemistry* **2004**, *2004*(5), 933.

9. Jarikote, D. V.; Murphy, P. V., Metathesis and Macrocycles with Embedded Carbohydrates. *European Journal of Organic Chemistry* **2010**, *2010*(26), 4959-4970.

10. Cao, S. G.; Guza, R. C.; Wisse, J. H.; Miller, J. S.; Evans, R.; Kingston, D. G. I., Ipomoeassins A-E, cytotoxic macrocyclic glycoresins from the leaves of Ipomoea squamosa from the Suriname rainforest. *Journal of Natural Products* **2005,** *68* (4), 487-492.

11. Cao S.; Norris A.; Wisse JH.; Miller JS.; Evans R.; Kingston DG., Ipomoeassin F, a new cytotoxic macrocyclic glycoresin from the leaves of Ipomoea squamosa from the Suriname rainforest. *Natural Product Research* **2007**; *21*(10), 872-876.

12. Fürstner, A.; Nagano, T. Total syntheses of ipomoeassin B and E. *Journal of the American Chemical Society* **2007**, *129*(7), 1906-1907.

13. Nagano, T.; Pospíšil, J.; Chollet, G.; Schulthoff, S.; Hickmann, V.; Moulin, E.; Herrmann, J.; Müller, R.; Fürstner, A., Total synthesis and biological evaluation of the cytotoxic resin glycosides ipomoeassin A-F and analogues. *Chemistry* **2009**, *15*(38), 9697-9706.

14. Postema, M. H. D.; TenDyke, K.; Cutter, J.; Kuznetsov, G.; Xu, Q. Total synthesis of ipomoeassin F. *Organic Letters* **2009**, *11*(6),1417-1420.

15. Zong G.; Barber E.; Aljewari H.; Zhou J.; Hu Z.; Du Y.; Shi WQ., Total Synthesis and Biological Evaluation of Ipomoeassin F and Its Unnatural 11R-Epimer. *The Journal of Organic Chemistry* **2015**, *80*(18), 9279-9291.

16. Zong G,.; Whisenhunt L.; Hu Z,.; Shi WQ., Synergistic contribution of tiglate and cinnamate to cytotoxicity of Ipomoeassin F. *The Journal of Organic Chemistry* **2017**, *82*(9), 4977-4985.

17. Kingston, D. G. L.; Cao, S. *the United States Patent US* 7,560,536 B2, **2009**.

18. Zong G.; Aljewari H.; Hu Z.; Shi WQ., Revealing the pharmacophore of ipomoeassin F through molecular editing. *Organic Letters* **2016**, *18*(7), 1674-1677.

19. Zong G.; Hirsch M.; Mondrik C.; Hu Z.; Shi WQ., Design, synthesis and biological evaluation of fucose-truncated monosaccharide analogues of ipomoeassin F. *Bioorganic & Medicinal Chemistry Letters* **2017**, *27*(12), 2752-2756.

20. Zong G, Sun X.; Bhakta R.; Whisenhunt L.; Hu Z.; Wang F.; Shi WQ., New insights into structure-activity relationship of ipomoeassin F from its bioisosteric 5-oxa/aza analogues. *European Journal of Medicinal Chemistry* **2018**, *144*, 751-757.

21. Gersch M.; Kreuzer J.; Sieber SA., Electrophilic natural products and their biological targets. *Natural Product Reports* **2012**, *29*(6), 659-682.

22. Zong G.; Aljewari H.; Hu Z.; Shi WQ., Revealing the pharmacophore of ipomoeassin F through molecular editing. *Organic Letters* **2016**, *18*(7), 1674-1677.

23. Cravatt BF.; Wright AT.; Kozarich JW., Activity-based protein profiling: from enzyme chemistry to proteomic chemistry. *Annual Review of Biochemistry* **2008**, *77*, 383-414.

24. Li X.; Hu Y., Identifying the cellular targets of bioactive small molecules with activity-based probes. *Current Medicinal Chemistry* **2010**, *17*(27), 3030-3044.

25. Heal WP.; Dang TH.; Tate EW., Activity-based probes: discovering new biology and new drug targets. *Chemical Society Reviews* **2011**, *40*(1), 246-257.

26. Kii I.; Shiraishi A.; Hiramatsu T.; Matsushita T.; Uekusa H.; Yoshida S.; Yamamoto M.; Kudo A.; Hagiwara M.; Hosoya T., Strain-promoted double-click reaction for chemical modification of azido-biomolecules. *Organic & Biomolecular Chemistry* **2010**, *8*(18), 4051-4055.

27. Tantama M.; Lin WC.; Licht S., An activity-based protein profiling probe for the nicotinic acetylcholine receptor. *Journal of the American Chemical Society* **2008**, *130*(47), 15766-15677.

28. Haldón E.; Nicasio MC.; Pérez PJ., Copper-catalysed azide-alkyne cycloadditions (CuAAC): an update. *Organic & Biomolecular Chemistry* **2015**, *13*(37), 9528-9550.

29. Holmes CP., Model Studies for New o-Nitrobenzyl Photolabile Linkers: Substituent Effects on the Rates of Photochemical Cleavage. *The Journal of Organic Chemistry* **1997**, *62*(8), 2370-2380.

30. Linxweiler M.; Schick B.; Zimmermann R., Let's talk about Secs: Sec61, Sec62 and Sec63 in signal transduction, oncology and personalized medicine. *Signal Transduction and Targeted Therapy* **2017**, *2*, 17002.

31. Greenfield JJ.; High S., The Sec61 complex is located in both the ER and the ER-Golgi intermediate compartment. *Journal of Cell Science* **1999**, *112*(Pt 10), 1477-1486.

32. McKenna M.; Simmonds RE.; High S., Mechanistic insights into the inhibition of Sec61-dependent co- and post-translational translocation by mycolactone. *Journal of Cell Science* **2016**, *129*(7), 1404-1415.

33. Candiano, G.; Bruschi, M.; Musante, L.; Santucci, L.; Ghiggeri, G. M.; Carnemolla, B.; Orecchia, P.; Zardi, L.; Righetti, P. G., Blue silver: a very sensitive colloidal Coomassie G-250 staining for proteome analysis. *Electrophoresis* **2004**, *25*(9), 1327-1333.

34. Dhamad, A. E.; Zhou, Z.; Zhou, J.; Du, Y. Systematic Proteomic Identification of the Heat Shock Proteins (Hsp) that Interact with Estrogen Receptor Alpha (ERα) and Biochemical Characterization of the ERα-Hsp70 Interaction. *PLoS One* **2016**, *11*(8), e0160312.

35. Zhou, Z.; Zhou, J.; Du, Y. Estrogen receptor alpha interacts with mitochondrial protein HADHB and affects beta-oxidation activity. *Molecular & Cellular Proteomics* **2012**, *11*(7), M111.011056.

36. Liu, H.; Sadygov, R. G.; Yates, J. R. A model for random sampling and estimation of relative protein abundance in shotgun proteomics. *Analytical Chemistry* **2004**, *76*(14), 4193-4201.

37. Old, W. M.; Meyer-Arendt, K.; Aveline-Wolf, L.; Pierce, K. G.; Mendoza, A.; Sevinsky, J. R.; Resing, K. A.; Ahn, N. G. Comparison of label-free methods for quantifying human proteins by shotgun proteomics. *Molecular & Cellular Proteomics* **2005**, *4*(10), 1487-1502.

38. Zybailov, B.; Coleman, M. K.; Florens, L.; Washburn, M. P. Correlation of relative abundance ratios derived from peptide ion chromatograms and spectrum counting for quantitative proteomic analysis using stable isotope labeling. *Analytical Chemistry* **2005**, *77*(19), 6218-6224.

CHAPTER 4. FUTURE PROJECT: APPLICATION FOR HIGH-THROUGHPUT SCREENING

As early as 1990s, high-throughput screening (HTS) of synthetic chemistry libraries against various potential therapeutic targets has been applied into pharmaceutic industry.[1] For recent decades, a significant number of natural products were isolated and characterized with the help of bioactivity screening.[2] Nowadays, HTS is considered as one of the most key tools in drug discovery within the pharmaceutical industry. With the employment of HTS, tens of thousands of compounds can be tested in a week to identify the specific mechanisms of different compounds.[3]

However, there is still a large numbers of potential interesting compounds that may be missed due the limit detecting sensitivity and screening throughput efficacy. With the application of new techniques and advances in data management, screening sensitivity has greatly improved. Mass spectrometry (MS)-based metabolomic profiling is one of those newly developed method. Even though this technique is acknowledged as a very sensitive screening approach, it is not easy to have it well established in practical throughput screening. Therefore, people are continuously looking for high-throughput strategies with 'low-tech' but robust output.

Sec61, a complex consisted of subunit α, β and γ, constitutes a heterotrimer.[4] Multiple heterotrimers cluster together to build up a transmembrane aqueous pore channel,[5-7] which enables of newly synthesized secretory proteins translocation and helps with membrane protein integration as well.[4,8] As discussed in Chapter 3, ipomoeassin F specifically binds Sec61α leading to its single digital nanomolar cytotoxicity IC_{50} value. This non-covalent binding or reversible covalent weak binding between ipomoeassin F probes and Sec61α can be outcompeted by adequate amounts of ipomoeasin F since they bind the same target protein. In future project, I will be trying to make the

competition easily monitorable with relatively small amounts of material and time, so that it could be used as a potential high throughput screening for Sec61α binding compound.

4.1.Fluorescent probe based HTS study

Fluorescent probes have been frequently used for exploring many kinds of bio-activities by taking advantage of their indispensable sensitivity and easily accessibility. They could be easily traceable at very low quantity, sensitive to ionic strength, PH, viscosity, temperature and hydrophobicity.[9] Moreover, the fluorescent probes can even present subcellular constitution by specific binding to regional specific molecules like DNA, proteins or lipids within organelles.

4.1.1. Mechanism for fluorescent probe based HTS research

Probe 4.1(Figure 4.1) was shown to be an active compound with strong emission signal when achieved with the proper excitation wavelength and to maintain favorable stability under reasonable continuous excitation.

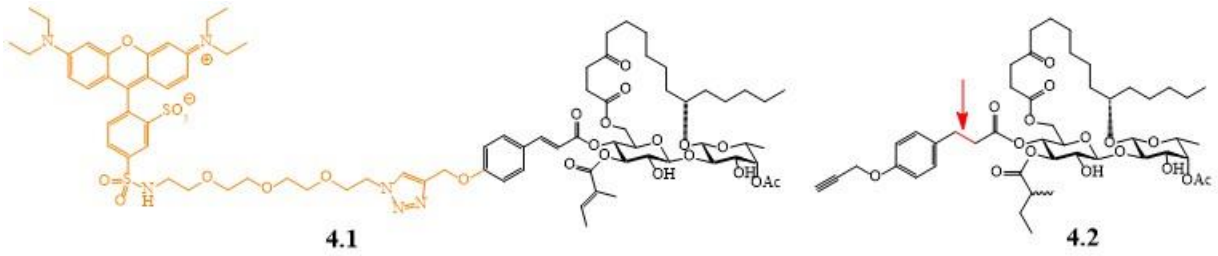

Figure 4. 1. Ipomoeassin F analogues **4.1, 4.2**.

The fluorescent intensity variation reflects probe - target protein complex binding and dissociation dynamics. As a result, ipomoeassin F that possesses strong potency and same target would perfectly compete probe **4.1** off the target protein binding site, therefore lessens the detectable fluorescent intensity (Figure 4.2B); while inactive analogue **4.2** that has no common binding site could not push **4.1** out of the protein binding pocket therefore causes no signal disturbance (Figure 4.2C). If the same competition was performed on an unknown compound,

detectable numerical fluorescent intensity would be a convenient and accurate indicator for whether this test compound harbors Sec61α affinity.

A.

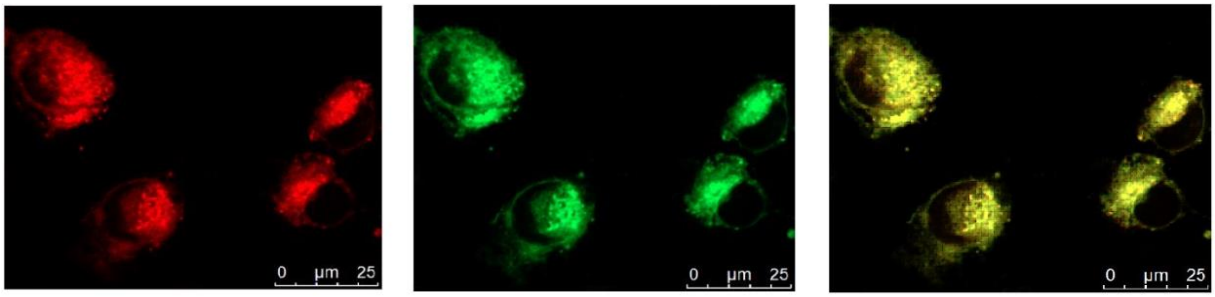

4.1, 0.2μM ER Tracker Merge

B.

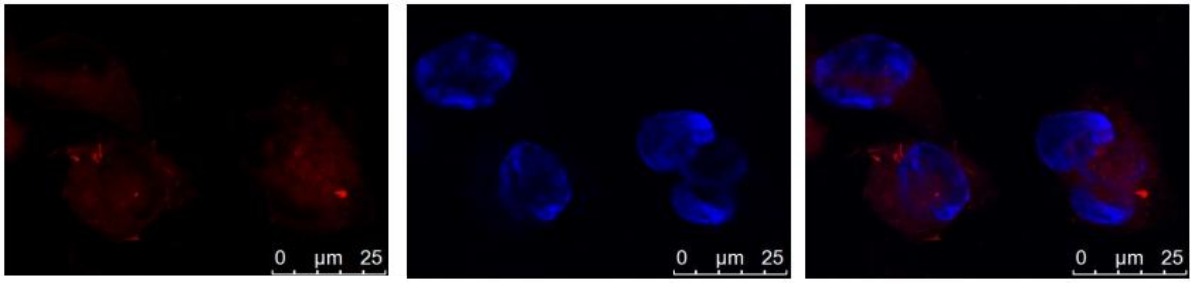

4.1 (0.2μM) + Ipom-F (20 μM) DAPI Merged

C.

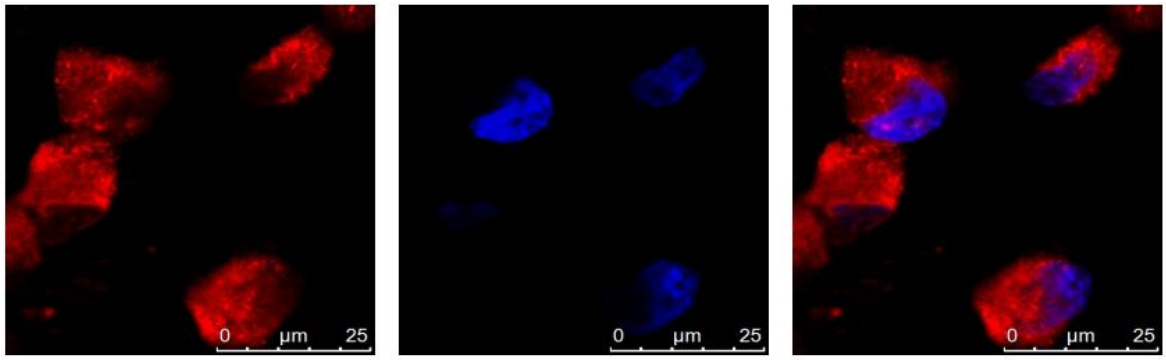

4.1 (0.2μM) + **4.2** (20 μM) DAPI Merged

Figure 4. 2. Live cell imaging-based competition experiments. (A) Cells were treated with 0.2 μM **4.1**. (B) Cells were treated with 20 μM ipomoeassin F and 0.2 μM **4.1**; (C) Cells were treated with 20 μM **4.2** and 0.2 μM **4.1**.

Due to the complicated synthesis of homemade positive control ipomoeassin F and negative control **4.2**, minimizing their required amount during the screening is critical to the feasibility as a potential HTS approach. Since HTS may be performed on tens of thousands of compounds, optimized time for the whole process is another critical factor that adds weigh to its potential availability for realistic application. In this project, I use probe **4.1** fluorescent signal intensity as an indicator, and ipomoeassin F and probe **4.2** are recruited as positive control and negative control respectively. The goal is to figure out the optimized efficacy on breast cancer cell line MDA-MB-231 so that it could be possibly used as an HTS for compounds that target Sec61α.

4.1.2. Optimal work concentration exploration for cell imaging

Work concentration of probe **4.1** is directly related to the corresponding competition controls, so the minimum amount for relative acceptable clear image is an ideal expected work concentration. Since the IC_{50} value of **4.1** is 253.4nM against MDA-MB-231, 500nM was set to be the highest testing concentration.

A.

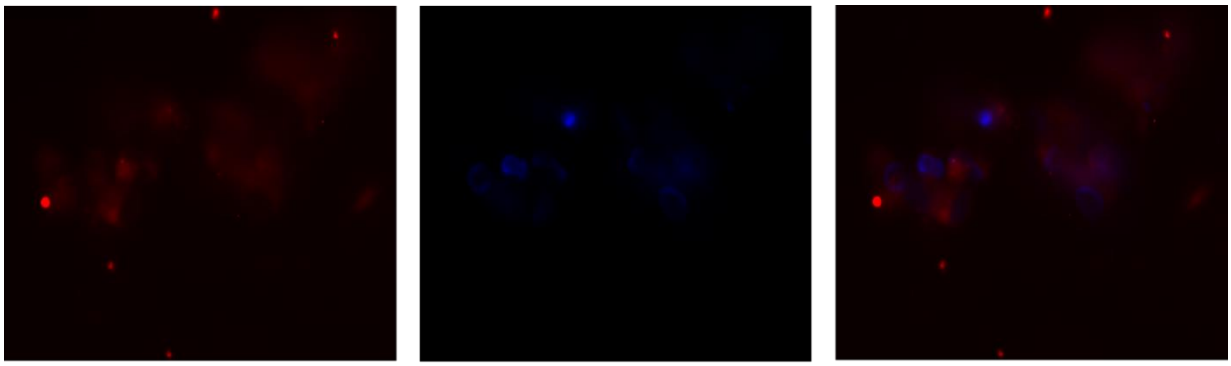

4.1, 25nM DAPI Merge

B.

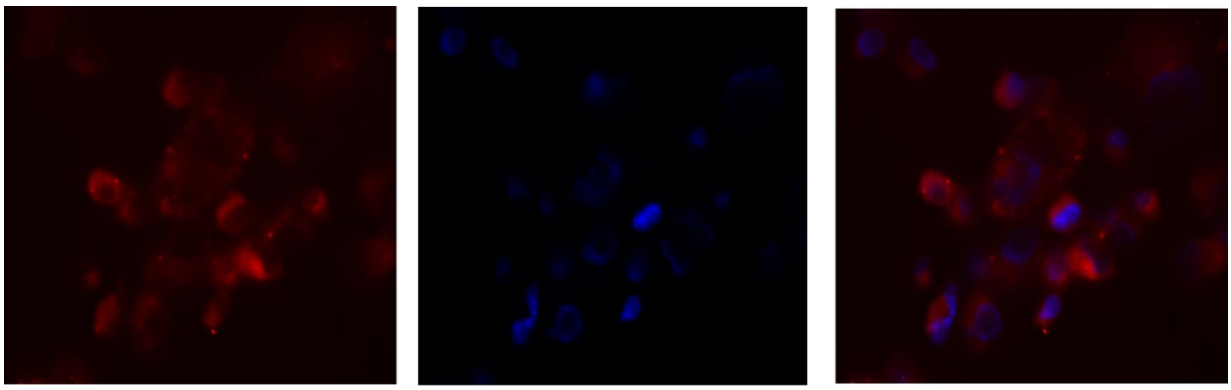

4.1, 50nM DAPI Merge

C.

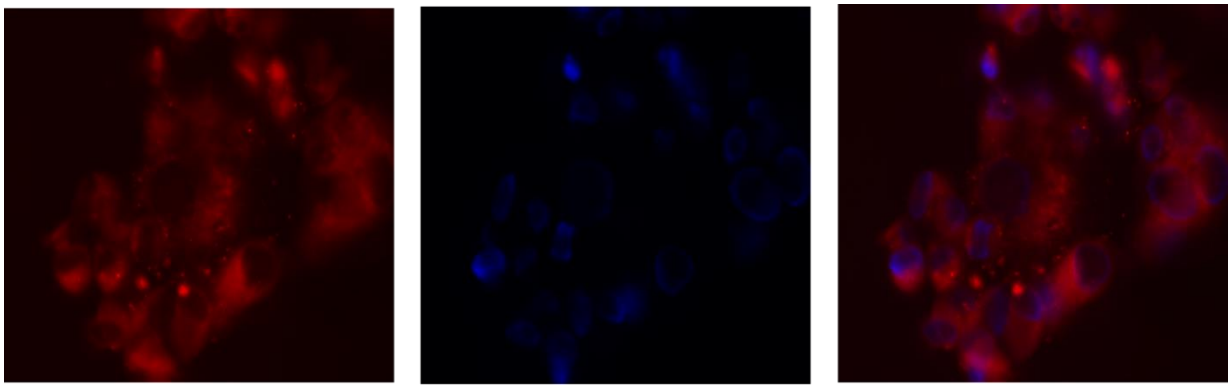

4.1, 100nM DAPI Merge

D.

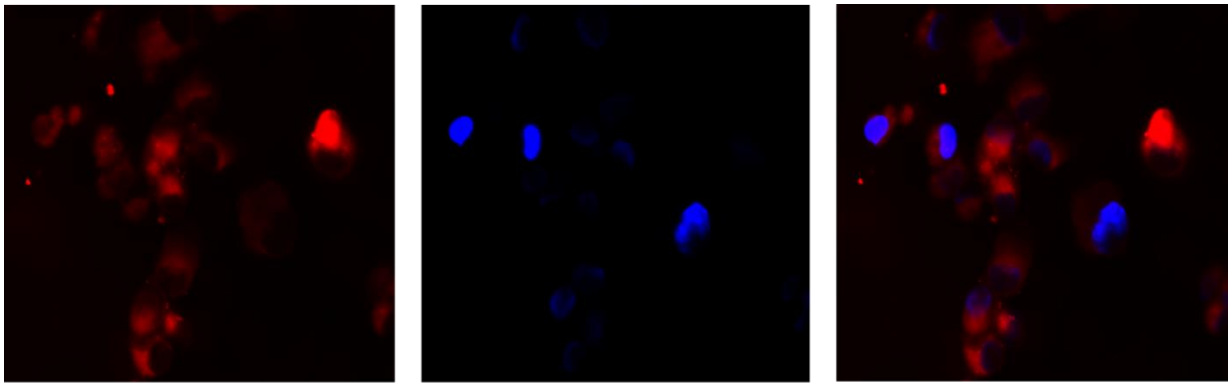

4.1, 200nM DAPI Merge

E.

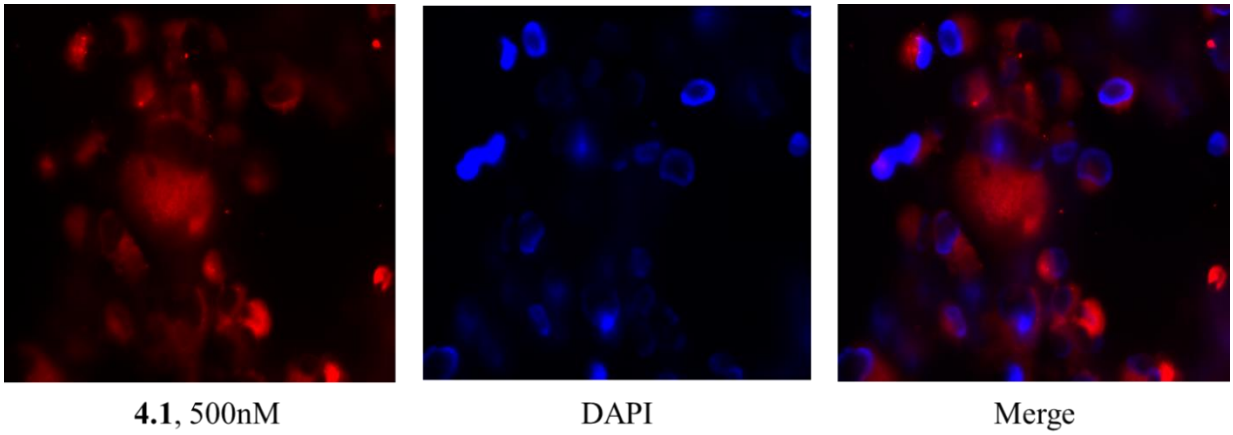

Figure 4. 3. Live cell imaging from **4.1** incubation at different concentration. (A) Cells were treated with 25nM **4.1**; (B) Cells were treated with 50nM **4.1**; (C) Cells were treated with 100nM **4.1**; (D) Cells were treated with 200nM **4.1**; (E) Cells were treated with 500nM **4.1**.

According to the image collected (Figure 4.3), when cells are treated with concentration below 100nM, cell image become clearer as we increase the work concentration; as the work concentration increased above 100nM, cell morphology is well detected, and signal intensity increase at very limited amount. As a result, 100nM is selected to be the best work concentration.

4.1.3. Optimal treatment time exploration for cell imaging

As a potential HTS test, consumption of positive control ipomoeassin F and negative control **4.2** is one of the biggest concerns, but time cost is also a critical unignorable factor. In order to push up the efficiency for competition test, we tried a serious of time to treat cells with probe **4.1** at work concentration 100nM.

A.

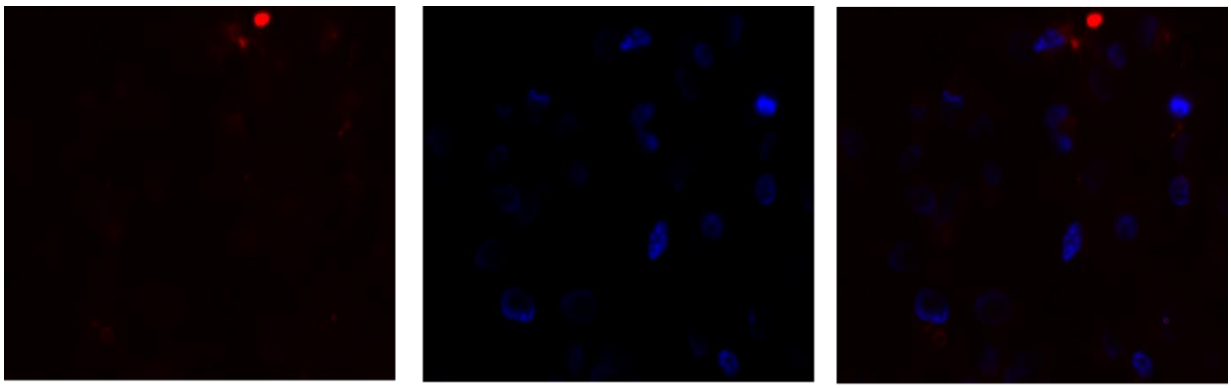

4.1, 5min DAPI Merge

B.

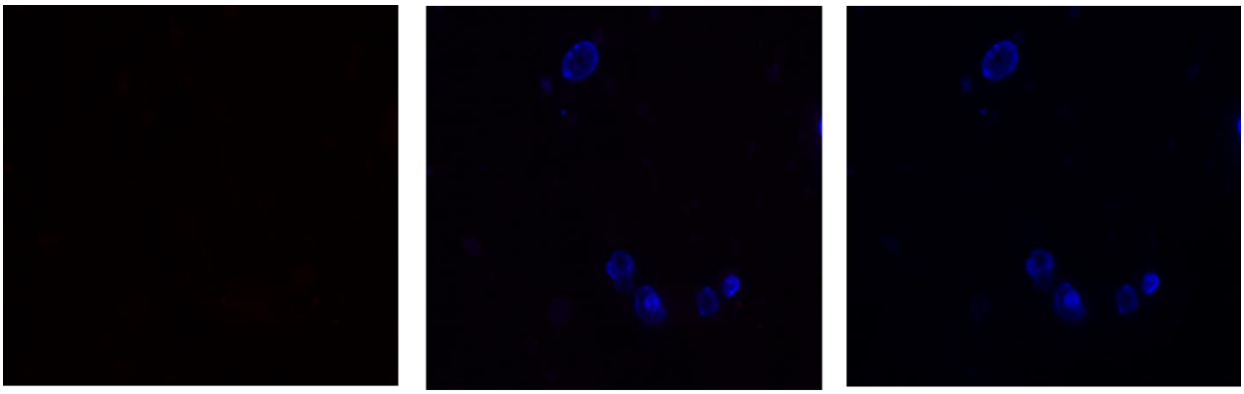

4.1, 15min DAPI Merge

C.

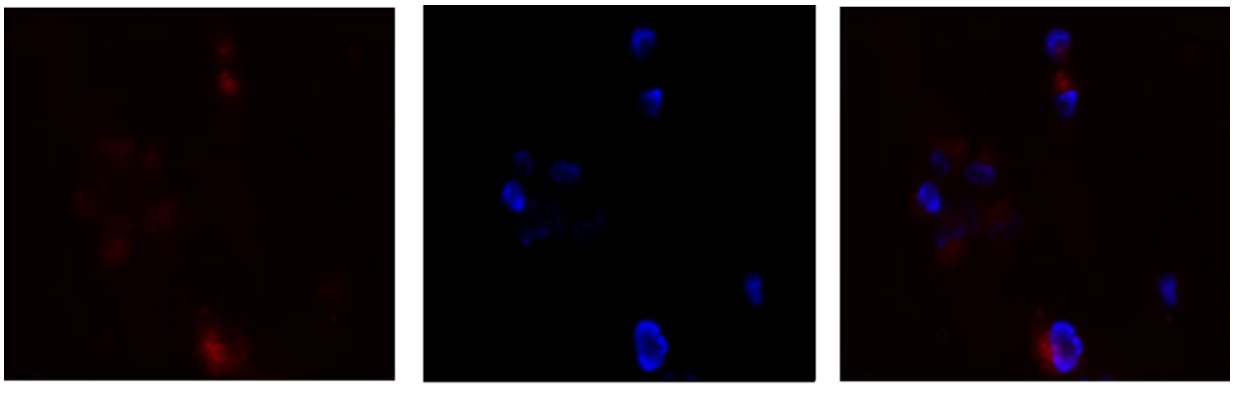

4.1, 30min DAPI Merge

D.

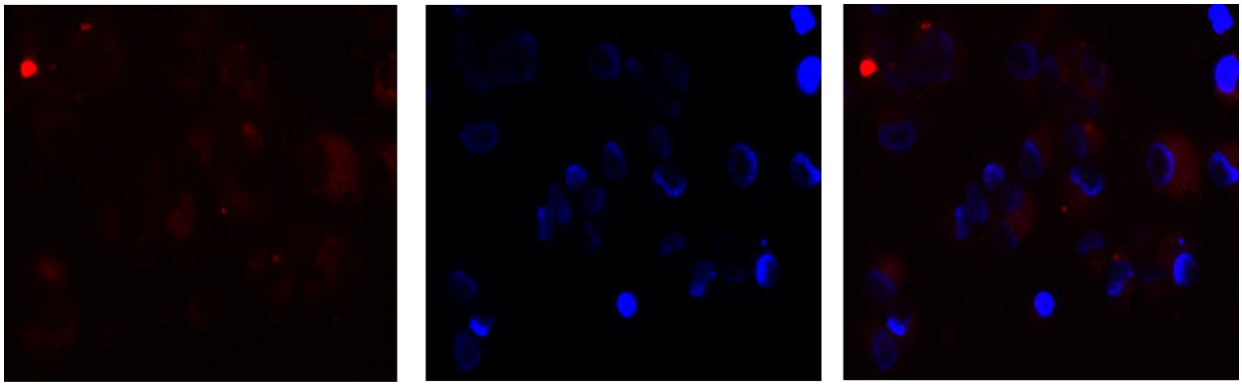

4.1, 45min DAPI Merge

E.

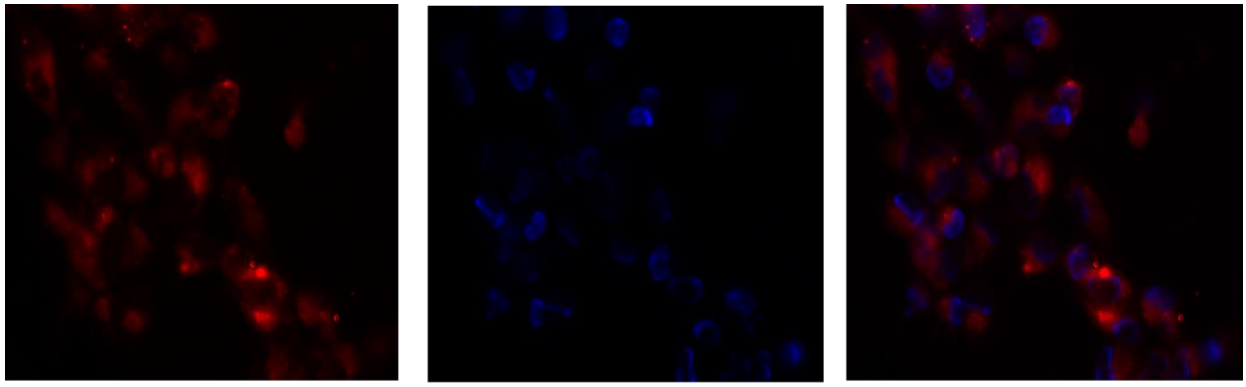

4.1, 60min DAPI Merge

F.

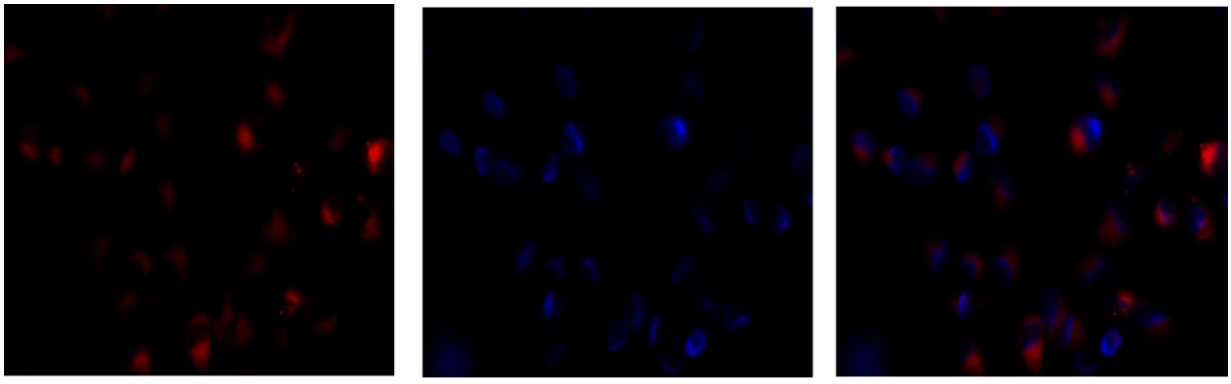

4.1, 2h DAPI Merge

G.

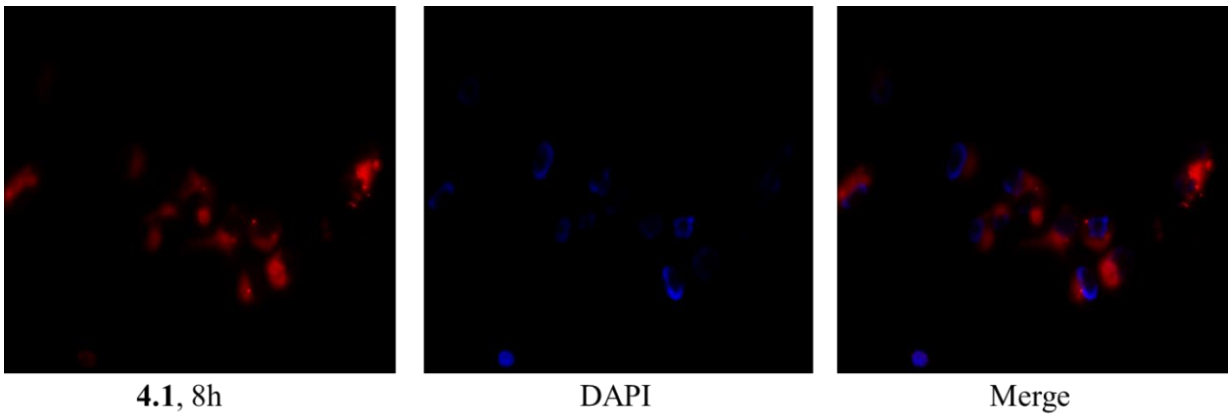

Figure 4. 4. Live cell imaging from **4.1** 100nM treatment at different time incubation: (A) Cells were incubated for 5min; (B) Cells were incubated for 15min; (C) Cells were incubated for 30min; (D) Cells were incubated for 45min; (E) Cells were incubated for 60min; (F) Cells were incubated for 2h; (G) Cells were incubated for 8h.

Without doubt, as the treatment time of **4.1** elongated, cell morphology is becoming more and more discernable (Figure 4.4). When the time goes beyond 1h, fluorescent intensity become stable even given 8h incubation. Therefore, 1h is optimized time when **4.1** labelling and disassociation become balanced.

4.1.4. Optimal fold competition of ipomoeassin F for cell imaging

Since the optimized work concentration for probe **4.1** is fixed at 100nM 1h, the best condition for competition become the next question. To better understand workable competition condition, we tried the competition between ipomoeassin F and probe **4.1** at the fold change ranging from 25-fold to 100-fold.

A.

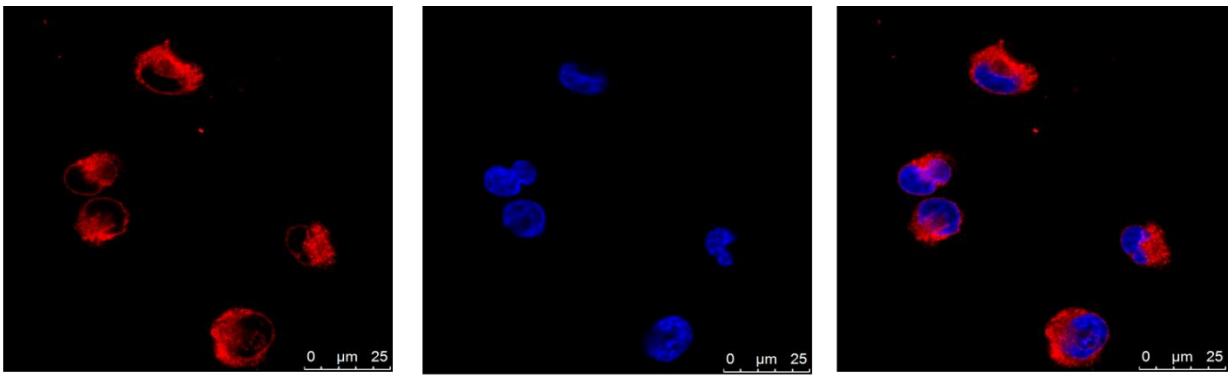

4.1 (0.1µM) + Ipom-F (0 µM) DAPI Merge

B.

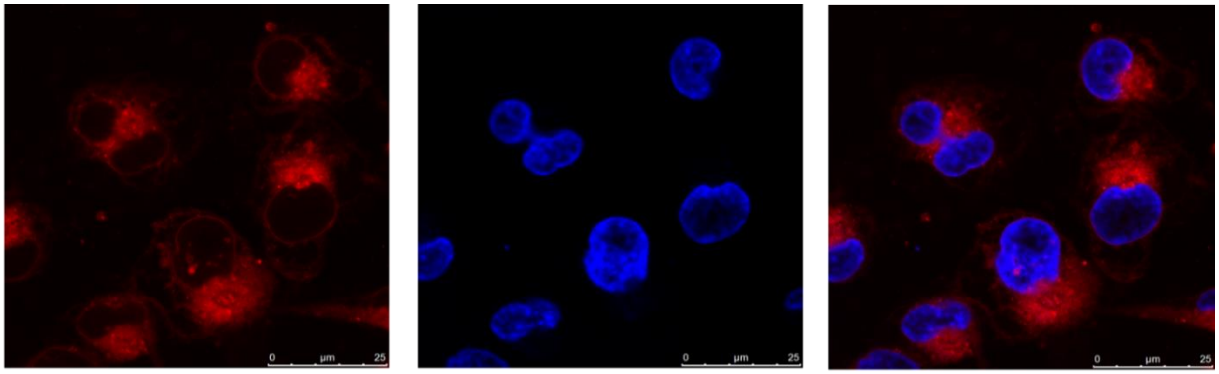

4.1 (0.1µM) + Ipom-F (2.5 µM) DAPI Merge

C.

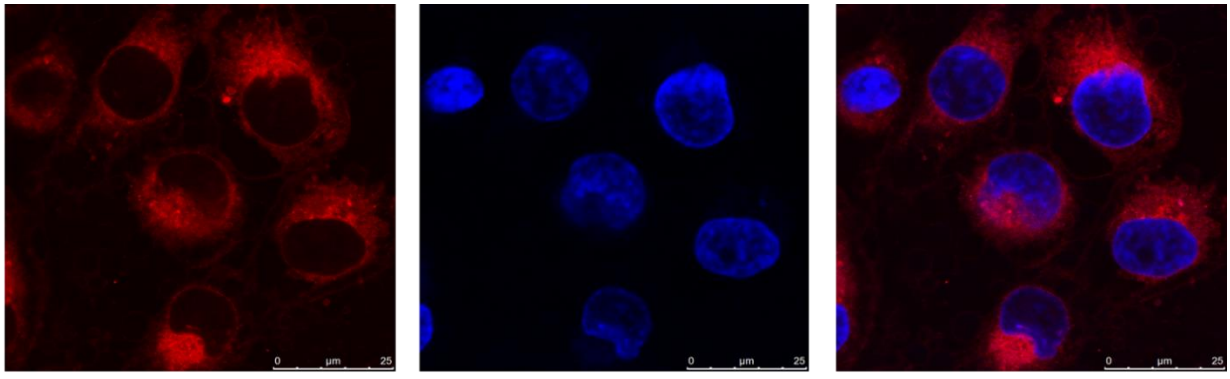

4.1 (0.1µM) + Ipom-F (5 µM) DAPI Merge

D.

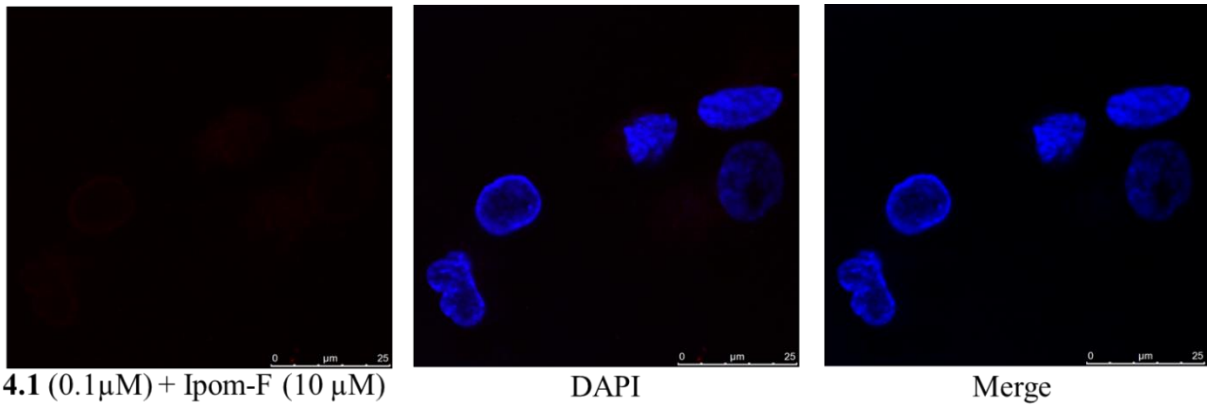

Figure 4. 5. Live cell confocal fluorescent microscopy imaging from 1h **4.1** 0.1 μM treatment and 30min ipomoeassin F competition at different competition fold difference: (A) Cells were treated with **4.1** without competition; (B) Cells were treated with **4.1** with 25-fold ipomoeassin F competition; (C) Cells were treated with **4.1** with 50 fold ipomoeassin F competition; (D) Cells were treated with **4.1** with 100 fold ipomoeassin F competition.

As expected (Figure 4.5), little competitive effect could be detected at 25 and 50-fold ipomoeassin F competition. However, when the concentration of ipomoeassin F increased to 100-fold competition, fluorescent signal was almost competed off. As a result, 100-fold competition is figured out to be the ideal condition for the potential HTS.

4.1.5. Optimal competition time of ipomoeassin F for cell imaging

As discussed above, 100-fold of ipomoeassin F completion almost removes fluorescent signal form probe **4.1** (Figure 4.5D), but the best competition time is unknown. Since the passive penetration of small molecular is very fast, the competition time increases gradually by every 5min, until the competition will not improve with passage of time.

A.

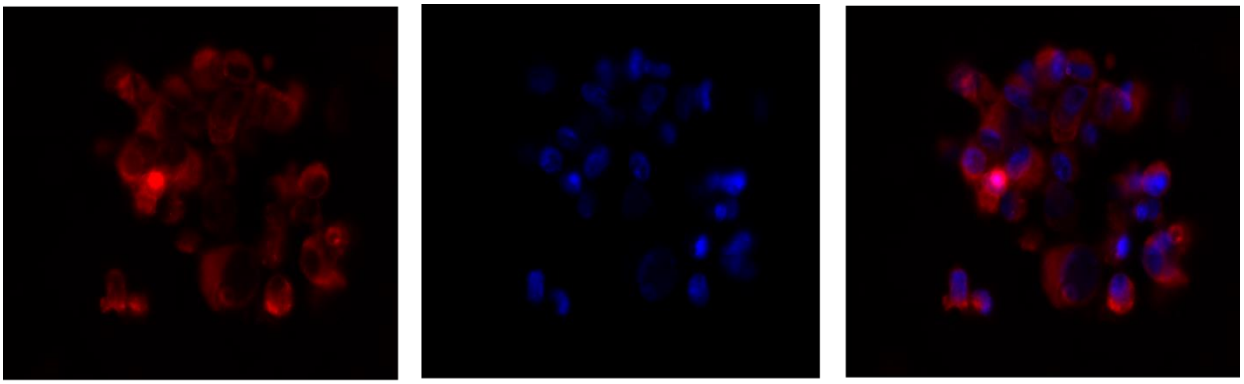

0 min competition DAPI Merge

B.

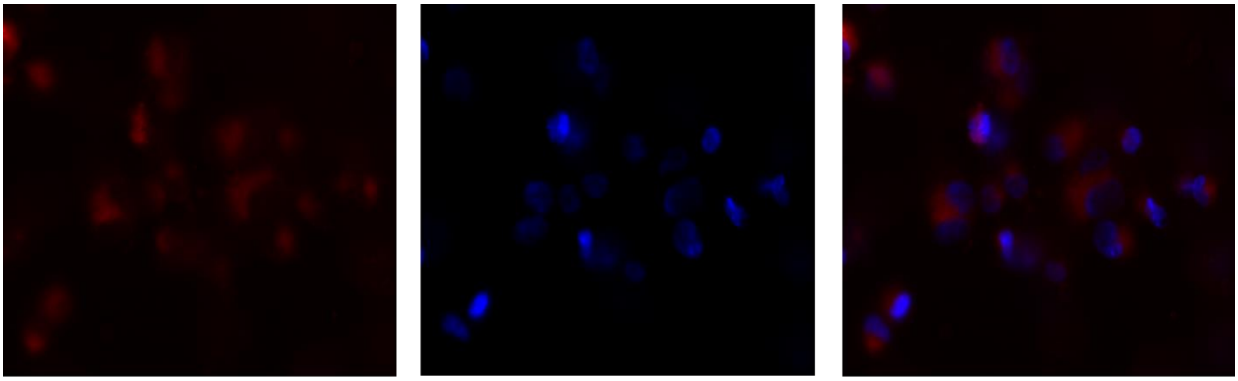

5 min competition DAPI Merge

C.

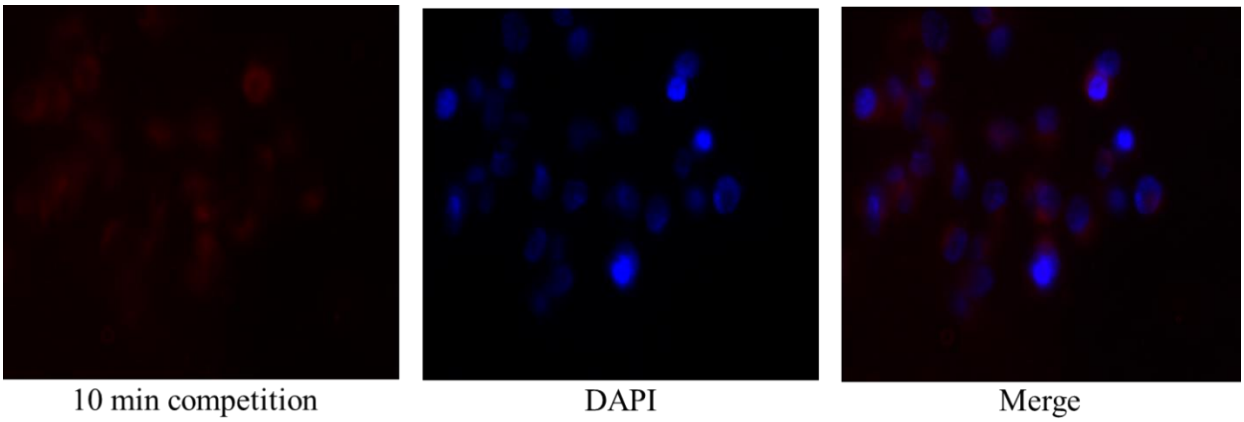

10 min competition DAPI Merge

D.

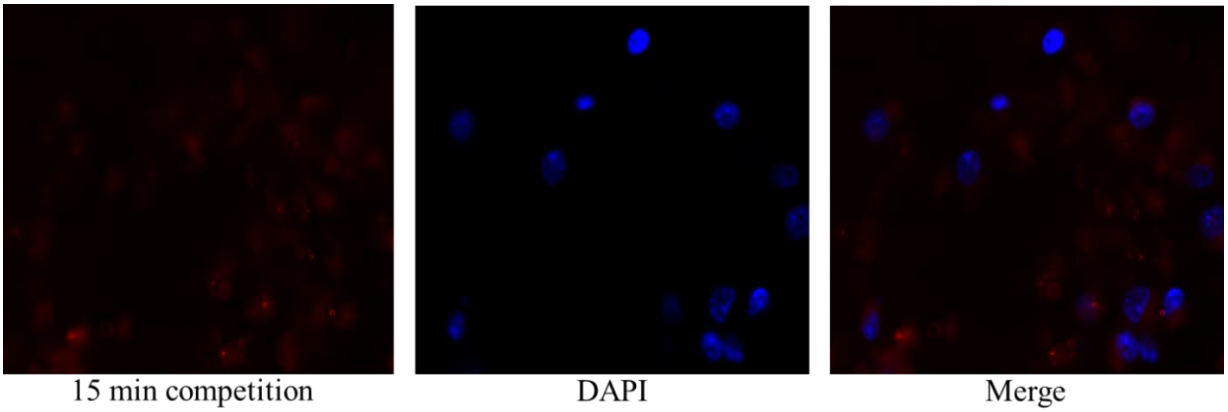

Figure 4. 6. Live cell imaging from 1h **4.1** 0.1 μM treatment and 100-fold ipomoeassin F competition at different competition time: (A) Cells were treated with **4.1** without competition; (B) Cells were treated with 5 min competition; (C) Cells were treated with 10 min competition; (D) Cells were treated with 15 min competition.

Probe **4.1** The fluorescent signal perishes fast within 10min competition and keeps a certain level ever since then. Compared with 1h incubation to reach peak binding for probe **4.1** at 100nM, high dosage (10μM) ipomoeassin F saturates the binding pocket within only 10 min, which significantly shorten screen time to 70min.

4.1.6. Procedure design for fluorescent probe based HTS research

Sharing the same target protein Sec61α, competition between ipomoeassin F and probe **4.1** are employed to isolate other compounds that hit the same target among large quantity of testing compounds. Fluorescent intensity variation vividly reflects the binding dynamics, so within proper work condition, the set of experiment enable potential application for HTS.

After systematic exploration, we found 1h treatment of probe **4.1** at 100nM work concentration followed by 10 min 100-fold ipomoeassin F (or testing compound) incubation is a

most suitable setting for the screening. As a result, procedure for fluorescent probe based HTS is designed as follow:

Step 1. Seed MDA-MB-231 cells into 96-well plate.

Step 2. Treat cells with medium containing 10μM positive control ipomoeassin F, negative control probe **4.2** and testing compound separately for 10min, followed by incubation with 100nM probe **4.1** for 1h in each group.

Step 3. Remove medium from each group and wash thoroughly with PBS for 3 times.

Step4. Collect fluorescent intensity reading from each group using plate reader at the optimized excitation and emission setting.

Step5. Evaluate the test compound reading with positive control and negative control result.

4.1.7. Result interpretation

Because of the stable and strong fluorescent properties, probe **4.1** is considered as an ideal candidate for target protein tracker. Solid result from positive control ipomoeassin F competition, negative control **4.2** competition and co-stain with ER tracker point to the conclusion that probe **4.1** binds to target protein Sec61α and the binding could be competed off by active compound that works on the identical binding site.

In the screening, fluorescent intensity from each test well represents the amount of **4.1** that firmly binds to Sec61α. Test compound that possesses strong affinity with Sec61α may easily compete off **4.1** like ipomoeassin F, leading to significant loss of fluorescent signal. Vice versa,

low Sec61α affinity compound has little chance to compete **4.1** off, giving rise to large fluorescent reading.

4.2.Biotin probe based HTS study

4.2.1. Mechanism for biotin probe based HTS research

Biotin modified probe **4.3** is proved to have specific binding with ER transmembrane protein Sec61α, and its binding can be competed away by ipomoeassin F that target the same site. Like the fluorescent probe based HTS study, proper condition and strategies for quantification would enable this probe a valuable potential candidate for HTS.

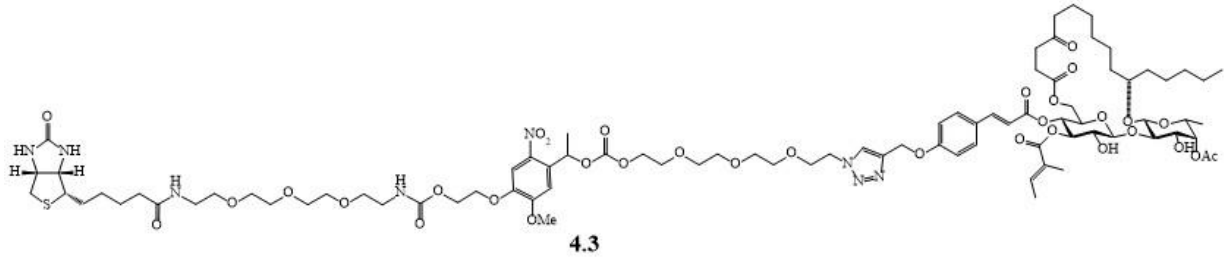

4.3

Figure 4. 7. Structure of ipomoeassin F analogues **4.3.**

Rather than generating detectable signal from the probe itself, **4.3** could excite secondary signal by biotin affinity strategies. For protein visualization, antibody-based detection approach western blot and ELISA are most commonly used due to the high sensitivity and specificity. However, western blot is not a first consideration for high throughput screening due to the fussy procedure. So, ELISA is applied to develop an easily accessible approach to effectively identify Sec61α affinity compounds by biotin probe competition. Due to the limited time and restriction of work condition, the following exploration for HTS application is designed for future work and lack of supportive experimental data.

4.2.2. HTS work condition optimization.

The Sec61α affinity compound screening is based on competition with probe **4.3** by using active compound ipomoeassin F and negative compound **4.2** as reference. Hence, standardize the work condition for competition and binding signal visualization is the key to perform HTS.

Firstly, the minimum ER microsome amount required for the screening will be evaluated to make sure enough target protein would be detectable in the visualization step. Based on the understanding of minimum number of ER microsome needed, the lowest work concentration *C1* of **4.3** for clear and stable visualization will be explored. Next, the optimized **4.3** incubation time *T1* would be determined. In the following step, optimized competition fold difference *F1* and its competition time *T2* for ipomoeassin F will be figured out. At last, since the commercial available anti-biotin antibody coated ELISA is standardized, conjugated antibody work condition in ELISA test will be optimized.

4.2.3. Procedure design for biotin probe based HTS research

In this project, our ultimate purpose is to quantitatively visualize the amount of **4.3** - Sec61α complex with the help of enzyme conjugated antibody or radioactive antibody. The procedure of biotin based HTS is listed as follow:

Step 1. Prepare sample as following

ER microsome is treated with positive control ipomoeassin F, negative control probe **4.2** and testing compound separately at the concentration of *C1*F1* for time *T2*, followed by incubation with probe **4.3** at the concentration of *C1* for time *T1* in each group. Then after multiple wash was performed in each group, n-dodecyl-ß-D-maltoside (DDM) will be added into each group to disrupt ER membrane structure.

Step 2. Add 100µl of sample from each group to anti-biotin polyclonal antibody coated 96 well plate and incubate in room temperature for 2 h.

Step3. Wash plate thoroughly before adding anti-Sec61α mono clonal secondary enzyme conjugated antibody and incubate in room temperature for 2h.

Step 4. Wash the plate thoroughly before adding substrate. Then read the plate after 0.5-1h room temperature incubation.

Step 5. Evaluate the test compound reading with positive control and negative control result

A.

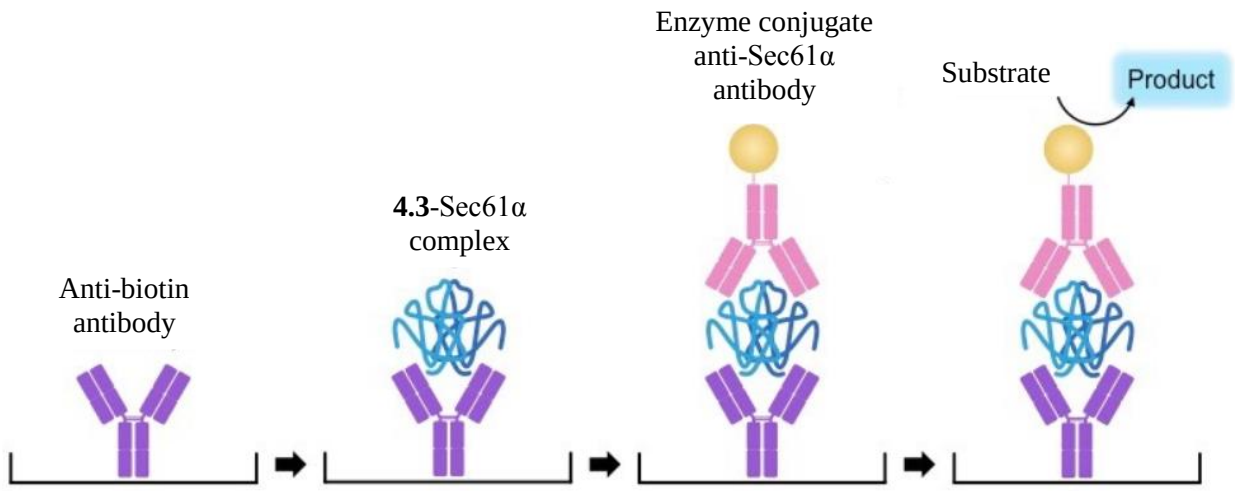

B.

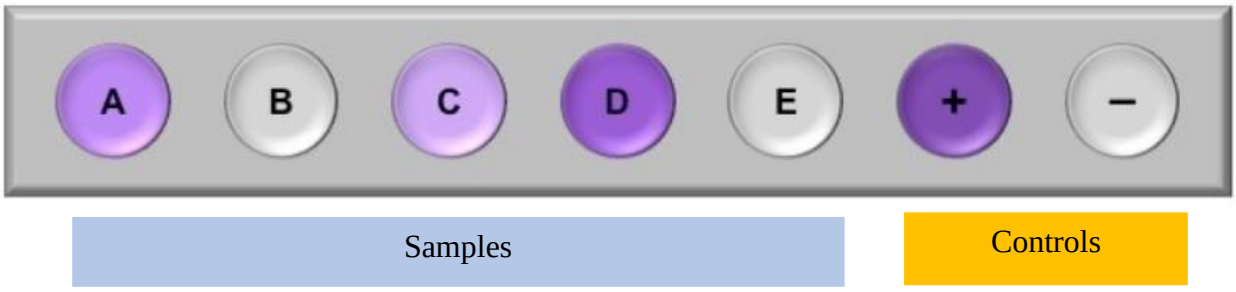

Figure 4. 8. Work flow of biotin-based HTS. (A) Elisa procedure diagram. (B) Testing result diagram. (diagrams are cited from http://ib.bioninja.com.au/options/untitled/b4-medicine/elisa.html)

4.2.4. Result interpretation

In the screening, cells are treated with high dosage ipomoeassin F, probe **4.2** and test compound respectively. Positive control ipomoeassin F saturates Sec61α binding site in the high concentration incubation, negative control does not consume any Sec61α binding site even in high concentration. As a result, in the following incubation step, probe **4.3** is not able to bind Sec61α in positive group but can freely bind Sec61α at its maximum capability. In this case, sample from positive group contain little **4.3**-Sec61α complex, while sample from negative group accumulate relatively large amount of **4.3**-Sec61α complex.

Since biotin is a key function group of **4.3**, coating antibody can easily capture **4.3**-Sec61α in negative group but keeps little such complex in positive group. In the following steps, only negative group would successfully bind enzyme conjugated antibody and catalyze substrate to produce detectable signals. Therefore, the stronger signal suggests the lower binding affinity between test compound and Sec61α, vice versa.

4.3.Conclusion

Sec61α is a critical ER transmembrane protein that play an indispensable role in protein translocation. Applying HTS to identify natural product or synthetic compound that work on Sec61α would provide abundant resources to develop anti-cancer drugs in medicinal chemistry.

Competition between probe **4.1** *vs* ipomoeassin F and probe **4.3** *vs* ipomoeassin F are well established and based on their common binding protein Sec61α. Stable fluorescent property of probe **4.1** enable its further potential application in HTS to search Sec61α high affinity compounds by the comparation of ipomoeassin F competition. Albeit a lot of work need to be done, the great sensitivity and easy accessibility endow the approach a promising future HTS. Unlike other probes, when **4.3** specifically binds Sec61α, the core structure is buried inside the complex, sprouting the

biotin group as a sticky end to provide extra binding site for ELISA quantitative visualization. Competition from Sec61α high affinity compound is expected to be reflected on the ELISA numerical reading, capacitating the potential application for ELISA-base HTS.

4.4.References

1. Katz L.; Baltz RH., Natural product discovery: past, present, and future. *Journal of Industrial Microbiology & Biotechnology* **2016**, *43*(2-3), 155-176.

2. Luo Y.; Cobb RE.; Zhao H., Recent advances in natural product discovery. *Current Opinion in Biotechnology* **2014**, *30*, 230-237.

3. Koehn FE., High impact technologies for natural products screening. *Progress in Drug Research* **2008**, *65:175*, 177-210.

4. Rapoport T. A.; Jungnickel B.; Kutay U., Protein transport across the eukaryotic endoplasmic reticulum and bacterial inner membranes. *Annual Review of Biochemistry* **1996**, *65*, 271-303.

5. Beckmann R.; Bubeck D.; Grassucci R.; Penczek P.; Verschoor A.; Blobel G.; Frank J., Alignment of conduits for the nascent polypeptide chain in the ribosome-Sec61 complex. *Science* **1997**, *278*, 2123-2126.

6. Hanein D.; Matlack K. E.; Jungnickel B.; Plath K.; Kalies K. U.; Miller K. R.; Rapoport T. A.; Akey C. W., Oligomeric rings of the Sec61p complex induced by ligands required for protein translocation. *Cell* 1996, 87, 721-732.

7. Greenfield JJ.; High S., The Sec61 complex is located in both the ER and the ER-Golgi intermediate compartment. *Journal of Cell Science* **1999**, *112* (Pt 10), 1477-1486.

8. High, S.; Laird, V., Membrane protein biosynthesis – All sewn up? *Trends in Cell Biology* **1997**, *7*, 206-210.

9. Duval R.; Duplais C., Fluorescent natural products as probes and tracers in biology. *Natural Product Reports* **2017**, *34*(2), 161-193.

SUMMARY AND CONCLUSIONS

Ipomeassin F is found to be one of promising natural products that would potentially curb cancer neoplasia. In order to better understand the property of this newly developed compound, we performed systematic SAR study and deep exploration on its MOA by using breast cancer cell line MDA-MB-231 and MCF-7 as models.

Based on the complicated SAR study, we reveal that lipophilicity is vital to retain potency of ipomoeassin F. Hydrophilic moieties in ipomoeassin F not only maintain the conformational stability but also work as vessel to efficiently deliver the compound into cells from aqueous environment. Impact significance of each group on ipomoeassin F potency is in the order of: D-Fucp >cinnamate >tiglate >alkene in cinnamate > alkene in tiglate > acetate > 3-OH-Fucp >cyclic skeleton ≈ ketone.

After treating cancer cells, ipomoeassin F would localize in ER and interact with the target protein Sec61α by non-covalent binding or weak reversible covalent binding. The binding pocket is deep inside the complex, and the firmly binding between ipomoeassin F and Sec61α requires membrane environment to sustain stability.

By employing ipomoeassin F analogues which share same target Sec61α, potential applications for Sec61α affinity compound HTS would be available. The application could be either analyzed by fluorescent intensity analysis or biotin-based ELISA signal analysis.

Appendix: Biosafety Approval Letter

February 10, 2017

MEMORANDUM

TO:	Dr. Wei Shi
FROM:	Ines Pinto, Biosafety Committee Chair
RE:	New Protocol
PROTOCOL #:	17024
PROTOCOL TITLE:	Molecular Engineering of Natural Glycoconjugates for Drug Discovery
APPROVED PROJECT PERIOD:	Start Date February 9, 2017 Expiration Date February 8, 2020

The Institutional Biosafety Committee (IBC) has approved Protocol 17024, "Molecular Engineering of Natural Glycoconjugates for Drug Discovery". You may begin your study.

If modifications are made to the protocol during the study, please submit a written request to the IBC for review and approval before initiating any changes.

The IBC appreciates your assistance and cooperation in complying with University and Federal guidelines for research involving hazardous biological materials.